CONDENSATION OF ZINC VAPOUR

by

Loucas Gourtsoyannis

CONDENSATION OF ZINC VAPOUR

by

Loucas Gourtsoyannis

A thesis submitted to the Faculty of Graduate Studies
and Research in partial fulfillment of the
requirements for the degree of
Master of Science

Department of Metallurgical Engineering
McGill University,
Montreal, Canada.

February, 1972.

ABSTRACT

The vapourization of pure liquid zinc and the condensation of zinc vapour on liquid lead have been experimentally studied using two gas-liquid metal contact methods: bubbling and jetting. Both vapourization methods yielded high efficiency, the jetting contact approach yielding the more reproducible results. Bubbling proved to be the most efficient zinc vapour condensation method.

A new approach to industrial condensation of zinc vapour from zinc blast furnace gas, namely, use of a bubble vacuum condenser, has been considered and a design of an industrial scale condenser has been formulated.

RÉSUMÉ

L'étude de l'évaporation du zinc liquide et de sa condensation sur du plomb liquide a été réalisée en considerant deux méthodes de contact entre le gaz et le métal: par barbottage et par balayage.

Les deux méthodes d'évaporation se caracterisent par une haute efficacité, le balayage donnant les résultats les plus reproductibles.

La condensation par barbottage s'est avérée la plus efficace.

La possibilité d'utiliser un condenseur à bulles sous vide, constitue une nouveauté parmi les techniques de condensation du zinc des gaz du haut-fourneau. Nous avons également conçu un condenseur d'échelle industrielle.

TABLE OF CONTENTS

Chapter		Page
I	INTRODUCTION	1
	1.1 Preliminary Remarks	1
	1.2 The Horizontal Retort Process	3
	1.3 The Vertical Retort Process	5
	1.4 The Wheaton-Najarian and Splash Condensers .	9
	1.5 The Zinc Blast Furnace	12
	1.6 The Lead Splash Condenser	14
	1.7 Present Work	14
II	THEORY OF THE PROCESSES AND PREVIOUS WORK	15
	2.1 General	15
	2.2 Enthalpy Considerations of Zinc Reduction. . .	15
	2.3 Thermodynamics of Zinc Production.	17
	2.4 Approach to Equilibrium Conditions During Zinc Production	19
	a) Retorts	19
	b) Zinc Blast Furnace.	20
	2.5 The Thermodynamics of Zinc Vapour Condensation	21
	2.5.1 Condensation of Zinc from Vertical Retort Gases	23
	a) Condensation	23
	b) Back-oxidation.	24
	c) Overall Effects	26

TABLE OF CONTENTS (Cont'd)

Chapter		Page
II (Cont'd)		
	2.5.2 Condensation of Zinc from Blast Furnace Gases	26
	a) Cooling Without Oxidation	28
	b) Back-oxidation	28
	c) Overall Effects	29
	2.5.3 Shock Chilling	30
	2.6 Thermal Considerations of Condensation	30
	a) Vacuum-Bubble Condenser (Wheaton-Najarian)	30
	b) Lead Splash Condenser (Zinc Blast Furnace)	31
	2.7 The Separation of Zinc from Lead	33
	2.8 Previous Work	35
III	EXPERIMENTAL	36
	3.1 General Description of Experiments	36
	3.2 Description of Apparatus	37
	3.2.1 Vapourizer	37
	3.2.2 Condenser	41
	3.2.3 Vapourizer-Condenser Connection	41
	3.2.4 The Sampling System	42
	3.2.5 Gas Circulation	44
	3.2.6 The Heating System	45

TABLE OF CONTENTS (Cont'd)

Chapter	Page
III (Cont'd)	
3.3 Operating Procedures	47
3.3.1 Assembly	47
3.3.2 Heating	48
3.3.3 Start of Experiment.	48
3.3.4 Procedures During Running	49
3.3.5 End of Experiment	50
3.3.6 Analysis of Samples	51
3.4 Experimental Results	52
3.4.1 Vapourization Results.	53
3.4.2 Vapourization into Argon Bubbles	53
3.4.3 Vapourization into an Argon Gas Jet. . .	57
3.4.4 Condensation Results	64
3.4.5 Condensation from Gas Bubbles	64
3.4.6 Condensation from a Gas Jet	70

TABLE OF CONTENTS (Cont'd)

Chapter		Page
IV	DISCUSSION	74
	4.1 Vapourization of Zinc from Liquid Zinc into Rising Argon Bubbles	74
	4.1.1 Rate Controlling Mechanisms in Vapourization Experiments (bubbling)	75
	4.2 Vapourization from Liquid Zinc into a Jet of Argon	83
	4.3 Problems in Interpreting the Vapourization Results	85
	4.4 Condensation Experiments	92
	4.5 Condensation of Zinc Vapour into Lead from Zinc-Argon Gas Bubbles.	93
	4.5.1 Rate Controlling Mechanisms in Bubbling Condensation Experiments	97
	4.6 Condensation of Zinc Vapour into Lead from a Jet of Zinc Argon Gas	102
	4.7 Industrial Implications	115
	4.7.1 The Use of Lead or of Zinc in the Bubble Condenser	116
	4.7.2 Design Calculation of Full Scale Bubble Condenser	118
	4.8 Suggestions for Future Experimental Work .	123
	4.9 Conclusions	124

TABLE OF CONTENTS (Cont'd)

	Page
APPENDIX A	125
ACKNOWLEDGEMENTS	134
LIST OF SYMBOLS	135
LIST OF FIGURES	137
LIST OF TABLES	140
REFERENCES	141

CHAPTER I

INTRODUCTION

1.1 PRELIMINARY REMARKS

Zinc is produced by two very different techniques:

a) by pyrometallurgical reduction of zinc oxide with carbon;

b) by leaching of zinc oxide in aqueous sulphuric acid solution followed by the recovery of the dissolved zinc by electrowinning.

Processes involving the reduction of zinc oxide by carbon, which form the subject of this thesis, today account for some 35 to 40 percent of world zinc production.

Fifty years ago, the pyrometallurgical production of zinc was almost exclusively by the horizontal retort process,[1] which involved the reduction of zinc oxide and condensation of the resultant zinc vapour in small individually charged retorts.

As a first attempt to replace the horizontal retort process, researchers attempted in the early 1900's to develop a blast furnace process which would continuously produce liquid zinc inside the furnace. An extensive thermodynamic study by Maier[2] proved, however, that such a blast furnace would have to operate under pressures much too high for industrial practice.

Thus this objective was abandoned in favour of producing zinc as a vapour and condensing it outside the furnace. Research into methods

of condensing zinc vapour from furnace gases resulted in the development of the present day techniques of contacting the gas with agitated, cool liquid metal.

Two of the main zinc reduction processes now in use are the vertical retort process and the zinc blast furnace process. Since both are continuous production processes of relatively large size in contrast to the small, batch-type horizontal retort process, they have brought about a considerable increase in production rate. These two processes now account for approximately 25 percent of the primary production of zinc.

The increased rates of zinc vapour production in the vertical retorts and the zinc blast furnaces demanded condensing techniques permitting high rates of condensation. The liquid metal condensers utilize direct intimate contact between the zinc-laden furnace gases and droplets or turbulent surfaces (i.e., bubble-liquid metal surfaces) of cool liquid metal and thus provide:

a) large surface area for condensation;

b) rapid heat transfer from the gas ('shock cooling').

These two conditions lead to the rapid rates of condensation required by the vertical retort and blast furnace processes. The zinc vapour condenses on the liquid metal surfaces and joins the liquid metal bath and hence the product zinc can be continuously produced and tapped.

As an introduction to the investigation, the remainder of this chapter describes current zinc oxide reduction processes and zinc vapour condensation techniques; and outlines the object of the research programme

described in this thesis.

1.2 THE HORIZONTAL RETORT PROCESS

In the horizontal retort process[1] the retorts are cylindrical, approximately 5 feet long with an inside diameter 8 to 9 inches. They are placed in a regenerative furnace (usually gas fired) as shown in Figure 1.-1.

The charge consists of a mixture of zinc calcine* and coal. Each retort is fitted with a fireclay condenser which is situated outside the furnace. Thus the condenser temperature is low enough to cause condensation of the zinc vapour which results from the reduction reactions taking place in the retort.

The gases from the retort pass slowly out through the condenser and the zinc vapour condenses as it contacts the cool condenser walls, thus forming a pool of zinc at the bottom of the condenser. In industrial practice this liquid zinc is removed by breaking the 'dam' of clay at the tip of the condenser, permitting the batch of zinc (usually 25 to 30 pounds) to flow into a mobile holding container. After each reduction and condensing cycle (usually 4 or 5 tappings of liquid zinc), the retort is emptied of residual matter and is recharged with the coal-calcine mixture.

A plant typically employs 40 retorts per ton of daily production capacity with some 800 retorts being heated in a single regenerative furnace.

It is clear that the horizontal retort process is extremely inefficient in terms of production rate, labour utilization, and thermal efficiency and hence it is rapidly disappearing as a viable industrial process.

---

*Oxidized zinc concentrates in fine form.

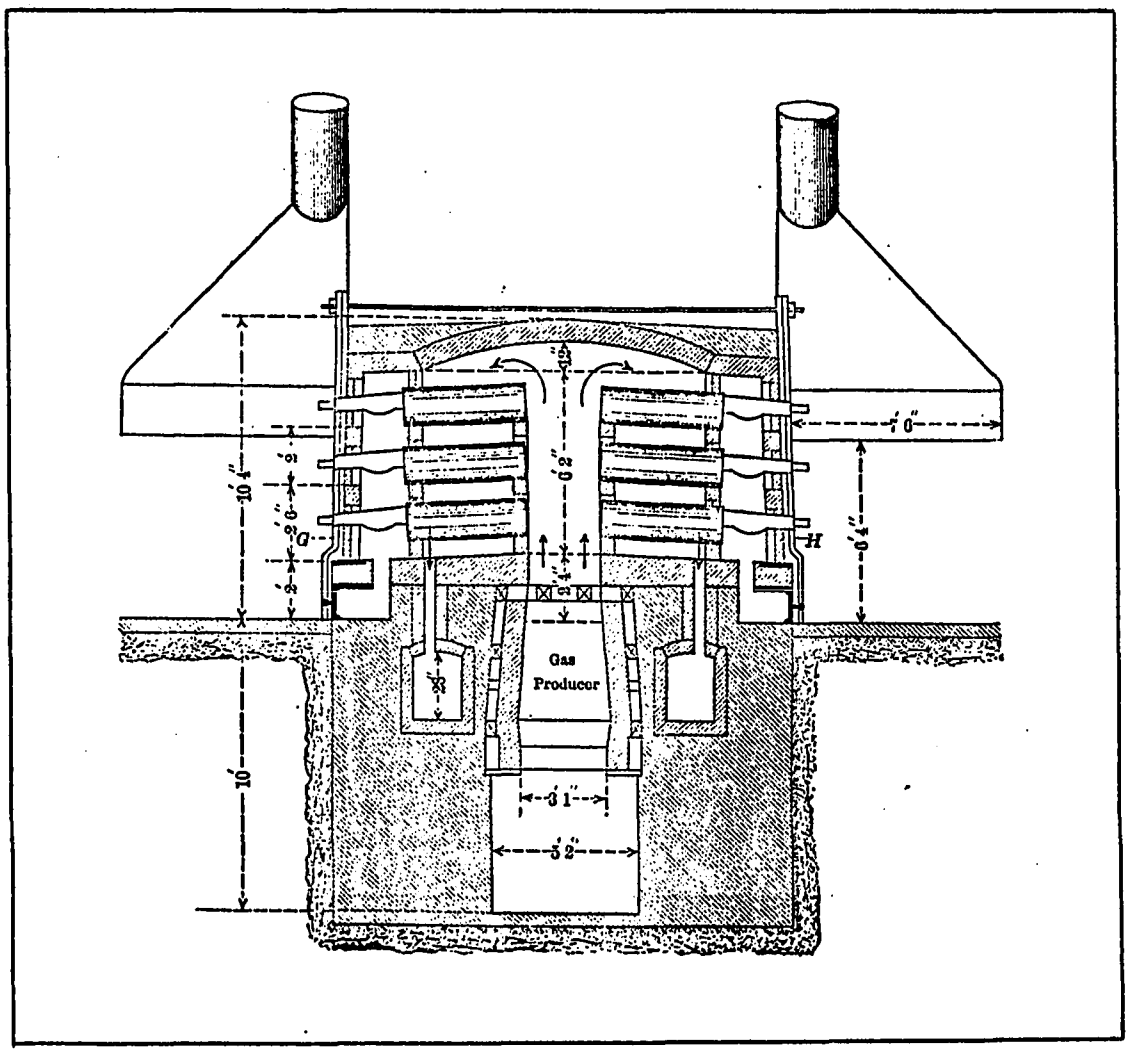

FIGURE 1.-1: Horizontal Retort Furnace.

1.3 THE VERTICAL RETORT PROCESS

The first improvement over the horizontal retort configuration was the vertical retort furnace[1] (Figure 1.-2) which permitted continuous charging, continuous removal of solid residue and continuous condensing and tapping of liquid zinc.

Although the chemical rate of reaction has not been substantially improved over the horizontal retort process, the use of silicon carbide as the retort wall material has permitted a much higher rate of heat transfer into the retort per unit area of retort wall.

The resultant higher rate of heat transfer has allowed the use of larger retort units, i.e., units with a lower surface area to contained volume ratio. These larger units provide enough cross-sectional area (plan dimensions 1 foot by 7 feet) to permit the continuous descent of charge in a vertical configuration and thus these retorts can be operated continuously. A zinc production rate of some 8 tons per day is common for retorts of these dimensions (typical height 30 feet).

A parallel development to the externally heated vertical retort has been that of the electrothermic zinc furnace which is, in simpler terms, a large vertical retort to which the heat is supplied by the passage of electric current through the solid charge (resistance heating) (Figure 1.-3). These units, although expensive to heat, have produced up to 80 tons of zinc per day.

A comparison between the two types of vertical retort systems is presented in Table 1.A.[1]

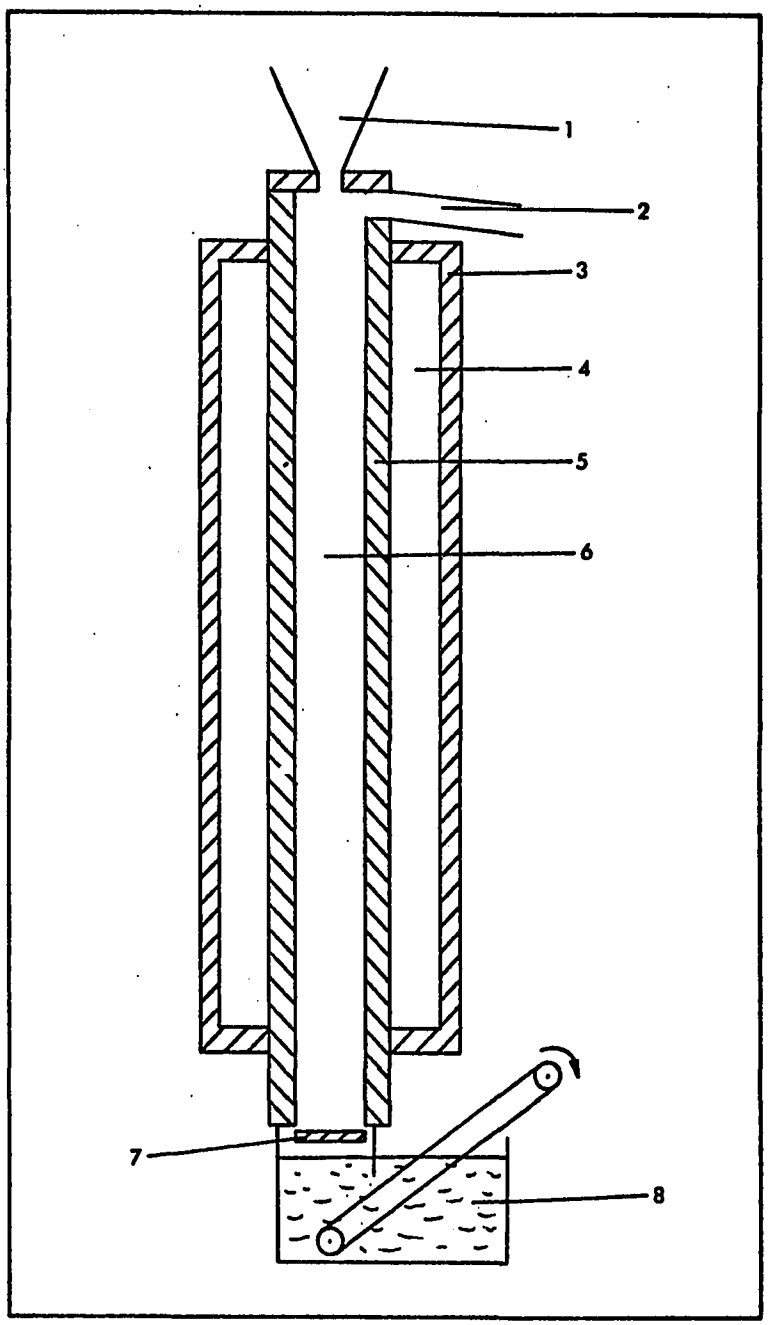

FIGURE 1.-2: Schematic diagram of vertical retort (out of scale)

1) Charging hopper; 2) Gas outlet to condensers; 3) Combustion chamber wall; 4) Combustion chamber; 5) Silicon carbide wall; 6) Reaction chamber; 7) Discharger; 8) Water seal.

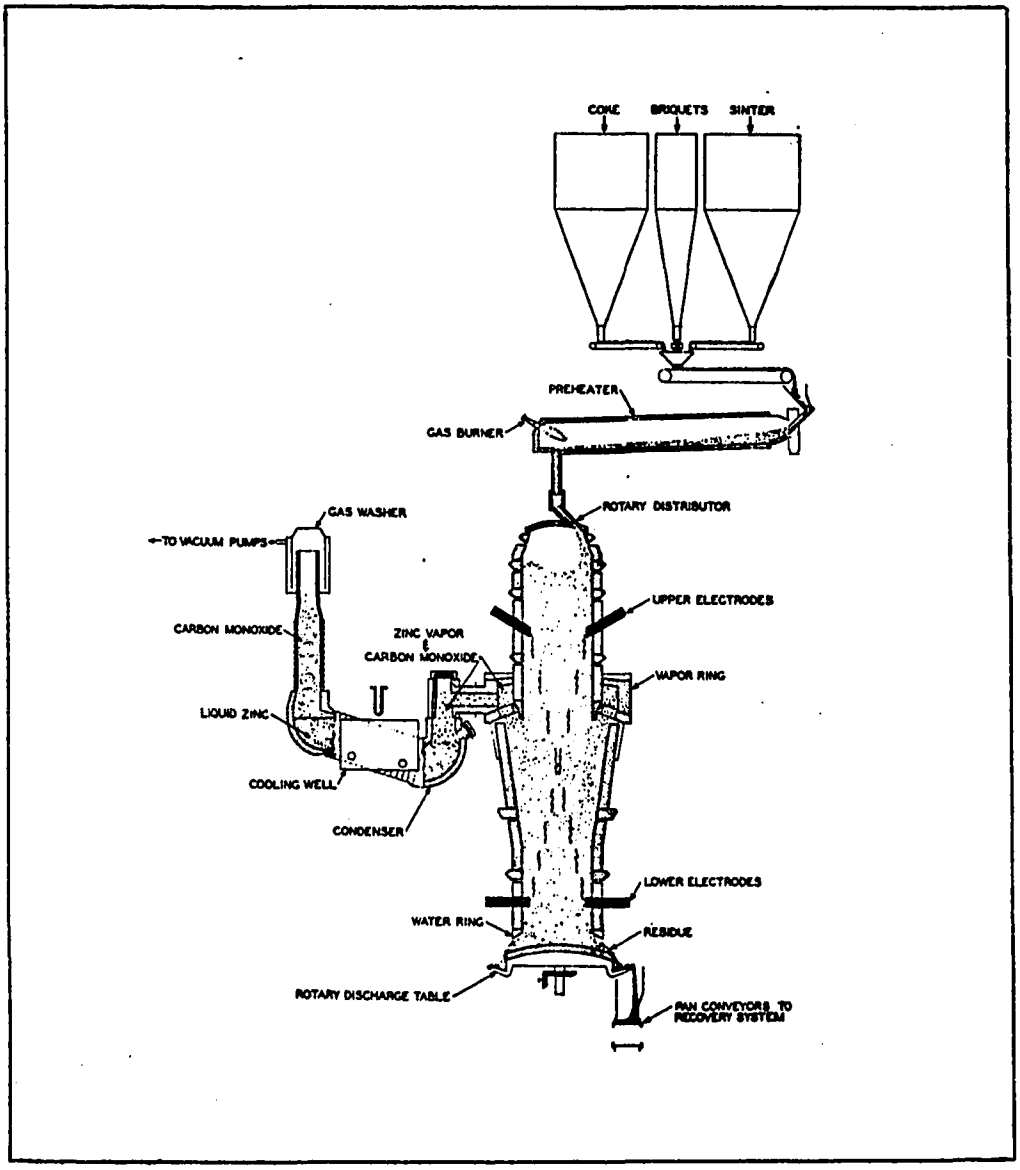

FIGURE 1.-3: St. Joseph Lead Company electrothermic zinc furnace.

TABLE 1.A

VERTICAL RETORT FURNACES

	Height	Horizontal Cross Section	Heating Method	Condenser Configuration	Zinc Production Rate
New Jersey Zinc Co. Retort	25-35 ft	Rectangular 1 foot x 7 feet	External Furnace	Splashing Liquid Zinc	5-8 tons/day
St. Joseph Lead Co. Electrothermic Process	32-45 ft	Circular, diameter 6-8 feet	Electrical Resistance	Bubbling Through Liquid Zinc	20-80 tons/day

1.4 THE WHEATON-NAJARIAN AND SPLASH CONDENSERS

The condensers employed with the vertical retorts are either the Wheaton-Najarian bubble type or the splash condenser type. Both employ zinc as the coolant metal.

The Wheaton-Najarian (or bubble-vacuum condenser)[3] consists of a U-shaped tube as shown in Figure 1.-4. The inlet end of the tube is connected to the output of the retort furnace, while the outlet end of the tube is connected to the vacuum pumps via a gas cleaning system. The U tube contains liquid zinc at about 500°C.

The application of vacuum (minimum pressure in leg 500 mm of Hg) on the output end causes the hot retort gases (1150°C) to bubble through the liquid zinc. The resultant cooling of the gases leads to zinc condensation.

The condenser leg, which is connected to the vacuum line, has a slope of approximately 30° (see Figure 1.-4) and it is fitted with refractory baffles and dams. These help to reduce bubble size and thus lead to better gas-liquid contact and smoother operation. The outside of the condenser is sprayed with water and water cooling pipes are immersed in the zinc bath to remove the heat absorbed from the furnace gases and from the zinc condensation process.

The zinc splash condenser[4, 5, 6, 7] is usually rectangular in plan and it is often divided into two or three compartments separated by dams (see Figure 1.-5). The liquid metal in the condenser circulates countercurrently to the furnace exit gases, while rotors of various types (horizontal, vertical, inclined) whirl in the liquid metal bath creating

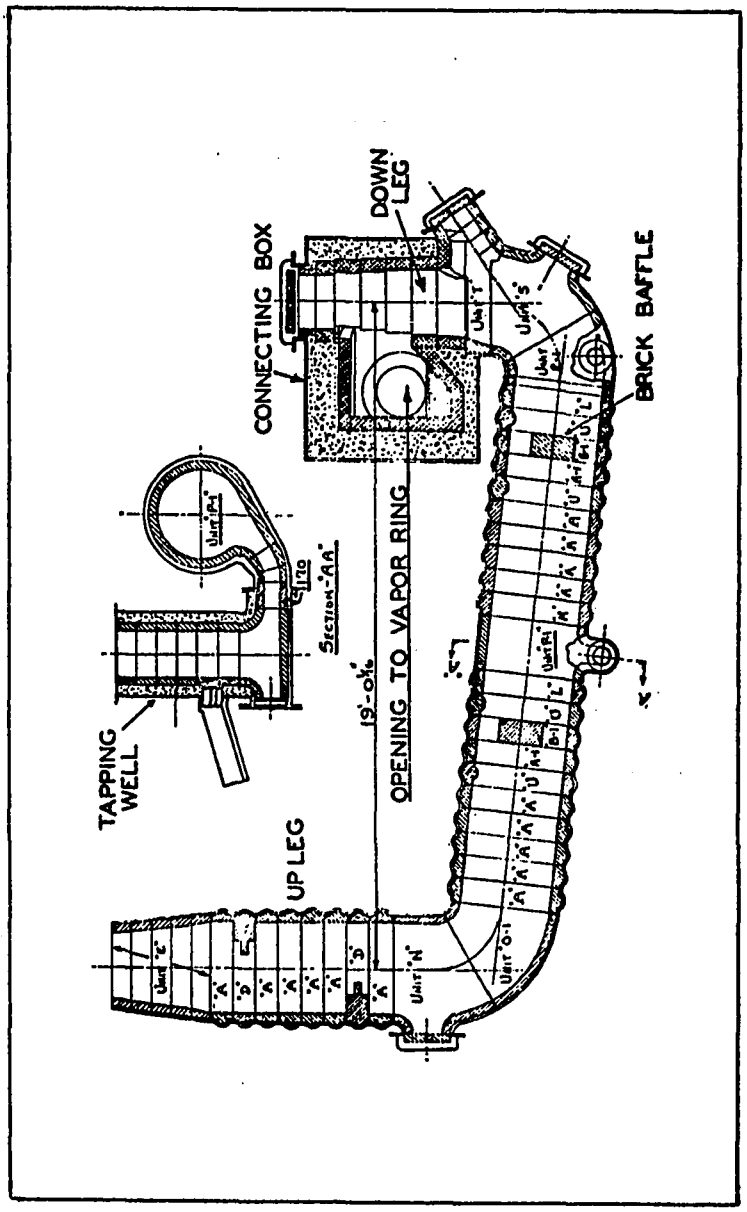

FIGURE 1.-4: Bubble vacuum condenser.

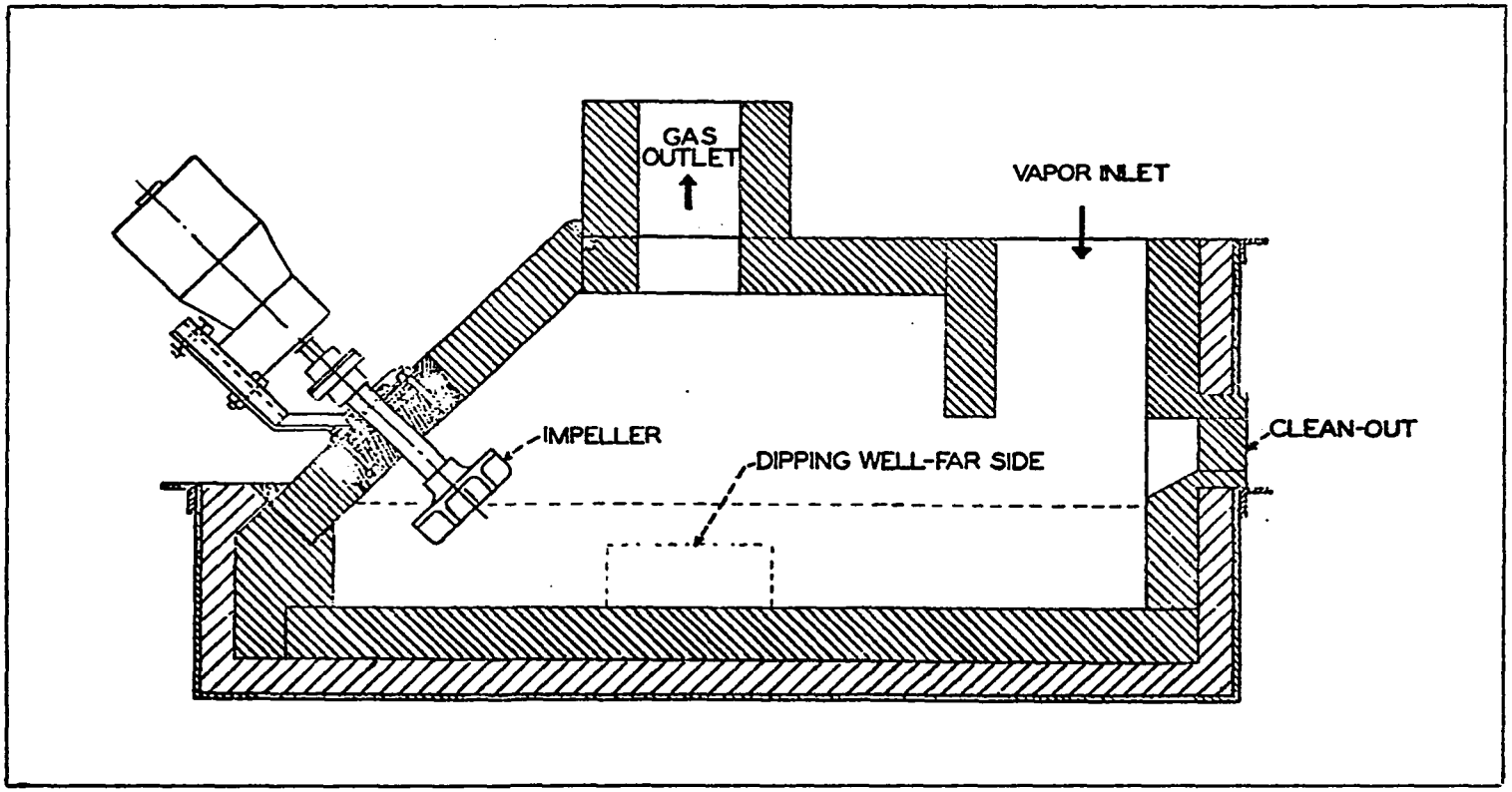

FIGURE 1.-5: Zinc splash condenser

showers of molten metal droplets. These metal droplets cool the furnace gases and the zinc vapour condenses on the droplet surfaces. The liquid zinc bath is cooled by means of immersed, water-cooled pipes.

Comparison between the bubble-vacuum and the splash condensers shows that from an engineering point of view the bubble condenser appears to be superior: it has practically no moving parts, it can be sealed effectively and it gives very high zinc recoveries (93-97%).

1.5 THE ZINC BLAST FURNACE

The zinc blast furnace or Imperial Smelting Furnace* is entirely different in concept to the retort process in that carbon is combusted with air inside the furnace. This difference has two major effects:[8]

1) Heat is provided directly inside the furnace, which permits the use of large furnace units.
2) The gases exiting from the furnace are high in CO_2 as a result of the air addition to the furnace.

In practice the carbon is added as coke while the zinc oxide is added as sinter. The blast air is preheated and injected via tuyères near the bottom of the furnace. Lead oxide is always present in the charge and lead is produced along with slag. These are tapped from the bottom of the furnace in liquid form.

As in the retort processes, the zinc is produced as a vapour and it is drawn off with furnace gases (N_2, CO_2, CO) near the top of the furnace (Figure 1.-6). The zinc is condensed in an external liquid metal condenser using lead as the cooling medium.

*The zinc blast furnace was developed by Imperial Smelting Corporation Limited and for promotional purposes is usually referred to as the Imperial Smelting Furnace. In this thesis the term zinc blast furnace will be used.

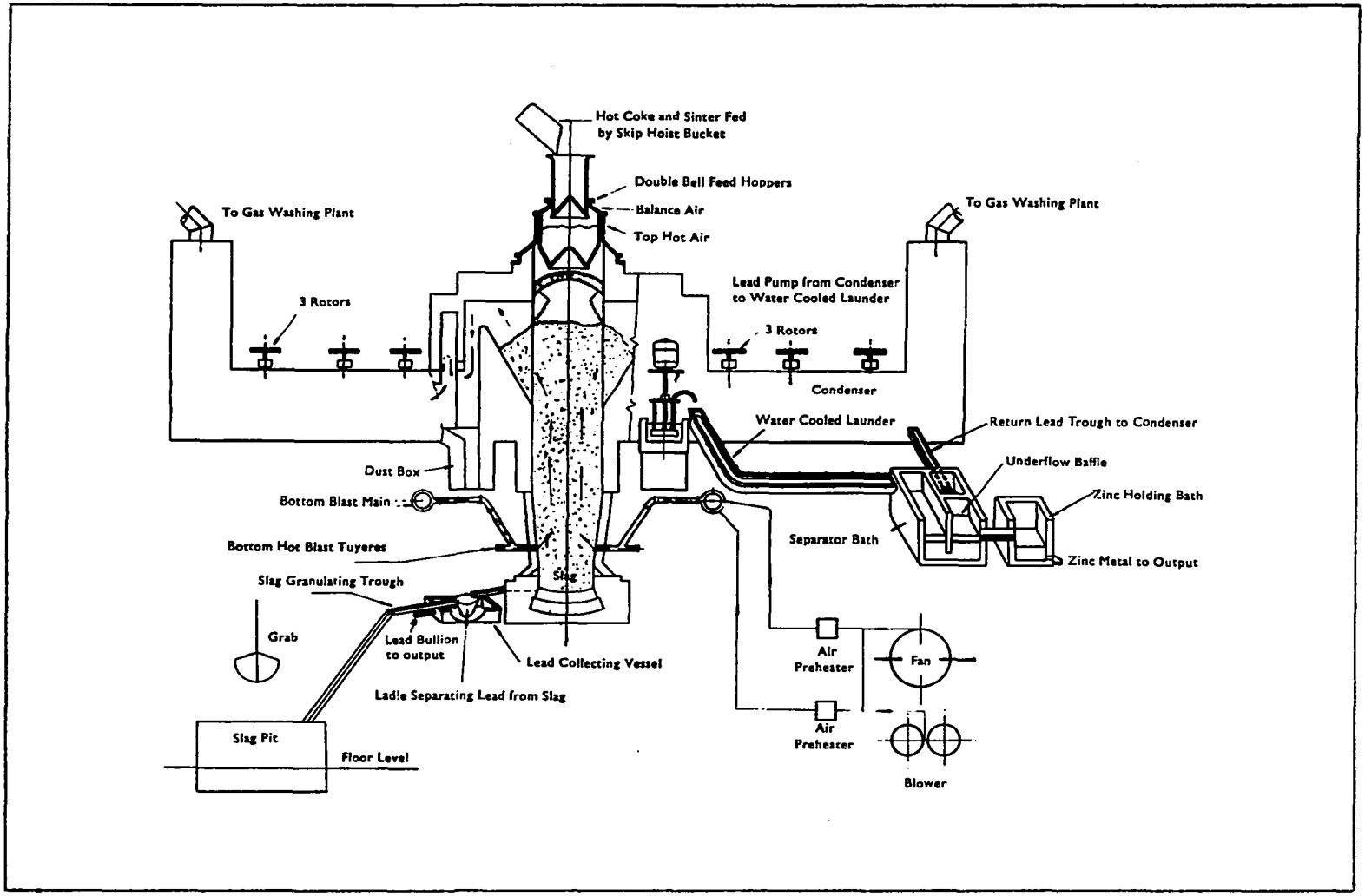

FIGURE 1.-6: Diagrammatic arrangement of zinc blast furnace.

1.6 THE LEAD SPLASH CONDENSER

The condenser used in the zinc blast furnace employs liquid lead as the absorbing medium. In all other respects, it is identical to the zinc splash condenser.

In the case of the lead condenser, the zinc vapour condenses and is absorbed in the lead. Subsequent water cooling of the resultant zinc-lead solution causes an immiscible zinc rich phase to separate and float on top of the zinc depleted lead. The zinc is skimmed off while the cooled lead is recycled to the condenser.

The zinc product (immiscible phase) contains 1 to 1 1/2 percent lead and hence almost all of this product must be subsequently refined by distillation.

1.7 PRESENT WORK

Industrial practice has shown that some 400 tons of lead must be pumped through the lead splash condenser for every ton of zinc produced.[9] This would suggest that the process is very inefficient and that optimum conditions for zinc condensation have yet to be established.

The object of this work has been to investigate the important factors and mechanisms that determine the kinetics and efficiency of zinc condensation on liquid lead and to suggest methods for improving the industrial processes.

The experimental programme consisted specifically of condensing zinc from various zinc-argon gas mixtures into liquid lead. The variables considered were lead bath temperature, zinc-in-gas concentration, gas flowrate, and condenser configuration.

CHAPTER II

THEORY OF THE PROCESSES AND PREVIOUS WORK

2.1 GENERAL

This chapter deals with the enthalpy, equilibrium, and kinetic aspects of:

a) the reduction of zinc oxide in retorts and the zinc blast furnace;

b) the condensation of zinc from the exit gases from reduction processes.

These processes are considered only in terms of zinc and the role of other metals (e.g., lead, cadmium) and other ore constituents are presented only when they significantly influence the reduction or condensation of zinc.

2.2 ENTHALPY CONSIDERATIONS OF ZINC REDUCTION

Reduction of ZnO in a retort furnace takes place by the reactions:[1]

$$ZnO_{(s)} + CO_{(g)} = CO_{2(g)} + Zn_{(v)} \qquad \Delta H^{o}_{1400^{o}K} = +43,850 \text{ cals}^{10} \qquad 2.-1$$

$$CO_{2(g)} + C_{(s)} = 2CO_{(g)} \qquad \Delta H^{o}_{1400^{o}K} = +39,600 \text{ cals}^{10} \qquad 2.-2$$

The process must be carried out at high temperature as the CO regeneration reaction (2.-2) becomes slow below about 900°C,[11] the exact temperature depending upon the surface characteristics of the carbon.

The initial production of CO_2 in the retort is by the reaction of residual air (oxygen) with the carbon.

The gases exiting from the retort are almost free of CO_2 (less than 1% CO_2)[12] so that the overall reaction for the retort process may be written:

$$ZnO_{(s)} + C_{(s)} = CO_{(g)} + Zn_{(v)} \qquad \Delta H^{o}_{1400^{o}K} = +83,450 \text{ cals}^{10} \qquad 2.-3$$

In fact it is doubtful whether this reaction contributes significantly to the reduction process due to the slow nature of the solid-solid reaction involved.[1]

It can be seen, however, that the net enthalpy deficiency for the process is very large, +83,450 calories per mole of zinc. In the retort processes this heat is supplied from an external furnace or by electrical resistance heating.

The reduction reactions, 2.-1 and 2.-2, are also the principal reactions of the zinc blast furnace. Two additional reactions take place in the tuyère zone where air is introduced,[8] i.e.:

$$C + \frac{1}{2}O_2 = CO \qquad \Delta H^{o}_{1400^{o}K} = -27,350 \text{ cals}^{10} \qquad 2.-4$$

$$CO + \frac{1}{2}O_2 = CO_2 \qquad \Delta H^{o}_{1400^{o}K} = -66,950 \text{ cals}^{10} \qquad 2.-5$$

The sum of these two reactions is:

$$C + O_2 = CO_2 \qquad \Delta H^{o}_{1400^{o}K} = -94,300 \text{ cals} \qquad 2.-6$$

which, as can be seen, leads to a net production of 94 Kilocalories per mole of carbon burnt. This can be compared with the overall reduction

reaction 2.-3 which was shown to consume 83,450 cals per mole of zinc.

Thus, the combustion of carbon particularly to CO_2 inside the furnace is an efficient way of providing heat for the endothermic reduction reactions.

The essential differences between the retort and the zinc blast furnace processes are:

1) the external supply of heat for the retort compared with the internal supply of heat by carbon combustion for the blast furnace;
2) the very low (less than 1%) concentration of CO_2 in the retort furnace exit gases compared with the considerable CO_2 concentration (11-13%)[13] in the zinc blast furnace gases.

2.3 THERMODYNAMICS OF ZINC PRODUCTION

As the above discussion has shown, the most important reaction in pyrometallurgical zinc production is reaction 2.-1:

$$ZnO_{(s)} + CO_{(g)} = CO_{2(g)} + Zn_{(v)}$$

The free energy of this reaction 2.-1, has been measured directly by Truesdale and Waring.[14] It has also been calculated from the free energy of formation data for CO and CO_2 which are well established experimentally[10] and from the free energy of formation data for ZnO as measured by several investigators.[15, 16] Table 2.A shows free energy data at various temperatures for reaction 2.-1. Values for the standard free energy of zinc oxide formation are also included.

TABLE 2.A

FREE ENERGY OF REACTION 2.-1 AND FREE ENERGY OF FORMATION OF ZnO

T°C	ΔG_T^o ZnO[15]	ΔG_T^o of reaction 2.-1 calculated	ΔG_T^o of reaction 2.-1 measured[14]
800	-59200	13900	
900	-54100	10800	11,400
1000	-48900	7800	8,600
1100			5,900

The free energy values used in all the calculation reported in this thesis were calculated from the linear free energy relations of Coughlin:[17] $\Delta G_T^o = 42,640-26.64T$. ΔG_T^o values, calculated from the Coughlin equation, lie within ± 600 calories of measured and calculated values.

Table 2.B gives values of ΔG_T^o of reaction 2.-1 for various temperatures and the calculated equilibrium constant (K) values for various temperatures. The importance of high reduction temperature for producing zinc at a high partial pressure is readily seen.

TABLE 2.B

FREE ENERGY AND EQUILIBRIUM CONSTANT OF REACTION 2.-1

T, °K	ΔG_T^o cals/mole	$K = \frac{P_{Zn} \cdot P_{CO_2}}{P_{CO}}$
700	24,000	3.10×10^{-7}
800	21,300	1.47×10^{-6}
900	18,700	2.9×10^{-5}
1000	16,000	3.2×10^{-4}
1100	13,300	2.25×10^{-3}
1200	10,700	1.15×10^{-2}
1300	8,000	4.51×10^{-2}
1400	5,300	1.47×10^{-1}
1500	2,700	4.07×10^{-1}

2.4 APPROACH TO EQUILIBRIUM CONDITIONS DURING ZINC PRODUCTION

a) Retorts

From the chemical equilibrium point of view, a retort is a system comprised of ZnO, C, Zn, CO, and CO_2.* There are two independent reactions between these species which are:[18]

$$ZnO + CO = Zn + CO_2$$

$$CO_2 + C = 2CO$$

while three phases are present: solid carbon, solid zinc oxide, and a gas phase. Since all the oxygen (as CO and CO_2) in the gas phase comes from the zinc oxide in the charge, there is an additional stoichiometric restriction which is:

$$P_{Zn} = P_{CO} + 2P_{CO_2} \qquad 2.-7$$

Application of the phase rule shows that the system is univariant, i.e., at a given temperature there is one total pressure value at which the system comes to equilibrium. At 1200°C this equilibrium pressure would be 24 atmospheres. In fact, the retorts are operated at virtually 1 atmosphere of pressure so that the system must be considerably out of equilibrium. Interestingly, P_{Zn} at equilibrium would be 6.5 atmospheres (1200°C) and a liquid zinc product would be obtained in the retort.

Under industrial conditions retorts are operated with an excess of carbon (i.e., 20-40% carbon by weight remains in the solid residue[1])

---

*P_{O_2} will be very small under these highly reducing conditions, and hence has been neglected in the calculations.

and the CO regeneration reaction

$$CO_2 + C = 2CO \qquad 2.-2$$

is virtually at equilibrium (i.e., 55% CO, less than 1% CO_2 in the exit gases).

Reaction 2.-1 is far out of equilibrium, the value of P_{Zn} being related to the values of P_{CO} and P_{CO_2} according to the stoichiometric equation 2.-7. In practice P_{Zn} = .45 atm P_{CO} = .55 atm, P_{CO_2} = .01 atm. The slightly high value of P_{CO} in excess of that predicted by stoichiometry is due to the reduction of iron oxide and other easily reduced oxides in the retort charge.

b) Zinc Blast Furnace

Conditions in the zinc blast furnace can be analyzed similarly to the retort process. Neglecting nitrogen as an inert species, there are five reactive species present in the furnace: C, ZnO, CO, CO_2, Zn. The oxygen which enters the system at the tuyères zone can be neglected as P_{O_2} is very low (10^{-17} atmospheres) above the tuyère zone of the furnace. As in the retort case, the two independent reactions may be written:

$$ZnO_{(s)} + CO_{(g)} = CO_{2_{(g)}} + Zn_{(v)} \qquad 2.-1$$

$$CO_{2_{(g)}} + C_{(s)} = 2CO_{(g)} \qquad 2.-2$$

In addition, there is a stoichiometric restriction in the system which can be expressed as follows:

$$n_{CO} + 2n_{CO_2} - n_{Zn} = n_{O_2}$$

where n_{O_2} = the number of moles of O_2 initially added to the system as air. According to the phase rule, the system is univariant, i.e., for every temperature there is one total pressure value for which the system can be at equilibrium. This value depends on the amount of oxygen initially introduced.

In practice, reaction 2.-1 approaches equilibrium but the CO regeneration reaction rate 2.-2 is slow at the charge level temperature (800°C) near the top of the furnace.

In practice the temperature of the gases leaving the furnace is raised from 800 to 1050°C by blasting air in above the charge level. This has the effect of oxidizing some CO, some $Zn_{(v)}$ and of supplying considerable reaction heat to the gases. The net purpose of the "top air" addition is to raise the gas temperature just prior to its entry to the condenser.

The gases leaving the furnace (1050°C) have a P_{CO}/P_{CO_2} ratio of 2.1[13] as compared with the equilibrium value of 1.4 for the reduction reaction 2.-1.

2.5 THERMODYNAMICS OF ZINC VAPOUR CONDENSATION

As shown in the previous sections, an important difference between the zinc blast furnace and the retort furnace processes is the much higher amount of CO_2 in the exit gases of the blast furnace. Table 2.C shows typical temperature and composition of the exit gases for the two processes.

TABLE 2.C

TEMPERATURE AND COMPOSITION OF ZINC FURNACES' EXHAUST GASES

	$T_{^oC}$	%CO	$\%CO_2$	$\%N_2$	%Zn
Vertical Retort[3]	1150	55	$\simeq 1.0$	0	45
Zinc Blast Furnace[13]	1050	25	12	55	8

Thus, the condensation of zinc vapour from the zinc blast furnace gases must be carried out under more oxidizing conditions than in the retort process. There is the distinct danger that zinc vapour will be oxidized to solid ZnO by the reverse of reaction 2.-1, i.e.,

$$CO_{2(g)} + Zn_{(v)} = CO_{(g)} + ZnO_{(s)} \qquad 2.-8$$

The most important problem associated with zinc condensation is how to condense the zinc vapour with a minimum of reoxidation. Reoxidation can occur in both the furnace and the condenser by reversing of the reaction 2.-1 as represented by equation 2.-8.

The degree to which the reoxidation reaction could take place to produce solid ZnO if equilibrium conditions were to be attained can be calculated from the equilibrium constant values

$$K = \frac{P_{Zn} \times P_{CO_2}}{P_{CO}}$$

given in Table 2.B. Thus, the zinc partial pressure at equilibrium with solid ZnO and a gas mixture of any given P_{CO}/P_{CO_2} ratio is given by:

TABLE 2.A

FREE ENERGY OF REACTION 2.-1 AND FREE ENERGY OF FORMATION OF ZnO

T°C	ΔG_T^o ZnO[15]	ΔG_T^o of reaction 2.-1 calculated	ΔG_T^o of reaction 2.-1 measured[14]
800	-59200	13900	
900	-54100	10800	11,400
1000	-48900	7800	8,600
1100			5,900

The free energy values used in all the calculation reported in this thesis were calculated from the linear free energy relations of Coughlin:[17] $\Delta G_T^o = 42,640-26.64T$. ΔG_T^o values, calculated from the Coughlin equation, lie within ± 600 calories of measured and calculated values.

Table 2.B gives values of ΔG_T^o of reaction 2.-1 for various temperatures and the calculated equilibrium constant (K) values for various temperatures. The importance of high reduction temperature for producing zinc at a high partial pressure is readily seen.

TABLE 2.B

FREE ENERGY AND EQUILIBRIUM CONSTANT OF REACTION 2.-1

T, °K	ΔG_T^o cals/mole	$K = \frac{P_{Zn} \cdot P_{CO_2}}{P_{CO}}$
700	24,000	3.10×10^{-7}
800	21,300	1.47×10^{-6}
900	18,700	2.9×10^{-5}
1000	16,000	3.2×10^{-4}
1100	13,300	2.25×10^{-3}
1200	10,700	1.15×10^{-2}
1300	8,000	4.51×10^{-2}
1400	5,300	1.47×10^{-1}
1500	2,700	4.07×10^{-1}
1600	16	9.95×10^{-1}

2.4 APPROACH TO EQUILIBRIUM CONDITIONS DURING ZINC PRODUCTION

a) Retorts

From the chemical equilibrium point of view, a retort is a system comprised of ZnO, C, Zn, CO, and CO_2.* There are two independent reactions between these species which are:[18]

$$ZnO + CO = Zn + CO_2$$

$$CO_2 + C = 2CO$$

while three phases are present: solid carbon, solid zinc oxide, and a gas phase. Since all the oxygen (as CO and CO_2) in the gas phase comes from the zinc oxide in the charge, there is an additional stoichiometric restriction which is:

$$P_{Zn} = P_{CO} + 2P_{CO_2} \qquad 2.-7$$

Application of the phase rule shows that the system is univariant, i.e., at a given temperature there is one total pressure value at which the system comes to equilibrium. At 1200°C this equilibrium pressure would be 24 atmospheres. In fact, the retorts are operated at virtually 1 atmosphere of pressure so that the system must be considerably out of equilibrium. Interestingly, P_{Zn} at equilibrium would be 6.5 atmospheres (1200°C) and a liquid zinc product would be obtained in the retort.

Under industrial conditions retorts are operated with an excess of carbon (i.e., 20-40% carbon by weight remains in the solid residue[1])

---

*P_{O_2} will be very small under these highly reducing conditions, and hence has been neglected in the calculations.

and the CO regeneration reaction

$$CO_2 + C = 2CO \qquad 2.-2$$

is virtually at equilibrium (i.e., 55% CO, less than 1% CO_2 in the exit gases).

Reaction 2.-1 is far out of equilibrium, the value of P_{Zn} being related to the values of P_{CO} and P_{CO_2} according to the stoichiometric equation 2.-7. In practice P_{Zn} = .45 atm P_{CO} = .55 atm, P_{CO_2} = .01 atm. The slightly high value of P_{CO} in excess of that predicted by stoichiometry is due to the reduction of iron oxide and other easily reduced oxides in the retort charge.

b) Zinc Blast Furnace

Conditions in the zinc blast furnace can be analyzed similarly to the retort process. Neglecting nitrogen as an inert species, there are five reactive species present in the furnace: C, ZnO, CO, CO_2, Zn. The oxygen which enters the system at the tuyères zone can be neglected as P_{O_2} is very low (10^{-17} atmospheres) above the tuyère zone of the furnace. As in the retort case, the two independent reactions may be written:

$$ZnO_{(s)} + CO_{(g)} = CO_{2(g)} + Zn_{(v)} \qquad 2.-1$$

$$CO_{2(g)} + C_{(s)} = 2CO_{(g)} \qquad 2.-2$$

In addition, there is a stoichiometric restriction in the system which can be expressed as follows:

$$n_{CO} + 2n_{CO_2} - n_{Zn} = n_{O_2}$$

where n_{O_2} = the number of moles of O_2 initially added to the system as air. According to the phase rule, the system is univariant, i.e., for every temperature there is one total pressure value for which the system can be at equilibrium. This value depends on the amount of oxygen initially introduced.

In practice, reaction 2.-1 approaches equilibrium but the CO regeneration reaction rate 2.-2 is slow at the charge level temperature (800°C) near the top of the furnace.

In practice the temperature of the gases leaving the furnace is raised from 800 to 1050°C by blasting air in above the charge level. This has the effect of oxidizing some CO, some $Zn_{(v)}$ and of supplying considerable reaction heat to the gases. The net purpose of the "top air" addition is to raise the gas temperature just prior to its entry to the condenser.

The gases leaving the furnace (1050°C) have a P_{CO}/P_{CO_2} ratio of 2.1[13] as compared with the equilibrium value of 1.4 for the reduction reaction 2.-1.

2.5 THERMODYNAMICS OF ZINC VAPOUR CONDENSATION

As shown in the previous sections, an important difference between the zinc blast furnace and the retort furnace processes is the much higher amount of CO_2 in the exit gases of the blast furnace. Table 2.C shows typical temperature and composition of the exit gases for the two processes.

TABLE 2.C

TEMPERATURE AND COMPOSITION OF ZINC FURNACES' EXHAUST GASES

	$T_{^oC}$	%CO	$\%CO_2$	$\%N_2$	%Zn
Vertical Retort[3]	1150	55	$\simeq 1.0$	0	45
Zinc Blast Furnace[13]	1050	25	12	55	8

Thus, the condensation of zinc vapour from the zinc blast furnace gases must be carried out under more oxidizing conditions than in the retort process. There is the distinct danger that zinc vapour will be oxidized to solid ZnO by the reverse of reaction 2.-1, i.e.,

$$CO_{2(g)} + Zn_{(v)} = CO_{(g)} + ZnO_{(s)} \qquad 2.-8$$

The most important problem associated with zinc condensation is how to condense the zinc vapour with a minimum of reoxidation. Reoxidation can occur in both the furnace and the condenser by reversing of the reaction 2.-1 as represented by equation 2.-8.

The degree to which the reoxidation reaction could take place to produce solid ZnO if equilibrium conditions were to be attained can be calculated from the equilibrium constant values

$$K = \frac{P_{Zn} \times P_{CO_2}}{P_{CO}}$$

given in Table 2.B. Thus, the zinc partial pressure at equilibrium with solid ZnO and a gas mixture of any given P_{CO}/P_{CO_2} ratio is given by:

$$P_{Zn} = \frac{P_{CO}}{P_{CO_2}} \cdot K$$

Figure 2.-1 gives a plot of the equilibrium pressure of zinc:

a) over pure zinc (line B, W, C) as a function of temperature (P^o_{Zn})

b) for the reaction:

$$Zn_{(v)} + CO_{2(g)} = CO_{(g)} + ZnO_{(s)} \qquad 2.-8$$

over solid ZnO.

In case (b), the equilibrium P_{Zn} is given as a function of the temperature and of the P_{CO}/P_{CO_2} ratio. P_{CO}/P_{CO_2} is treated as an independent variable, i.e., there is no predetermined P_{CO}/P_{CO_2} ratio for any given P_{Zn}.

Figure 2.-1 is helpful in describing condensation and reoxidation phenomena in the retort system.

2.5.1 CONDENSATION OF ZINC FROM VERTICAL RETORT GASES

a) Condensation

The retort gases contain zinc at a partial pressure of .45 atmospheres and they are at 1150°C. This point is plotted as point A on Figure 2.-1. Cooling without condensation is represented by moving leftwards along line A, B, i.e., lowering of temperature at a constant P_{Zn} of .45 atmospheres until the dew point is reached at point B.

Equilibrium condensation of zinc upon further cooling below the dew point, point B (830°C in the P_{Zn} = .45 atmospheres case), follows

the line BC with the zinc partial pressure falling with a decreased temperature to the normal condensation temperature 500°C (point C).

b) Back-oxidation

The P_{CO}/P_{CO_2} ratio in the retort gases is 55 while the P_{CO}/P_{CO_2} ratio in equilibrium with pure solid ZnO and a P_{Zn} of .45 at 1150°C is 2.5. Thus the gases leaving the retort have an excess of CO with respect to the equilibrium value and no back oxidation can take place at 1150°C.

Figure 2.-1 shows, however, that the P_{CO}/P_{CO_2} ratio in equilibrium with pure solid ZnO and a P_{Zn} of .45 atmospheres increases with decreasing temperature until at 900°C the equilibrium ratio is 55, i.e., the same as that in the retort gases. Thus cooling the gases (without condensation) has brought the P_{CO}/P_{CO_2} ratio and P_{Zn} into equilibrium with pure solid ZnO at 900°C, point D.

Note that at the dew point temperature (830°C) the P_{CO}/P_{CO_2} ratio in equilibrium with P_{Zn} = .45 and pure solid ZnO is approximately 170. This means that the retort gases cooled to this temperature contain an excess of CO_2 and the back oxidation reaction is favoured.

Further, inspection of the condensation line BC shows that during condensation, i.e., cooling to 500°C, the normal operating temperature of the condenser, the P_{CO}/P_{CO_2} ratio in equilibrium with pure ZnO and the equilibrium P_{Zn} over pure liquid zinc increases until at 500°C the equilibrium P_{CO}/P_{CO_2} ratio is 3000. Thus the retort gases contain an excess of CO_2 (at a P_{CO}/P_{CO_2} ratio of 55) and back oxidation is still favoured.

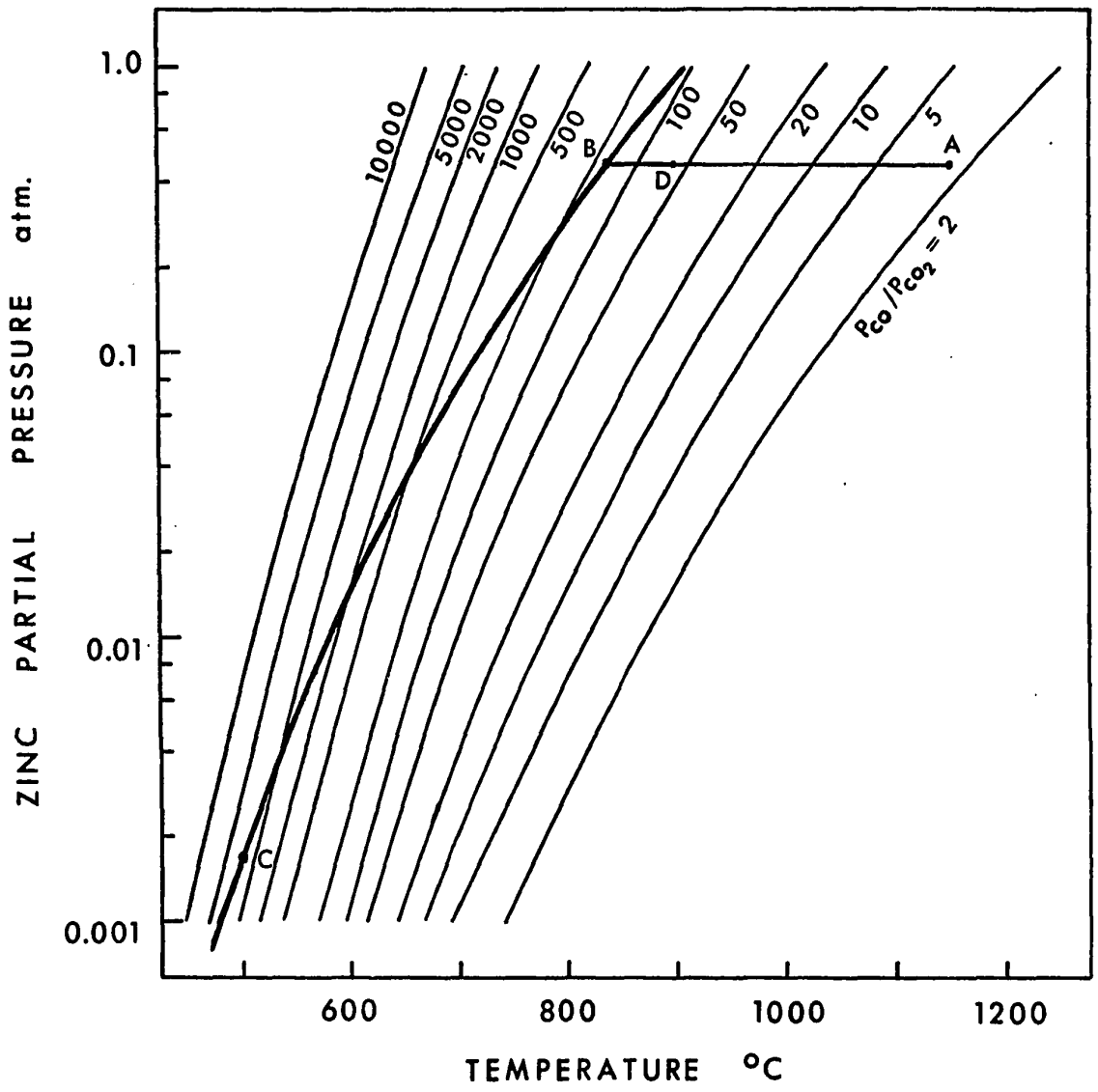

FIGURE 2.-1: Condensation of zinc vapour from vertical retort gas.

Thus cooling of the retort gases below 900°C, point D, forces the retort gases into an oxidizing position with regard to the zinc vapour in the gases.

c) Overall Effects

Stoichiometry shows, however, that since the retort gas composition is 45 vol. % Zn, 55 vol. % CO, 1 vol. % CO_2, one mole of gas contains only .01 moles of CO_2 and hence only .01 moles of the zinc vapour can be oxidized.

Thus back oxidation will destroy a maximum of 2% of the zinc vapour input into the condenser.

The condenser efficiency from retort gases is usually 93% to 97% with both reoxidation and non condensation contributing to this loss (P_{Zn} over liquid zinc at 500°C = .002 atmospheres).

2.5.2 CONDENSATION OF ZINC FROM BLAST FURNACE GASES

The gas exiting from the zinc blast furnace is much higher in CO_2 than the retort gases (11% or over). The zinc pressure is lower, typically 0.08 atmospheres, while the temperature of the gas is 1050°C. This point is plotted as point S in Figure 2.-2.

Figure 2.-2 is similar to Figure 2.-1 with the exception that the zinc vapour pressure curve (line U T) represents the equilibrium pressure of zinc over a 2.25 weight percent zinc-in-lead alloy, where the 2.25 percent zinc is typical of the coolant alloy as it leaves the lead splash condenser.

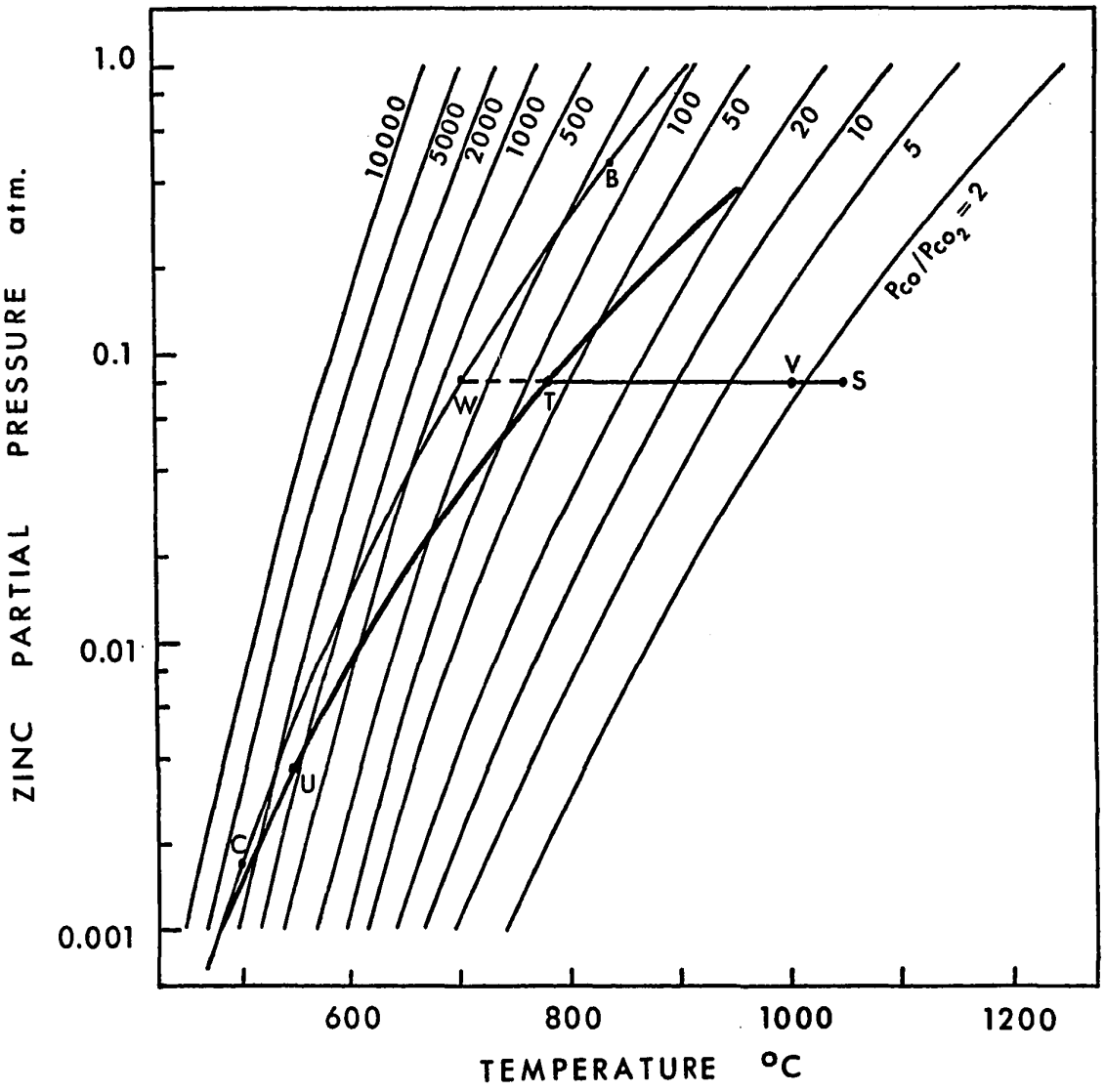

FIGURE 2.-2: Condensation of zinc vapour from zinc blast furnace gas.

In this case the vapour pressure of zinc over the zinc-lead alloy has been calculated using the expression:

$$P_{Zn} = a_{Zn(\text{in alloy})} \cdot P^{o}_{Zn(\text{over pure zinc})}$$

where a_{Zn} activity of zinc in the zinc-in-lead alloy as calculated from the zinc partial excess free energy of mixing expression as reported by Hultgren.[19]

a) Cooling Without Oxidation

Cooling without condensation of gas S is represented by moving along line S T, i.e., lowering of temperature at a constant zinc pressure of P_{Zn} = 0.08 atmospheres. Because the zinc is at less than unit activity condensation and absorption in liquid lead can occur at point T (780°C) which is a higher temperature than the dew point temperature, point W (700°C), over pure liquid zinc. Equilibrium condensation of zinc upon further cooling below 780°C (point T) follows line T U, showing the fall of the equilibrium zinc partial pressure with temperature to the normal splash condenser temperature of 550°C (point U).

b) Back-oxidation

The P_{CO}/P_{CO_2} ratio in the blast furnace gases is 2.1 while the P_{CO}/P_{CO_2} ratio in equilibrium with pure solid ZnO and a P_{Zn} of .08 atmospheres at 1050°C is 1.4. Thus the furnace gases contain a slight excess of CO at 1050°C and back oxidation is not favoured.

Figure 2.-2 shows, however, that the P_{CO}/P_{CO_2} ratio in equilibrium with pure solid ZnO and a P_{Zn} of .08 atmospheres increases

with decreasing temperature until at 1000°C (point V) the equilibrium P_{CO}/P_{CO_2} ratio is 2.1, i.e., the same as that in the blast furnace exit gases. Thus cooling the furnace gases without condensation has brought the P_{CO}/P_{CO_2} ratio and P_{Zn} into equilibrium with pure solid ZnO at 1000°C, point V.

Similarly to the case of the retort gases above, any cooling below 1000°C, point V, forces the furnace gases into an oxidizing position with respect to the zinc vapour, and oxidation can occur during virtually the entire condensation process.

c) Overall Effects

The composition of the blast furnace gases is typically 8% Zn, 12% CO_2, 25% CO and 55% N_2.

At the condenser temperature (550°C), back-oxidation having been permitted to occur, the P_{CO}/P_{CO_2} ratio in equilibrium with the 2.25 zinc-in-lead working alloy would be 1200. Thus, the CO_2 in the blast furnace gases clearly will tend, by back-oxidation of the zinc vapour during cooling, to bring itself to a very low level, less than .001 atmospheres.

Stoichiometry shows that 1 mole of blast furnace gas contains .08 moles of zinc and .12 moles of CO_2, so that virtually all of the zinc will be (if equilibrium is attained) back-oxidized by the CO_2 during the cooling process. It should be noted that the absorption of zinc in the working lead lowers the equilibrium CO/CO_2 ratio from 1600 (for pure zinc) to 1200 (2.25 weight percent zinc-in-lead), but that this change has

very little effect on the stoichiometry of the back-oxidation reaction.

Clearly a procedure which prevents the attainment of equilibrium conditions of the back-oxidation reaction is necessary, if liquid zinc is to be recovered.

2.5.3 SHOCK CHILLING

Industrial practice has shown that the "back oxidation" of zinc vapour during condensation of blast furnace gases can be avoided to a large degree by shock chilling of the gas with splashes of cool liquid lead and that recoveries of zinc metal from the gases are typically 88-90% for the lead splash condenser. Shock cooling is further examined in the discussion section.

2.6 THERMAL CONSIDERATIONS OF CONDENSATION

In addition to the mass transfer of zinc from the vapour to the liquid metal condensing medium, large quantities of heat must also be extracted:

a) from the furnace gases to cool the system to a suitable condensing temperature;

b) to extract the heat evolved during the condensation of the zinc vapour.

The magnitude of the heat transfer required during condensation is shown below for the vacuum-bubble condenser (vertical retort furnace) and the lead splash condenser (zinc blast furnace).

a) Vacuum-Bubble Condenser (Wheaton-Najarian)

The typical operating conditions of the vacuum-bubble condenser are given in Table 2.D.[3]

TABLE 2.D

WORKING CONDITIONS OF THE VACUUM-BUBBLE CONDENSER

	Gas temp.	Liq. Zn temp.	Gas composition CO	CO_2	Zn
Input to condenser	1150°C	500°C	54%	1.0%	45%
Output from condenser	500°C	500°C (maintained by water cooling condenser)	100%	0%	0.2%

Using the above data, an enthalpy balance gives:[10]

Heat liberated from cooling CO	5,800 cals/mole of zinc condensed
Heat liberated from cooling and condensing zinc	31,500 cals/mole of zinc condensed
TOTAL	37,300 cals/mole of zinc condensed

Thus, some 37,000 calories of heat must be absorbed by the zinc condensing medium for every mole of zinc condensed. The use of small bubbles (estimated volume 10-20 cm^3) rising along a 30 foot inclined path through liquid zinc adequately transfers the heat to the zinc.

b) Lead Splash Condenser (Zinc Blast Furnace)

The exiting gas from a zinc blast furnace is considerably less concentrated in zinc than the retort gases, with the result that a much greater amount of heat must be extracted per mole of zinc vapour. Table 2.E shows the working conditions of a typical lead splash condenser.[13]

TABLE 2.E

WORKING CONDITIONS OF THE LEAD ZINC SPLASH CONDENSER

	T_{oC} gas	T_{oC} lead	Wt % Zn in lead	Gas Composition %CO	%CO_2	%N_2	%Zn vapour gas phase
Input	1050	440	2.02	25	12	55	8
Output	450	550	2.26	28	13	59	.04

Using the above data, an enthalpy balance gives (calories per mole of zinc[10]):

Heat liberated from cooling N_2	31,700 cals
Heat liberated from cooling CO	14,650 cals
Heat liberated from cooling CO_2	11,650 cals
Heat liberated from zinc condensation and cooling	31,350 cals
Heat liberated by mixing of zinc in lead	-4,700 cals[20]
TOTAL	84,650 cals

It is interesting to note that the solution of zinc into the lead condensing medium requires some heat with the total result that heat liberated by the zinc during condensation and absorption ($\simeq$ 27,000 cals) represents 1/3 of the total heat which must be absorbed by the lead condensing medium. It can also be seen that per gram mole of zinc, the lead splash condenser must absorb some 2 1/2 times the heat absorbed by the vacuum-bubble zinc condenser operating in conjunction with a retort.

It can also be calculated that 126 moles of lead per mole of zinc produced must enter the condenser at 440°C, absorb the heat liberated from the gases and the zinc condensation, and exit at a temperature of 550°C, which is equivalent to 400 tons of lead per ton of zinc condensed. Thus, very large tonnages of lead must be pumped around the system to absorb the heat from the gases. This quantity of lead circulation could, of course, be reduced if water cooling in the condenser were employed.

2.7 THE SEPARATION OF ZINC FROM LEAD

The hot zincy lead exiting from the lead splash condenser at 550°C is cooled in water cooled launders to 440°C. This results in the removal of the heat absorbed by the lead in the condenser and the separation of zinc from lead.

The separation of zinc from lead is based on the immiscibility gap of the Zn-Pb binary system (see Figure 2.-3). Thus, at 550°C the maximum solubility of zinc in lead is 4.60 wt % while at 440°C it is 2.02 wt %.[19]

In practice the zinc-rich alloy at the condenser output is only partially saturated with zinc and it contains 2.26% zinc at 550°C (point A). By cooling to 440°C the solubility limit is reached (point B) and a zinc-rich phase containing 1.05 wt % Pb, separates and floats on top of the zincy-lead. The final zinc concentration in the lead rich phase is thus lowered to its saturation value of 2.02 wt % at 440°C (point C). The zinc yield then becomes 2.26-2.02 = .24%. From the yield it can be calculated that 400 tons of lead must be circulated to produce one ton of zinc.

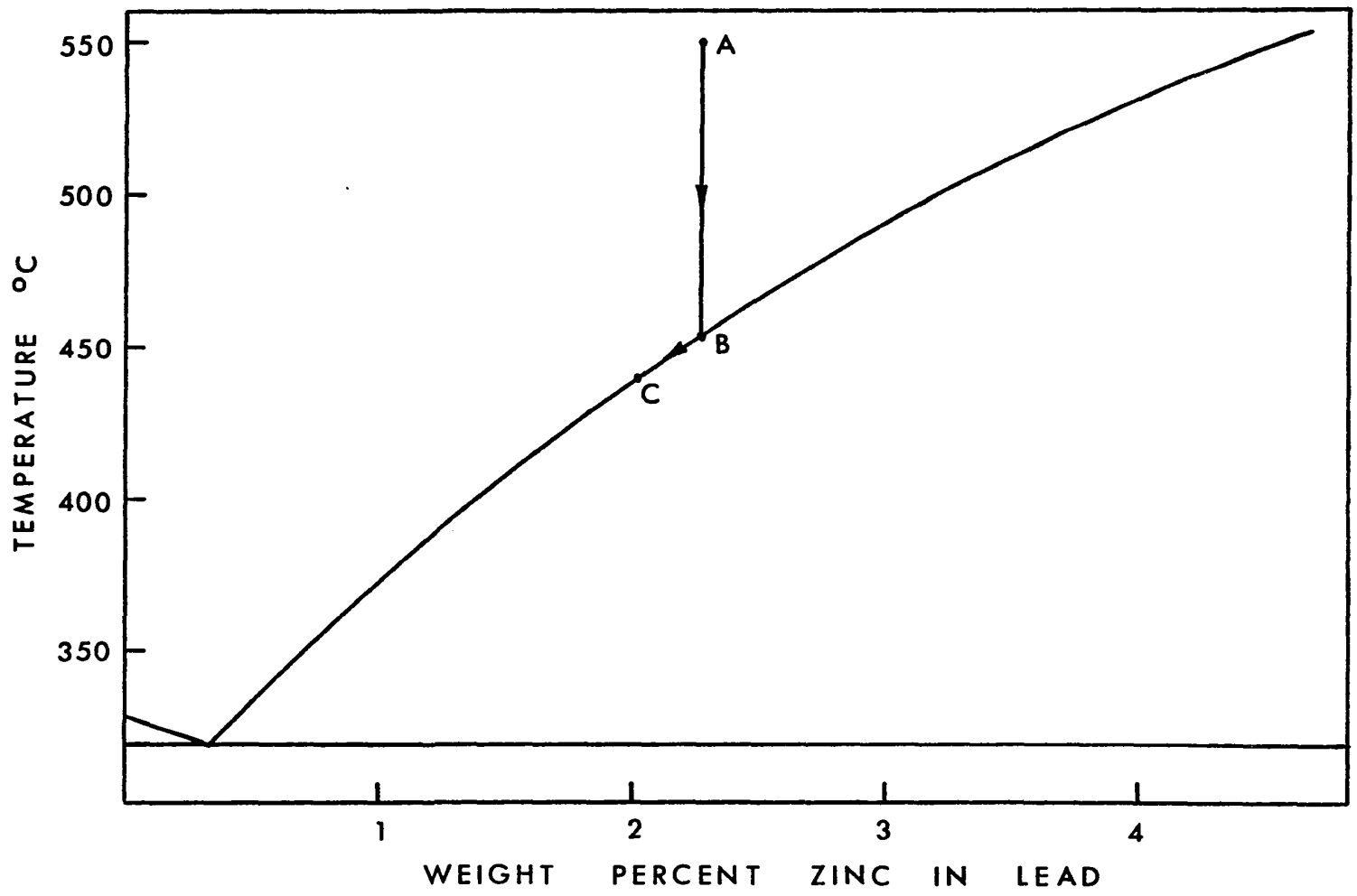

FIGURE 2.-3: The separation of zinc from lead (lead-zinc phase diagram)[19]

If maximum solubility conditions could be attained at 550°C (4.6 wt % zinc in lead), the zinc yield would be 4.6 - 2.0 = 2.6% and only 40 tons of lead would be required to produce 1 ton of zinc, which would be a marked improvement on present performance. As the enthalpy balance showed, however, cooling would have to be carried out in the condenser to make the low lead configuration work.

2.8 PREVIOUS WORK

The work of N.A. Warner[21] is the only laboratory scale study to have been carried out on zinc condensation on liquid lead. The work involved the absorption of zinc vapour by liquid lead using countercurrent gas liquid flow in a packed column. The author concluded that the rate controlling step in the absorption process was gaseous diffusion of zinc vapour to the gas-liquid lead interfaces. He suggested therefore that the phenomenon should be considered more as an absorption than a condensation process, since the term 'condensation' implies physical liquefaction of a vapour as a result of cooling.[21]

On the industrial scale, zinc condensation experiments were reported by H.K. Najarian[3] for the development of the Wheaton-Najarian Vacuum Condenser. In this work Najarian describes the first qualitative experiments which showed zinc vapour could be efficiently condensed by bubbling through liquid zinc at 500°C.

It is apparent, however, that the quantity of experimental work on zinc condensation has been limited, a condition which, in part, led to the present experimental programme.

CHAPTER III

EXPERIMENTAL

3.1 GENERAL DESCRIPTION OF EXPERIMENTS

The experimental programme was designed to measure rates and efficiencies of:

a) vapourization of pure zinc into argon gas;

b) condensation of the resultant zinc vapour into liquid lead.

The vapourization and condensation experiments were performed under dynamic gas flow conditions. The four types of experiments were:

a) vapourization of pure liquid zinc into rising argon bubbles;

b) vapourization of pure liquid zinc into rising argon bubbles and subsequent condensation of zinc vapour into liquid lead as the zinc laden gas bubbles rose through liquid lead;

c) vapourization of pure liquid zinc into a jet of argon and subsequent condensation of zinc vapour into liquid lead from a jet of zinc laden gas;

d) vapourization of pure liquid zinc into a jet of argon and subsequent condensation of zinc vapour into liquid lead from zinc laden gas bubbles.

The principal variables were gas flow configuration (bubbles or jet), flow rate of gas, lance position, and the temperature of the liquid metals.

In basic terms the experiments consisted of directing a stream of argon (as bubbles or as a jet) into liquid zinc and of directing the resultant zinc laden gas (argon as bubbles or as a jet) into a liquid lead bath.

The concentration of zinc in the gas leaving the vapourizer (entering the condenser) and the concentration of zinc in the gas leaving the condenser were measured. These measurements permitted the determination of rates and efficiencies of vapourization and of rates of condensation of zinc vapour into liquid lead.

3.2 DESCRIPTION OF APPARATUS

The main parts of the experimental apparatus were:

1) zinc vapourizer;
2) lead condenser;
3) twin sampling system: one unit for samples of the vapourizer output and a second unit for samples of the condenser output gas.

A detailed description of the main and auxiliary parts of the apparatus follows.

3.2.1 VAPOURIZER

The liquid zinc was contained in a Mullite V30 (McDanel Refractory Porcelain Co., 510 Ninth Ave., Beaver Falls, Pa. 15010, U.S.A.) crucible (1) shown in Figure 3.-1. The dimensions of the crucible were: height: 30.5 cm; inside diameter: 5 cm; outside diameter, 6 cm. The depth of the liquid zinc was 15 cm.

FIGURE 3.-1: Schematic diagram of experimental apparatus

1. Zinc crucible
2. Liquid zinc level
3. Stainless steel vapourizer vessel
4. Access vapourizer pipes
5. Vapourizer lance
6. Thermocouple probes
7. Thermocouple probes
8. Condenser stainless steel vessel
9. Lead crucible
10. Liquid lead level
11. Condenser access pipes
12. Thermocouple probes
13. Thermocouple probes
14. Piston cylinder
15. Bottom access pipe
16. Clamp
17. Connecting pipe
18. Condenser lance
19. Sampling tubes
20. Sampling tubes
21. Manifolds
22. Manifolds

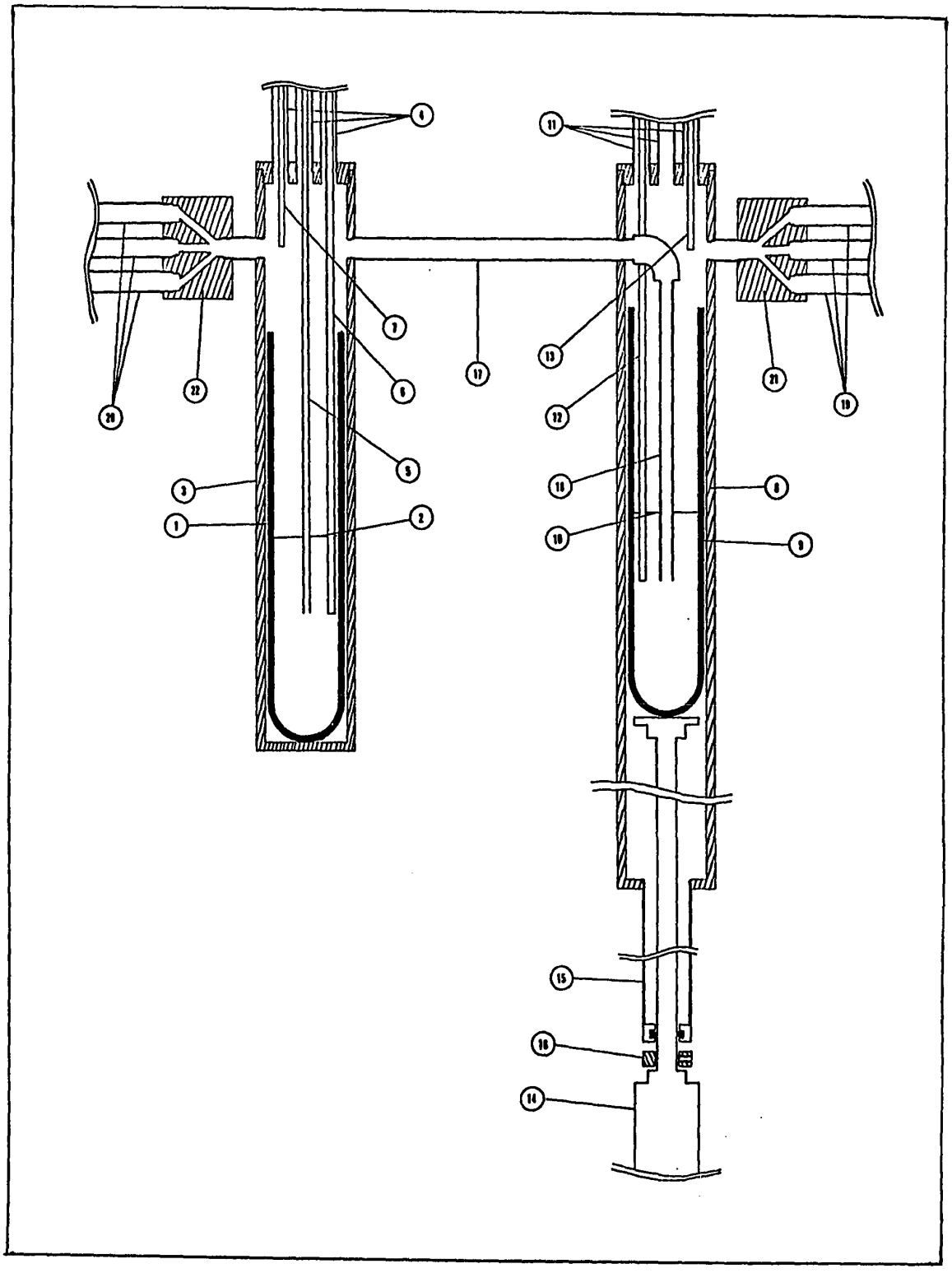
4
11
7
13
6
17
22
21
19
20
12
5
10
8
3
2
1
10
9
15
16
14

The vapourizer apparatus was made gas tight by enclosing the crucible assembly in a stainless (S.S. 304 Atlas, Atlas Alloys, 241 Hymus Blvd., Pointe Claire, Montreal, Que.) steel vessel: (3) height: 43 cm; inside diameter: 6.35 cm; outside diameter: 7.6 cm. The 304 Atlas stainless steel proved to be capable of withstanding the temperature of operation (900°C maximum) and corrosion from the zinc vapours. The bottom plate of the steel vessel was welded to the tube while the top cover was threaded to allow easy access.

Entry into the vapourizer assembly was facilitated by threading four steel (1/4" standard) pipes (4) through the top cover of the stainless steel container arranged as shown in Figure 3.-2. These pipes provided access for:

a) A blowing lance (5) (via central access pipe) through which the argon stream was introduced into the vapourizer (lance material Mullite V30, McDanel) i.d. .24 cm, o.d. .48 cm.

b) A thermocouple probe (6) (Pt-Pt 13% Rh) immersed in the liquid zinc bath.

c) A thermocouple probe (7) (Pt-Pt 13% Rh) which measured the temperature of the gases above the liquid zinc bath.

The top ends of these three steel pipes were equipped with Gyro-lock (Kirk Equipment Ltd., 375 Victoria Ave., Montreal 6, Que.) vacuum tight tube fittings with teflon ferrules. These fittings completed the gas tight nature of the vapourizer while still permitting the easy insertion and withdrawal of the argon lance and thermocouples.

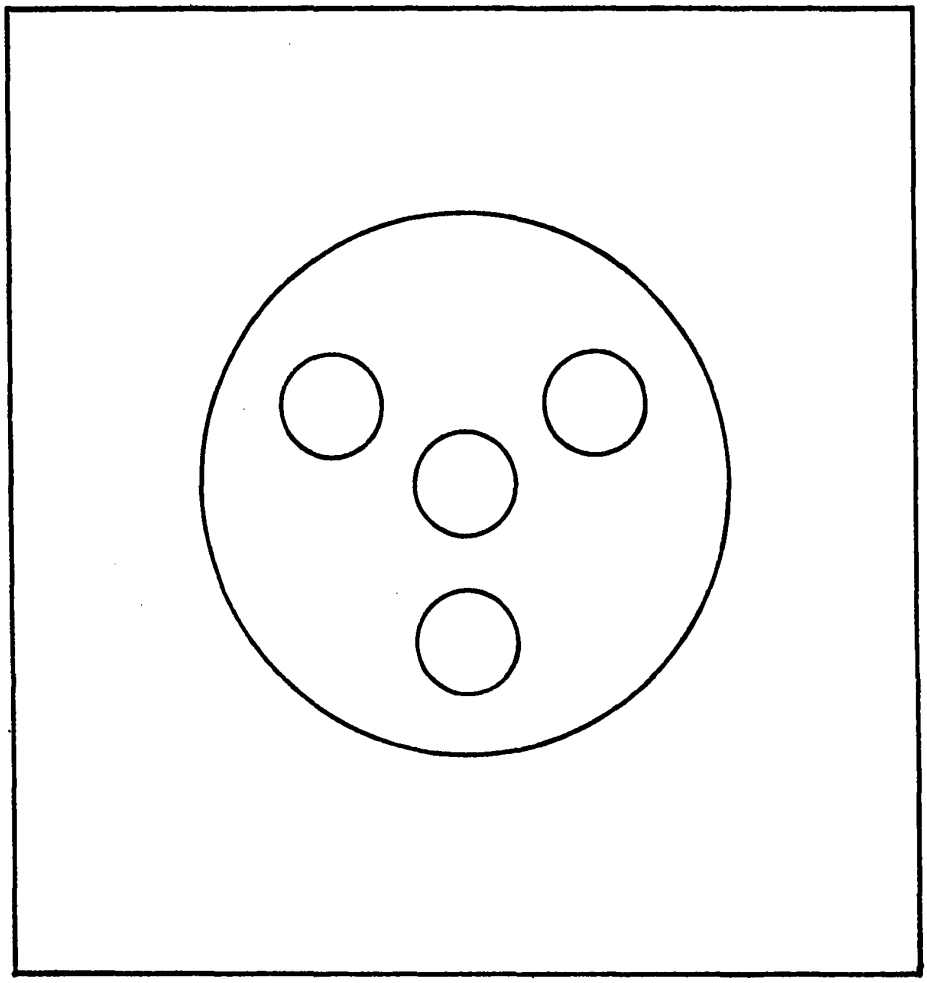

FIGURE 3.-2: Arrangement of vapourizer access pipes

The fourth pipe was used as an exhaust port during heating of the assembly. This pipe was fitted with a pressure gauge during the actual vapourization runs to measure the head pressure in the vapourizer.

3.2.2 CONDENSER

The condenser unit consisted of a Mullite crucible (9) identical to that used in the vapourizer. The crucible contained liquid lead the depth of which was approximately 15 cm. The crucible assembly was enclosed in a cylindrical stainless steel vessel (8) similar to that used in the vapourizer, 68 cm long.

The top cover, penetrated by three 1/4" standard pipes, (11) was threaded onto the stainless steel vessel. Two pipes were fitted through the cover with Gyrolock ferrules and were used for the entry of thermocouple probes (12), (13). The third pipe was used as an exhaust during heating of the assembly. It was closed with an O-ring fitting during the actual condensation experiments.

The bottom cover of the steel vessel was threaded onto the tube. It was penetrated by a 1/2" standard steel pipe (15) which provided access for a piston cylinder (14) which was used for vertical positioning of the inner mullite crucible (and lead) of the condenser assembly.

3.2.3 VAPOURIZER-CONDENSER CONNECTION

The condenser was connected to the vapourizer via a 3/8" standard stainless steel pipe (17) (S.S. Atlas 316) 20 cm long, which penetrated through the steel walls of the vapourizer and condenser vessels. The end of the connecting pipe inside the condenser was fitted via a 90^{o} bent

connector with a stainless steel (S.S. Atlas 316 1/4" standard pipe (18) directed vertically down the centre of the condenser. This vertical pipe was the condenser lance. Since this lance was immobile in the assembly, the piston arrangement described in the previous paragraph was designed to move the lead condenser bath (mullite crucible) vertically into its desired position with respect to the condenser lance.

3.2.4 THE SAMPLING SYSTEM

The sampling system consisted of a vapourizer unit (19) and a condenser unit, (20) the positions of which are shown in Figure 3.-1. Each of the sampling units consisted of 6 sampling tubes of 3/8" standard stainless steel (S.S. Atlas) pipes. Each sampling tube was operated individually so that five samples (plus a blank) could be taken during the course of each experiment.

The six sampling tubes were threaded into a manifold (3" diameter) (21), (22) which was connected opposite to the vapourizer-condense connection via a single 3/8" standard stainless steel pipe. The lengths of the sampling tubes were approximately 50 cm. Approximately 27 cm of each tube was inside the heating furnace while the remainder protruded out as shown in Figures 3.-3 and 3.-4. This arrangement ensured that:

1) no condensation of zinc vapour could occur inside the manifold or in the first 8 cm of the sampling tubes;
2) all the zinc vapour in the gas stream condensed in the cold end of the sampling tubes.

Fiberglass filters were placed inside the sampling tubes, near their outlet end, to trap the entrained zinc dust which formed in the

FIGURE 3.-3: View of the experimental furnace, temperature controllers and powerstats. The split furnace is closed as it would be during an experimental run. The sampling tubes are protruding out of the furnace.

FIGURE 3.-4: View of the experimental furnace with the split furnace open to expose the vapourizer (left) and condenser (right) vessels. The areas of varying darkness on the split of the furnace correspond to the temperature profile during operation.

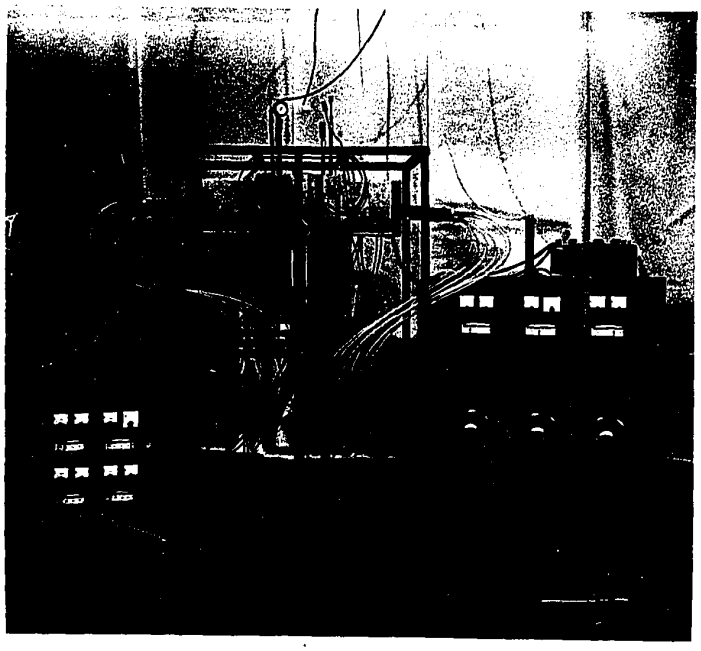

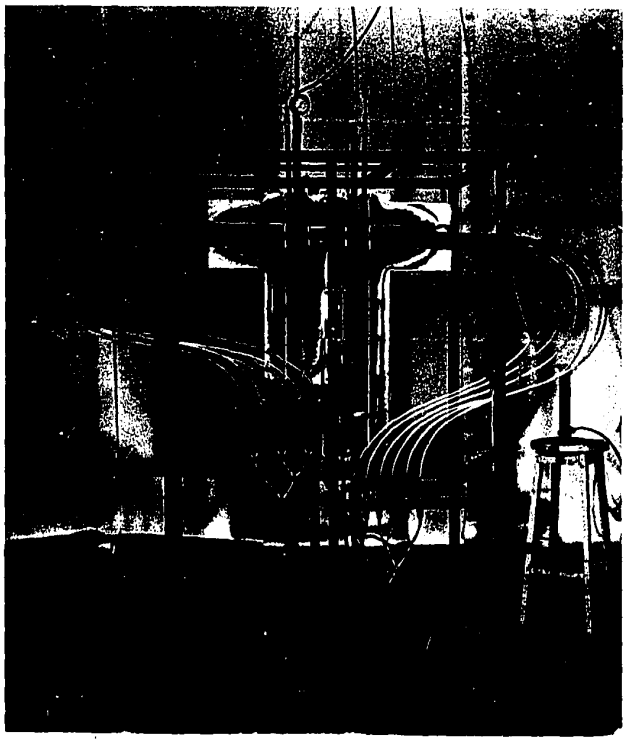

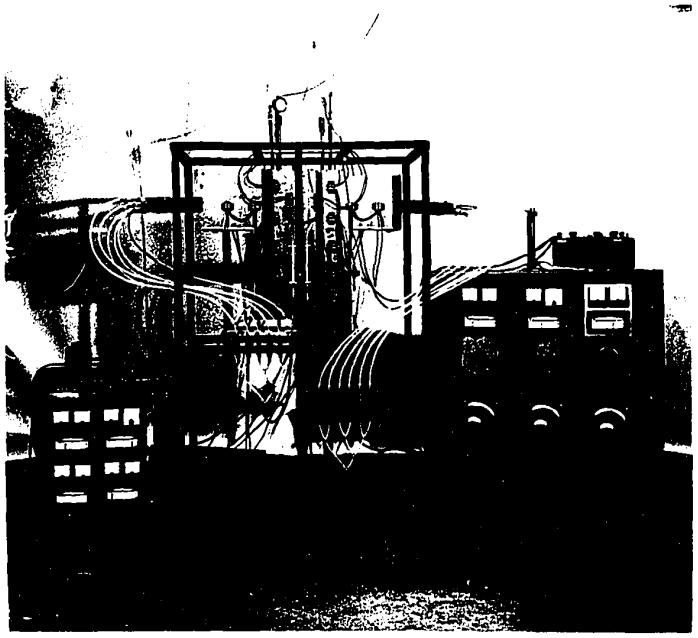

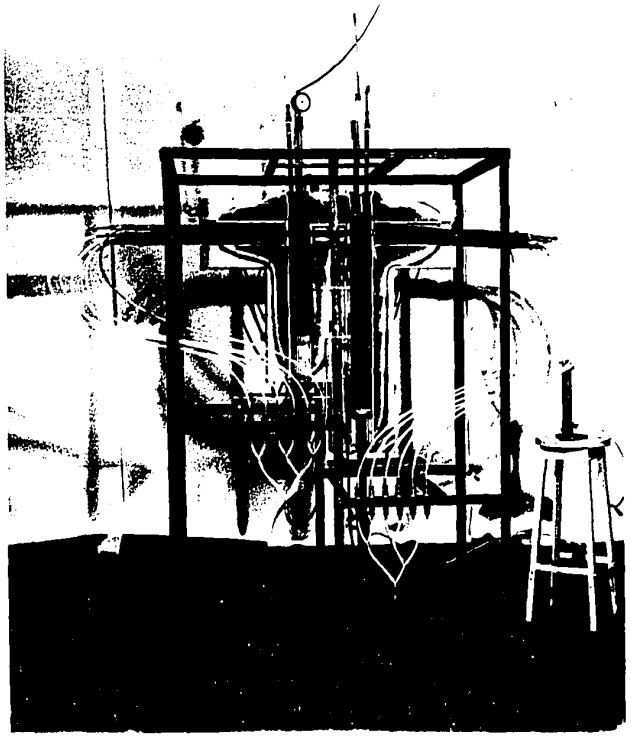

sampling tubes. The outlet end of each tube was connected via a polyethelene tube to a needle valve and finally to a rotameter type flowmeter which was used to measure the output argon flowrate. The opening and closing of the needle valves connected to the sampling tubes permitted individual operation of any chosen sampling tube.

The actual measurement in the sampling tube was the weight of zinc condensed. Measurement of the flowrate of gas through the tube and of the time the gas had been passed, permitted calculation of both the total amount of zinc in the gas and the zinc concentration (partial pressure).

It is estimated that the volume of gas through a specific sampling tube could be measured $\pm$ 10% and that the quantity of zinc could be measured $\pm$ 3% so that the overall sampling accuracies expressed as zinc-in-gas concentration were within $\pm$ 15%.

3.2.5 GAS CIRCULATION

Argon was used exclusively as the carrier gas for the zinc vapour. The input was passed at a fixed flowrate via a rotameter type flowmeter into the vapourizer system.

The zinc laden gas exiting from the vapourizer was divided into two streams: one stream was directed to the vapourizer sampling system while a second stream was directed to the condenser via the condenser lance. All of the second stream was directed finally through the condenser sampling system.

The flowrate of gas through the vapourizer sampling system was measured on the sampling system flowmeter. The flowrate through the

vapourizer sampling system was controlled by each sample tube needle valve.

3.2.6 THE HEATING SYSTEM

The vapourizer, condenser, connecting tube, and part of the sampling tubes were enclosed in an especially designed split furnace shown in Figures 3.-4, 3.-5. Each half of the split furnace was equipped with 18 semicylindrical resistance heating elements.

The elements directly opposite each other on the two sides of the split were connected in parallel.

These heating element pairs were connected to each other in such a way that the furnace was divided into seven individually controlled zones. Table 3.A shows the distribution of heating elements in each zone. Figure 3.-5 shows the wiring diagram of one side of the split.

TABLE 3.A

DISTRIBUTION OF HEATING ELEMENTS IN THE FURNACE

Section	No. of elements on each side of split	No. of elements on both sides of split
1) Vapourizer centre section	3	6
2) Vapourizer end section	2	4
3) Vapourizer sampling section	2	4
4) Connecting tube section	2	4
5) Condenser centre section	4	8
6) Condenser end section	3	6
7) Condenser sampling section	2	4
TOTAL	18	36

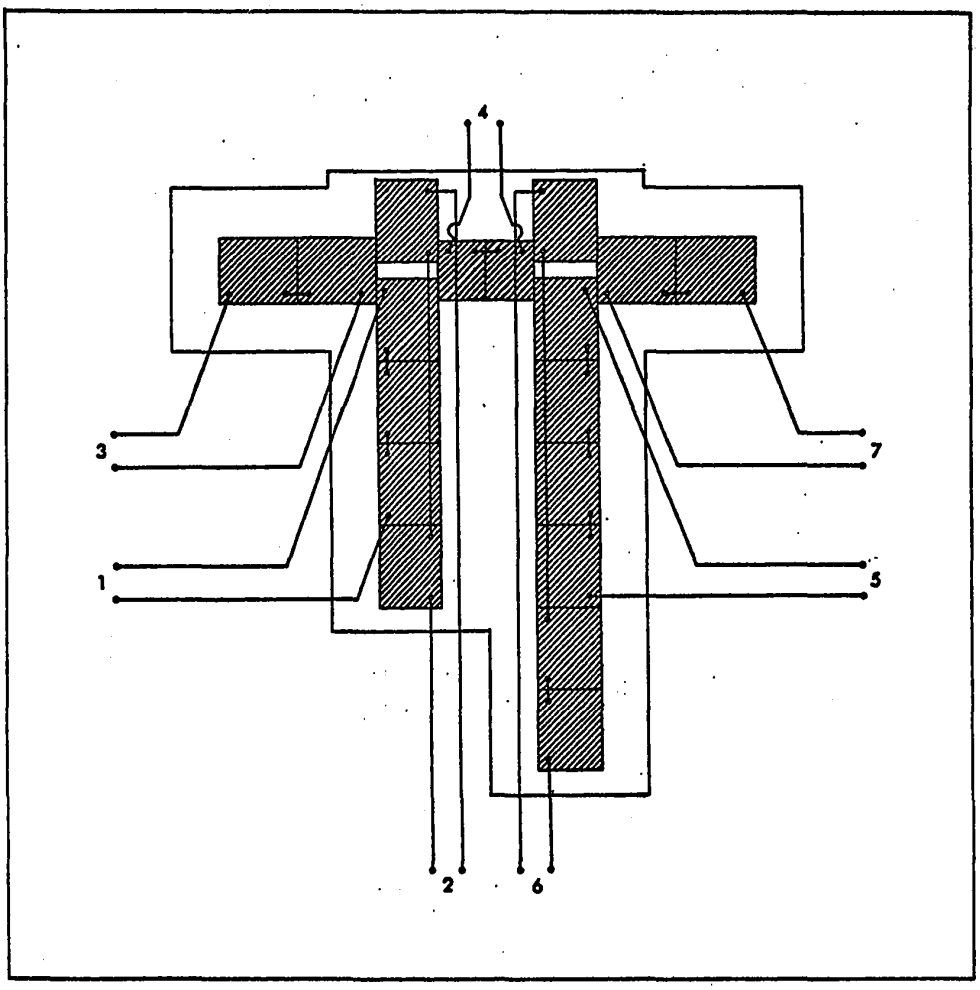

FIGURE 3.-5: Schematic and wiring diagram of one side of the furnace.

The temperatures of the various sections were regulated by controller, based on temperature reading inputs from thermocouple probes (Pt-Pt 13% Rh.) imbedded in the heating unit of each zone. A temperature control of $\pm 5^{o}C$ was obtained during furnace operation.

3.3 OPERATING PROCEDURES

3.3.1 ASSEMBLY

The basic steel assembly consisted of the vapourizer, condenser, connection tube and condenser lance, and the sample tube manifolds. These parts and the vapourizer bottom cover and condenser top cover were more or less permanently connected.

The first step in each series of experiments was to place new solid zinc in the mullite vapourizer crucible and new solid lead into the mullite condenser crucible. The zinc crucible was then placed into the steel vapourizer vessel and the vapourizer top cover was threaded on. This thread connection and all thread connections of the assembly were sealed with Sauereisen refractory cement (Fisher Scientific Co., Ltd., 8555 Devonshire Road, Montreal 301, Que.) Clean sample tubes were then threaded into sample manifolds.

At this point the vapourizer-condenser assembly was mounted into position on the furnace frame. The condenser crucible and lead were then placed inside the steel condenser vessel and the bottom cover and piston device were threaded into position.

Finally, the split heating furnace was closed and the wire connections and PVC sampling tube connections (Figure 3.-3) were completed.

3.3.2 HEATING

Heating was initiated with the input power at maximum value. A flow of argon was maintained throughout the heating period to flush the system of air and to prevent oxidation of the metals and the steel vessel. The argon was blown into the vapourizer through the vapourizer lance and into the condenser via a small lance positioned in place of one of the two condenser thermocouples. During this time the sampler needle valves were all closed while the exhaust pipes on top of both vapourizer and condenser were maintained open. This arrangement prevented the flow of gas through the sampling tubes during preheating.

Once the lead was molten, the piston cylinder was employed to push the lead crucible upwards until the condenser lance was well immersed in the lead bath. This manoeuvre blocked any gas circulation between the condenser and the vapourizer during the remainder of the preheating period.

When the temperature began to approach the desired value, the power was turned down to the appropriate level for each heating zone. The temperatures were so chosen as to ensure that the temperatures of the zones above the liquid zinc and liquid lead baths were higher by 50 to 100^{o}C than those of the corresponding liquid metal baths.

Similarly the connecting tube and the parts of the sampling tubes inside the furnace were heated to sufficient temperature to ensure that condensation would not occur except in the cold end of the sampling tubes.

3.3.3 START OF EXPERIMENT

When the desired temperatures were reached, the vapourizer lance was lowered until it touched the liquid zinc surface. This position was

detected by the vibration of the lance and the fluctuations of the gas flowmeter. The lance was then moved to the required position (as a bubbler or as a lance) and its location was fixed by the Gyrolock fitting.

The piston in the condenser assembly was then adjusted and the lead crucible was moved to the desired position. The precise position of the lead surface relative to the fixed position of the condenser lance was determined by placing a straight copper wire of known length down through one of the top lid holes, parallel to the condenser lance. A simple electric circuit was provided so that contact with the lead caused a small lamp to light, thus showing the exact position of the lead surface.

After melting and positioning, argon flows were cut off and the pressure gauge was fitted to the vapourizer exhaust valve. At the same time, the condenser thermocouple was positioned in place of the temporary argon input lance and the condenser exhaust pipe was closed.

At the start of an experimental run, the needle valve of one of the sample tubes in each of the vapourizer and condenser samples was opened, followed by the initiation of argon flow through the vapourizer lance. The relative proportions of gas flow from the vapourizer to the condenser and to the vapourizer sampling system were adjusted by means of the vapourizer sampler needle valve.

3.3.4 PROCEDURES DURING RUNNING

Each sampling tube was used for a fixed length of time (typically 10 min.). At the end of this length of time, argon flow through the lance was shut off, the two open needle valves were closed, and the

adjacent two valves were opened. Argon flow through the lance was then restarted, always within one minute of the previous argon shutoff.

During the argon blowing time, the zinc dust depositing on the sampling tube filters changed the flow resistance of the system and manipulation of the open manifold valves was required to ensure a constant ratio of gas flow distribution.

Five tubes from each sampling system were used during a complete experiment, the sixth being used as a blank to determine the presence of any zinc entering the tubes by thermal diffusion during the heating up period. Flow through the tubes was prevented by a closed needle valve at the sampler exit, but some Zn diffusion might take place into the tube via the open furnace connection. This was checked by using a 'blank' sampling tube.

3.3.5 END OF EXPERIMENT

At the end of an experiment, the power was switched off, the immersed thermocouples and lance were pulled out of the melts, and the lead crucible was slipped down to its lowest position. The pressure gauge and the seal of the exhaust pipes were removed and the system was flushed with argon in a manner identical to that followed during the heating cycle.

The furnace was allowed to cool for approximately 18 hours, at which time the assembly was dismantled. The mullite crucible and lead were removed from the condenser after each experiment and the crucible was mechanically cleaned of its zinc-lead alloy. The zinc in the vapourizer was not contaminated and thus, the vapourizer part of the assembly

was opened only every ten or so experiments to replace the evaporated zinc.

3.3.6 ANALYSIS OF SAMPLES

The actual measurements from the experiments were the weights of zinc condensed in the sampling tube, i.e., on the sampling tube walls and in the filters of the sampling tubes.

The best technique for recovering all the zinc in the sampling tubes appeared to be to place the entire sampling tube in a solvent for zinc and to measure the concentration of zinc in the known volume of solution. Thus, each sampling tube was immersed in 500 ml of 20% by volume aqueous hydrochloric acid solution in ungraduated cylinders. The tubes were left in the solution for 24 hours at room temperature. The resulting solutions were filtered into 1000 ml volumetric flasks and were made up to 1000 ml. These solutions were subsequently diluted by between five and one thousand times, depending on the weight of zinc deposited in each sampling tube. The chemical analysis was accurate for zinc concentrations up to 8 p.p.m. in solution and the above dilution range ensured that the final solutions were in the right concentration range. The dilution was done in one step for dilution ratios up to 40 and in two steps for higher dilution ratios. The dilute solutions were analyzed by the atomic absorption flame-spectrophotometry method using either:

a) Unicam S.P. 90 spectrophotometer or,

b) Perkin-Elmer 403 spectrophotometer.

The procedure of the instrumental analysis consisted of feeding a series of standard solutions (1, 2, 4, 6, 8, 10 p.p.m. for the Unicam unit and .5, 1, 2, 3 p.p.m. for the Perkin-Elmer unit) to calibrate the apparatus, followed by feeding the series of sample solutions. The sample solutions' concentrations were deduced by comparison of the light absorbance readings to the calibration curve.

The standard solutions were made by dilution from a master zinc aqueous 1000 p.p.m. solution (Hartman-Leddon Co., Philadelphia, U.S.A.). These solutions were checked versus a master .1M solution made by dissolution of an exactly weighed amount of pure zinc metal (Fisher Scientific Co., Ltd.) and the agreement proved to be within 1%. The standard solutions were replaced every week to avoid any alteration with time.

3.4 EXPERIMENTAL RESULTS

As described in section 3.1, the principal experiments were either simple vapourization experiments or integrated vapourization and condensation experiments. Since the vapourization and condensation processes were operated independently of each other, the experimental results are classified in two sections: vapourization results and condensation results. These sections are further subdivided into results of bubbling and jetting configuration experiments. All experimental results are tabulated in Appendix A.

3.4.1 VAPOURIZATION RESULTS

The basic experimental results of vapourization are reported in the form of zinc concentration in the output gas (g cm^{-3} and mole fraction). The variables investigated were:

a) method of argon introduction: bubbling or jetting;

b) temperature of the zinc bath;

c) argon flowrate.

3.4.2 VAPOURIZATION INTO ARGON BUBBLES

Seventeen experiments were performed involving vapourization of pure liquid zinc into argon gas bubbles rising through the zinc. Eleven were simple vapourization experiments, while the other six were part of integrated vapourization-condensation experiments. The experiments were designed to:

a) investigate the feasibility of producing a steady stream of gas carrying zinc vapour at a desired concentration which could be subsequently used in condensation tests;

b) investigate the dependence of the zinc-in-gas concentration upon zinc bath temperature;

c) determine the rate controlling mechanisms of zinc vapourization into gas bubbles.

Figure 3.-6 shows a typical plot of the experimental vapourization results. The zinc vapour concentration in the gas stream, expressed in grams of zinc per cm^3 of argon gas (measured at 1 atmosphere pressure, $0^{o}C$) is plotted versus the time of blowing through each

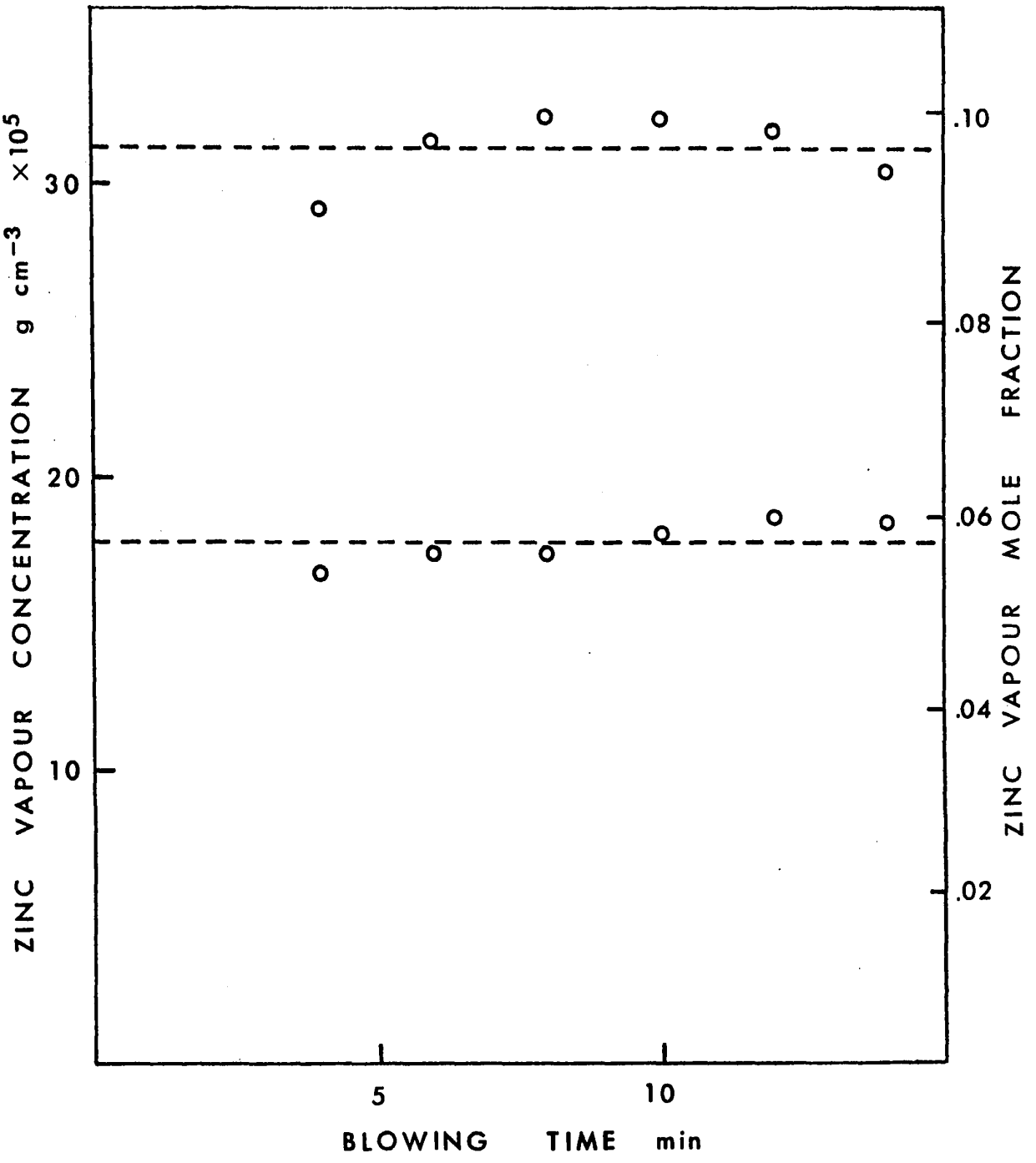

FIGURE 3.-6: Typical vapourization results (bubbling)

sampling tube. The scale on the right hand side of the graph shows the zinc vapour concentration expressed as zinc mole fraction in the gas stream. Each point corresponds to the analysis of a single sample tube and represents the time at the end of each sample blow (from time = 0).

It can be seen that a stream of gas with a steady zinc vapour concentration was produced. The maximum fluctuation of the measured values for the two experiments represented in Figure 3.-6 about the mean value was ± 7% of the average value. The typical fluctuation for most of the vapourization experiments was less than ± 25%, while for four of the experiments it was between 30-55%. The latter high fluctuation of the experimental values could not be explained in terms of the experimental errors involved and it is believed that the scatter was due to splashes of liquid zinc being ejected into the higher temperature region of the vapourizer. This splashing would result in unexpectedly high zinc vapour concentrations in the gas phase.

Figure 3.-7 shows the average zinc concentration values for each experiment plotted versus zinc bath temperature. This figure shows that, almost certainly due to an increased equilibrium vapour pressure with temperature, the zinc-in-gas concentration increases markedly with bath temperature. Thus a desired zinc concentration can be achieved by varying of the temperature of the zinc bath. This finding was used in subsequent condensation experiments in which the desired high zinc vapour concentrations were obtained by raising the temperature of the vapourizer.

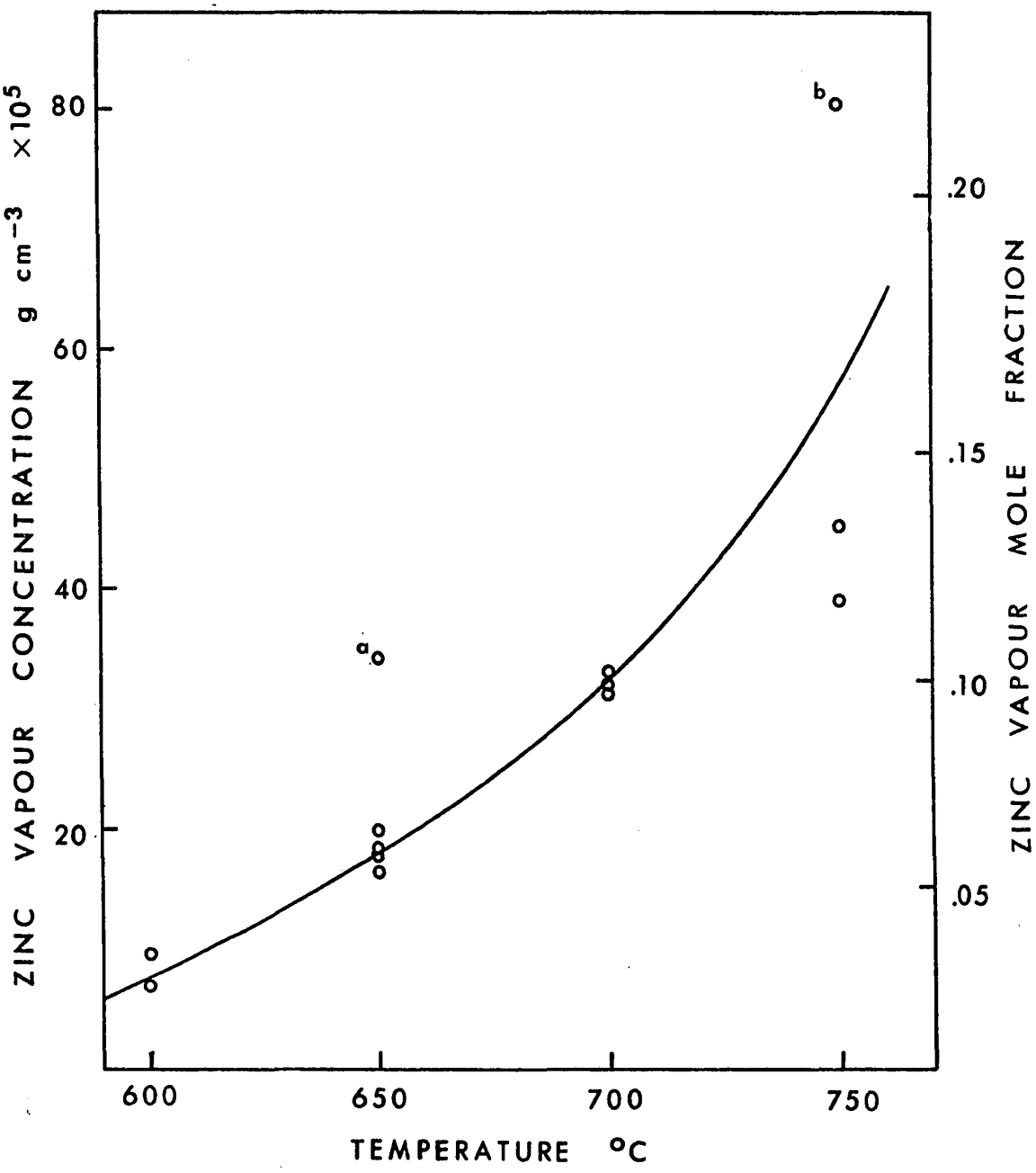

FIGURE 3.-7: Zinc vapourization results (bubbling)

Figure 3.-7 shows also that the reproducibility of the zinc in gas concentration is quite good but shows some wide scatter especially at the highest temperature (750°C). Thus the reproducibility of the vapourization results indicated the potential usefulness of this vapourization method for providing gas streams of desired zinc concentrations. It is believed that the very high values of zinc vapour concentration (points a, b Fig. 3.-7) is due to the splashing effect as was mentioned above. An attempt to avoid this effect was made by adopting the jetting vapourization method which was used in the later experiments.

Figure 3.-8 summarizes the experimental rates of vapourization of zinc from the zinc bath into argon bubbles. The vapourization rates are plotted as zinc g-moles sec^{-1} versus liquid zinc temperature. As the argon flowrates were constant for all experiments, the vapourization rate curve has the same form as the zinc-in-gas concentration curve and shows the same temperature dependence.

3.4.3 VAPOURIZATION INTO AN ARGON GAS JET

Thirteen experiments were performed in which zinc was vapourized from a pure liquid zinc bath into an argon gas jet. All tests were part of an integrated vapourization-condensation experimental programme. The condensation parts of the experiments involved condensation of zinc vapour on liquid lead from an argon-zinc gas jet while the other four experiments involved condensation of zinc vapour from zinc-laden argon bubbles rising in liquid lead.

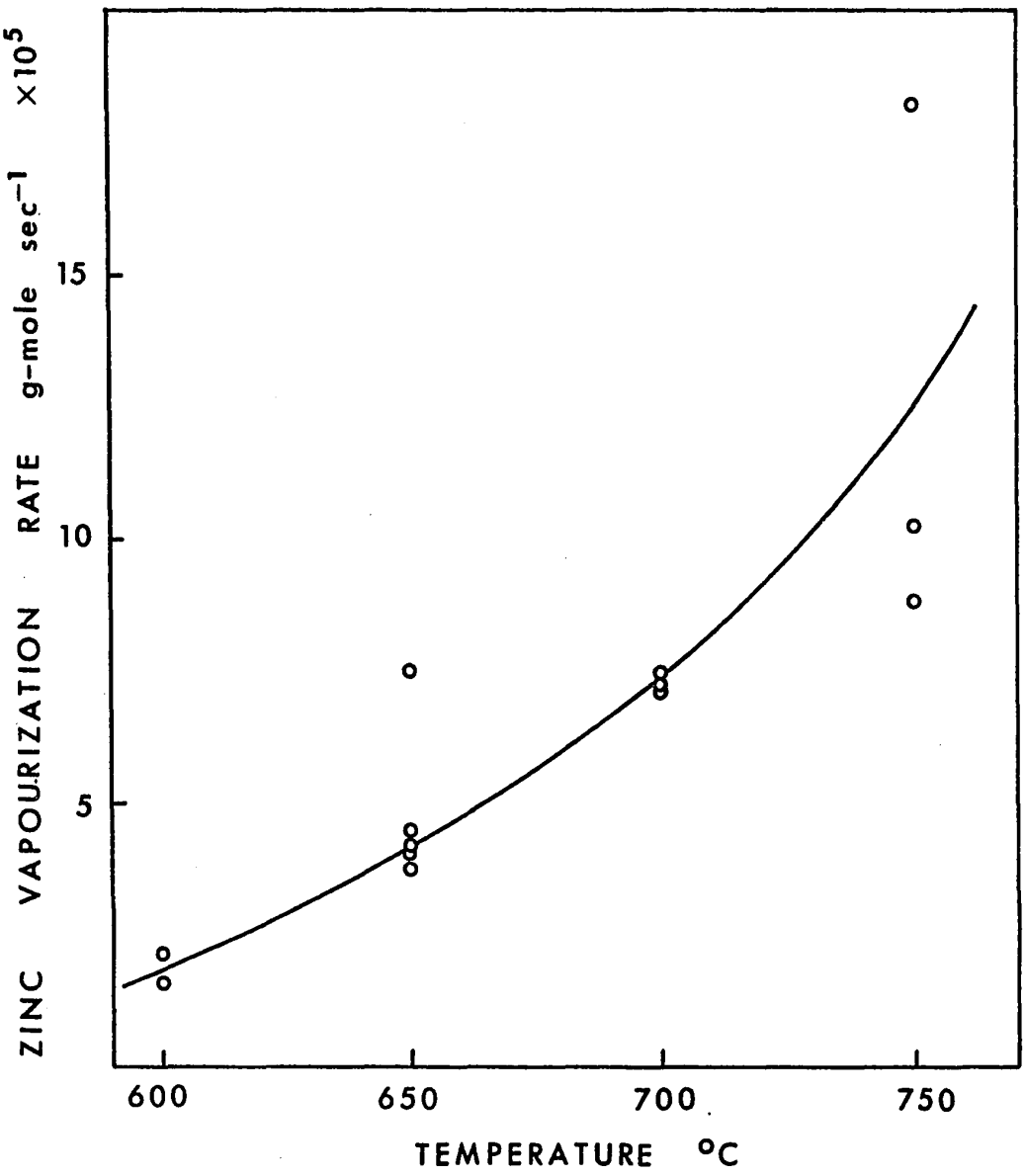

FIGURE 3.-8: Zinc vapourization rates (bubbling)

Vapourization into jet experiments were designed to:

a) investigate the feasibility of reproducing a steady stream of argon gas carrying zinc vapour at a concentration which would be suitable for the condensation experiments, i.e., to improve upon the bubbling vapourization performance;

b) investigate the dependence of the zinc vapour concentration in the gas stream on the zinc bath temperature;

c) investigate the dependence of the zinc vapour concentration in the gas stream on the argon gas flowrate;

d) determine the rate controlling mechanisms of zinc vapourization into an argon jet.

Figure 3.-9 shows a typical plot of the experimental results of jetting experiments. The zinc vapour concentration expressed in grams of zinc per cm^3 of pure argon gas (1 atmosphere pressure, 0^oC) and mole fraction of zinc is plotted versus vapourization time. Each point corresponds to the analysis of a single sample tube while the arrows indicate the time each sample tube was employed. The dashed lines indicate the time average of zinc concentration over an entire experiment.

It can be readily seen that the zinc vapour concentrations in the gas streams were steady throughout the experimental runs. Thus, the jetting vapourization configuration also proved to be a suitable technique for the production of a steady stream of zinc laden gas with a constant concentration of zinc vapour. The fluctuation of the zinc vapour concentration values about the mean value for the two experiments reported in Figure 3.-9 was $\pm$ 5% while it was within $\pm$ 20% for most of the

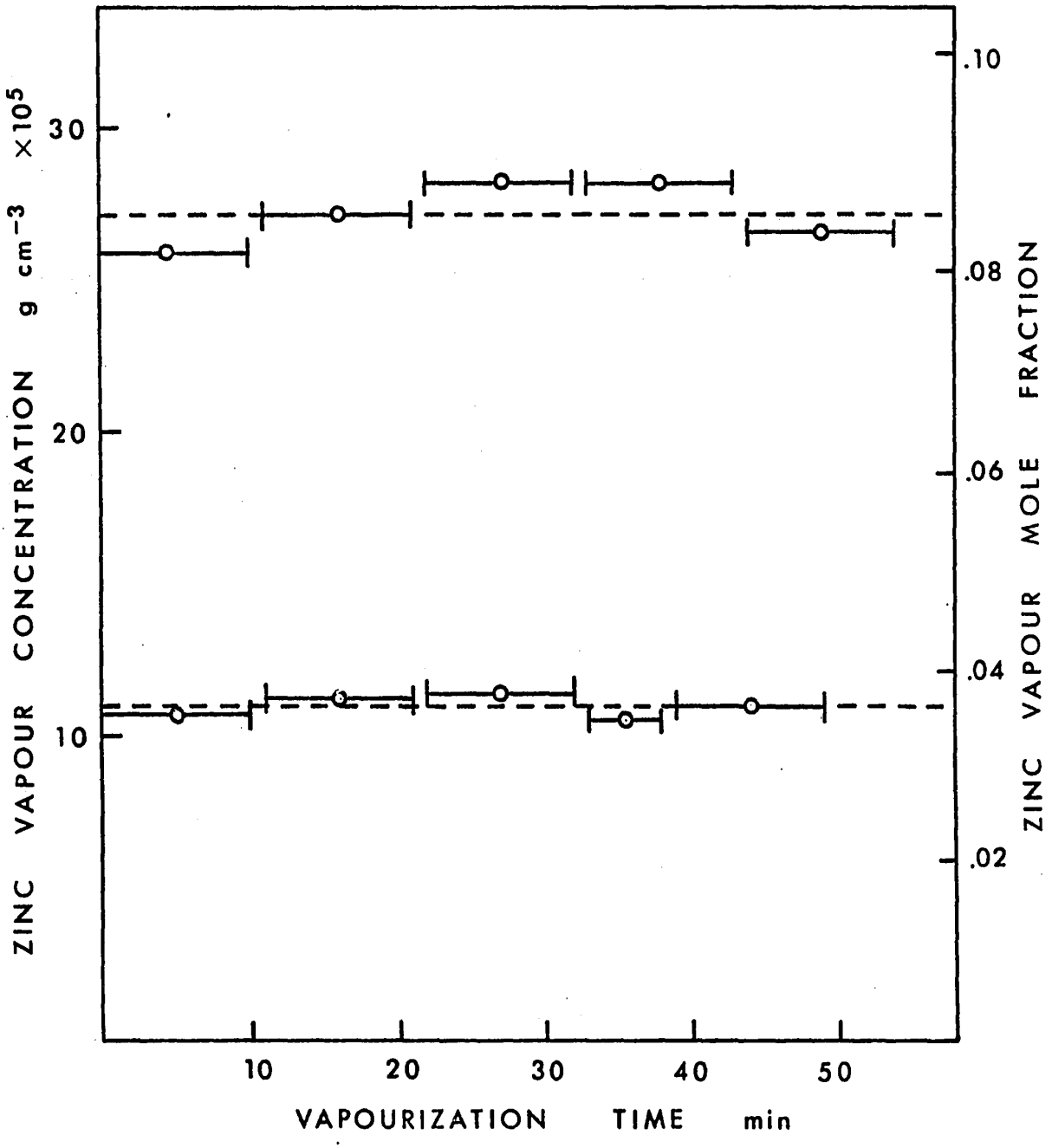

FIGURE 3.-9: Typical vapourization results (jetting).

experiments.

It was found, during the course of the experiments, that unsteady zinc-in-gas concentrations were always obtained in experiments which immediately followed meltdown of new zinc. A typical curve is shown in Figure 3.-10 showing high initial zinc in gas concentration falling off with time. This behaviour indicates the splashing and adherence of zinc droplets on the walls of hotter regions of the apparatus during meltdown. Steady results were obtained after sixty minutes of jetting following initial meltdown.

A similar problem was encountered during jetting experiments which followed vapourization into argon bubble experiments.

The dependence of zinc vapour concentration on the temperature of the liquid zinc bath and on the argon gas flowrate is illustrated in Figure 3.-11 in which average zinc vapour concentration values are plotted versus liquid zinc bath temperature. The experimental gas zinc concentration values show a scatter in the order of $\pm$ 20% between comparable experiments. A trend towards decreasing zinc vapour concentration with increasing flowrate can be seen from Figure 3.-11. The number of experiments is too limited, however, to regard this trend as being conclusive.

Comparing the jetting results with the bubbling vapourization results shows:

1) a lower scatter of the zinc concentration values for the jetting configuration than for the bubbling configuration;

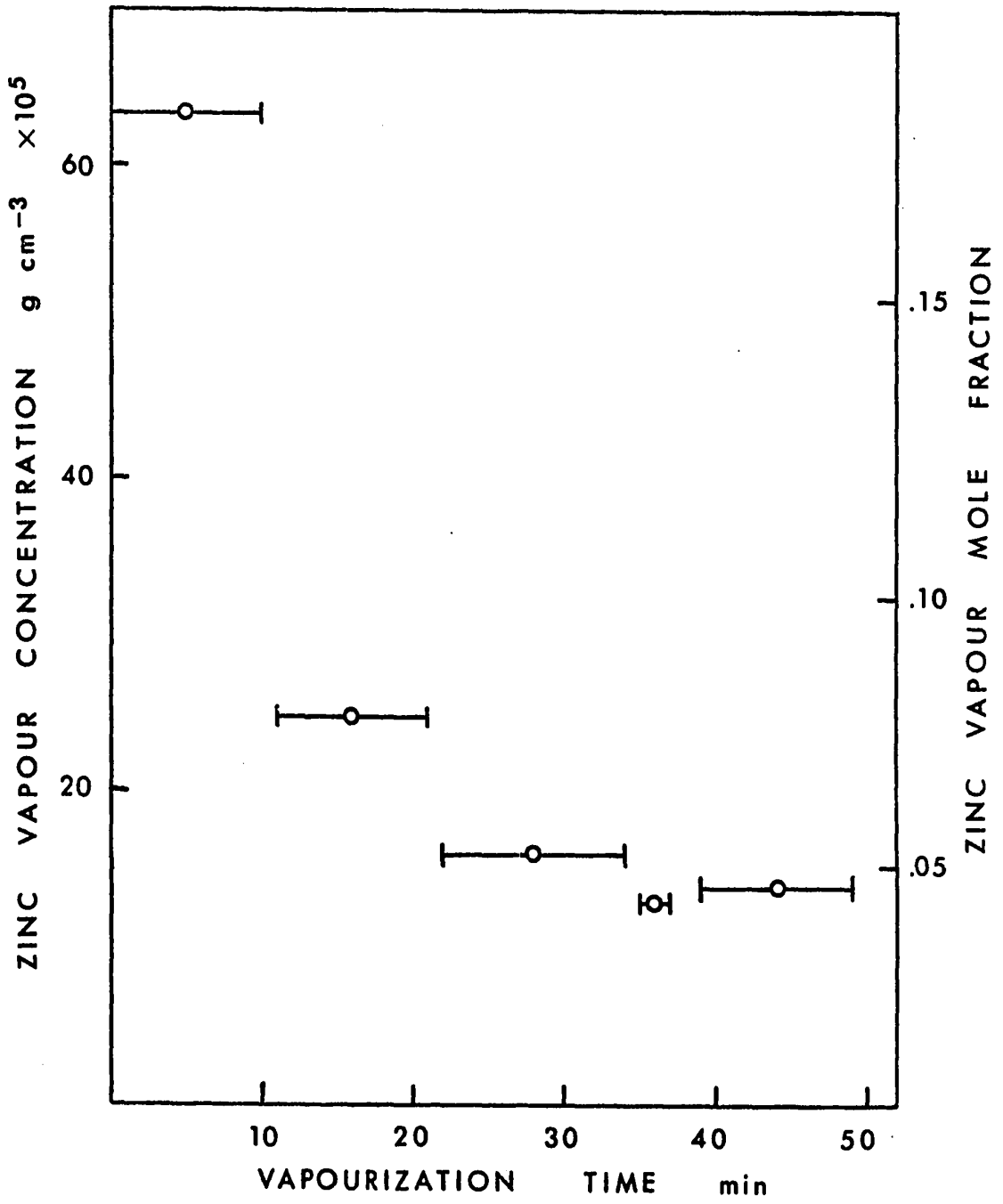

FIGURE 3.-10: Effect of new zinc meltdown on zinc-in-gas concentration.

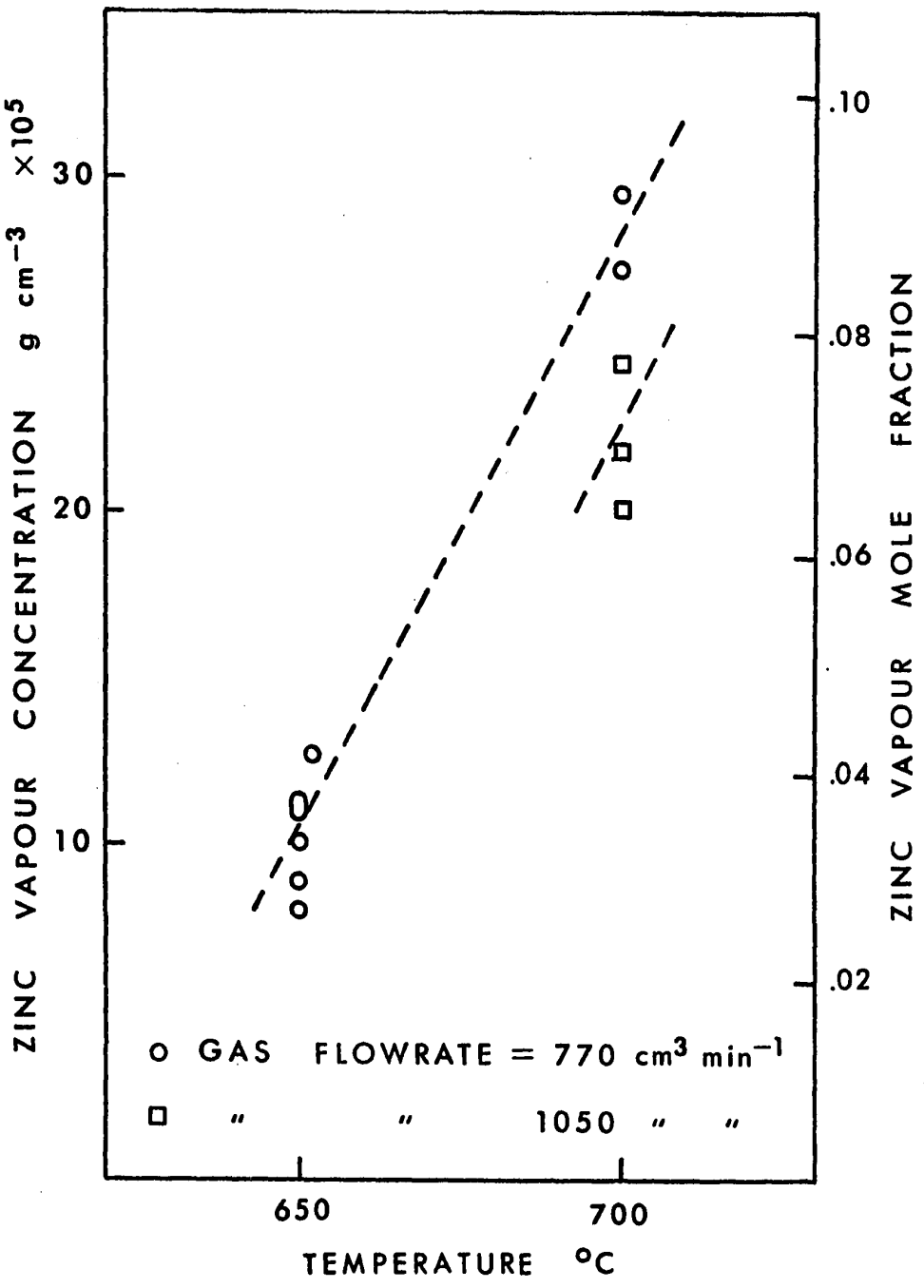

FIGURE 3.-11: Zinc vapourization results (jetting)

2) the zinc vapour concentration values are considerably lower for the jetting configuration than for the bubbling configuration.

The rates of zinc vapourization are summarized in Figure 3.-12. The rates of vapourization, calculated from the average zinc vapour concentration values for each experiment and expressed as g-moles of zinc per second are plotted versus zinc bath temperature for the two argon flowrates. The marked dependence of vapourization rates upon temperature is again shown while the effect of argon flowrate appears to be minimal over the limited range examined.

3.4.4 CONDENSATION RESULTS

The experimental results of the condensation of zinc into lead are reported in the form of zinc concentration in the input gas to the condenser and output gas from the condenser. The variables are:

a) mode of gas introduction: bubbling or jetting,

b) temperature of the lead bath.

3.4.5 CONDENSATION FROM GAS BUBBLES

Nine experiments were performed involving condensation of zinc vapour from zinc-laden argon gas bubbles rising through liquid lead. In six of them the zinc-laden gas stream was produced by bubbling of argon gas through liquid zinc while in the other three, jetting was the vapourization method applied. These experiments were designed to:

1) investigate the efficiency of condensation of zinc vapour on liquid lead from zinc-laden argon gas bubbles rising in

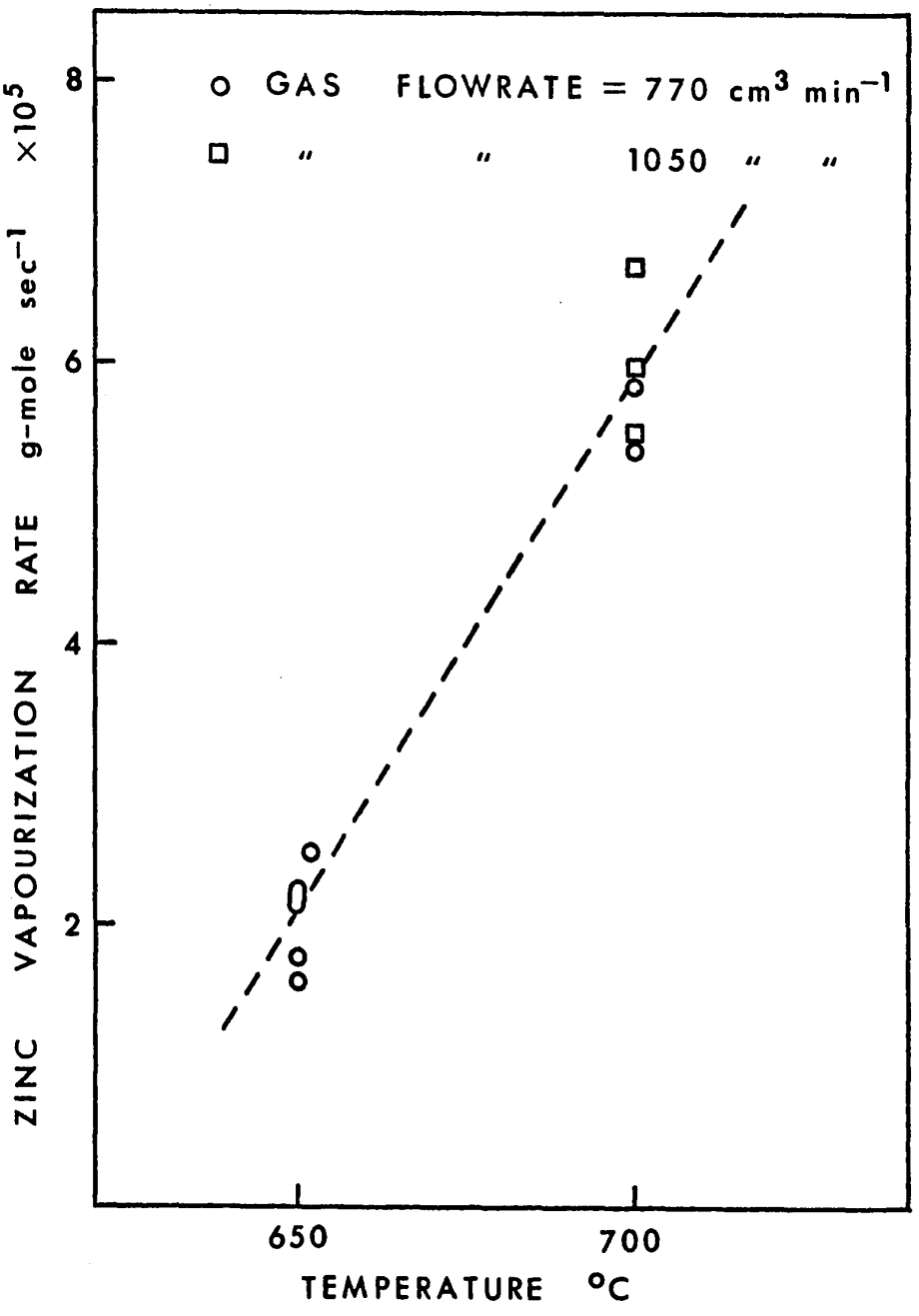

FIGURE 3.-12: Zinc vapourization rates (jetting)

liquid lead;

2) investigate the effect of liquid lead temperatures on condensation efficiency;

3) investigate the mechanisms of zinc vapour condensation on liquid lead from zinc-laden argon gas bubbles rising in liquid lead.

Figure 3.-13 shows an example plot of zinc concentration in the input (upper points, circles) and the output (lower points, squares) gas from the condenser, expressed in grams of zinc per cm^3 of pure argon gas (1 atmosphere at 0^oC) and zinc vapour mole fraction versus experimental time.

It can be seen that the zinc concentration in the input gas is more or less constant ($\pm$ 20%, consistent with the bubbling vapourization results) while the output zinc concentration increases markedly with time. It can also be seen that, throughout the experiment, as the output zinc concentration from the condenser is very much lower than the input zinc concentration, a considerable amount of condensation has taken place. The experiments showed then that a high condensation efficiency was achieved and that the efficiency decreased with time.

The effect of the lead bath temperature can be illustrated by comparison of Figures 3.-13, 3.-14, 3.-15 in which the gas zinc concentration is plotted versus experimental time for various lead bath temperatures. It is apparent that the output zinc vapour concentration decreases with decreasing lead bath temperature, which is equivalent to a condensation efficiency increase with decreasing lead bath temperature.

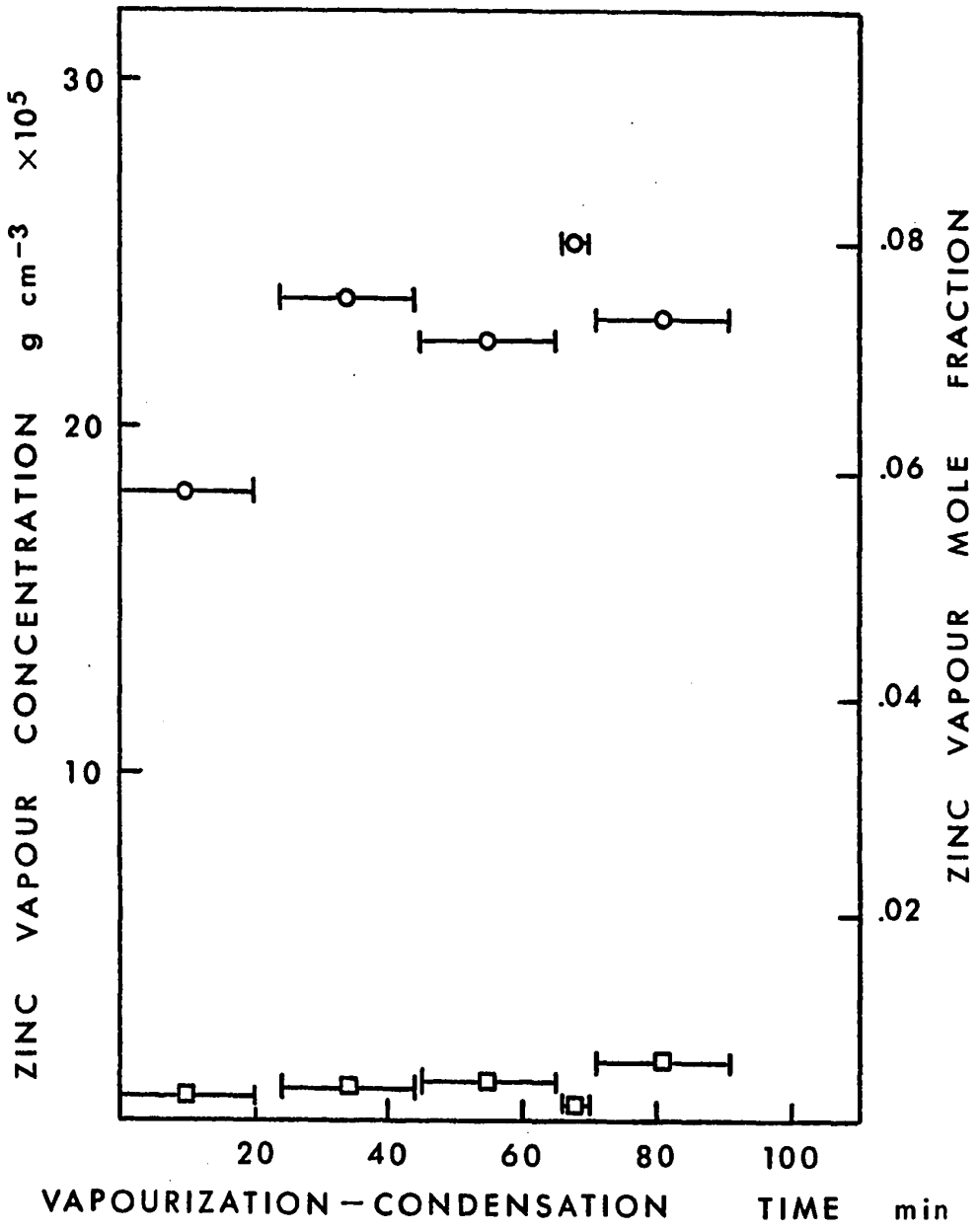

FIGURE 3.-13: Typical zinc condensation results (bubbling) (lead bath temperature 650°C).

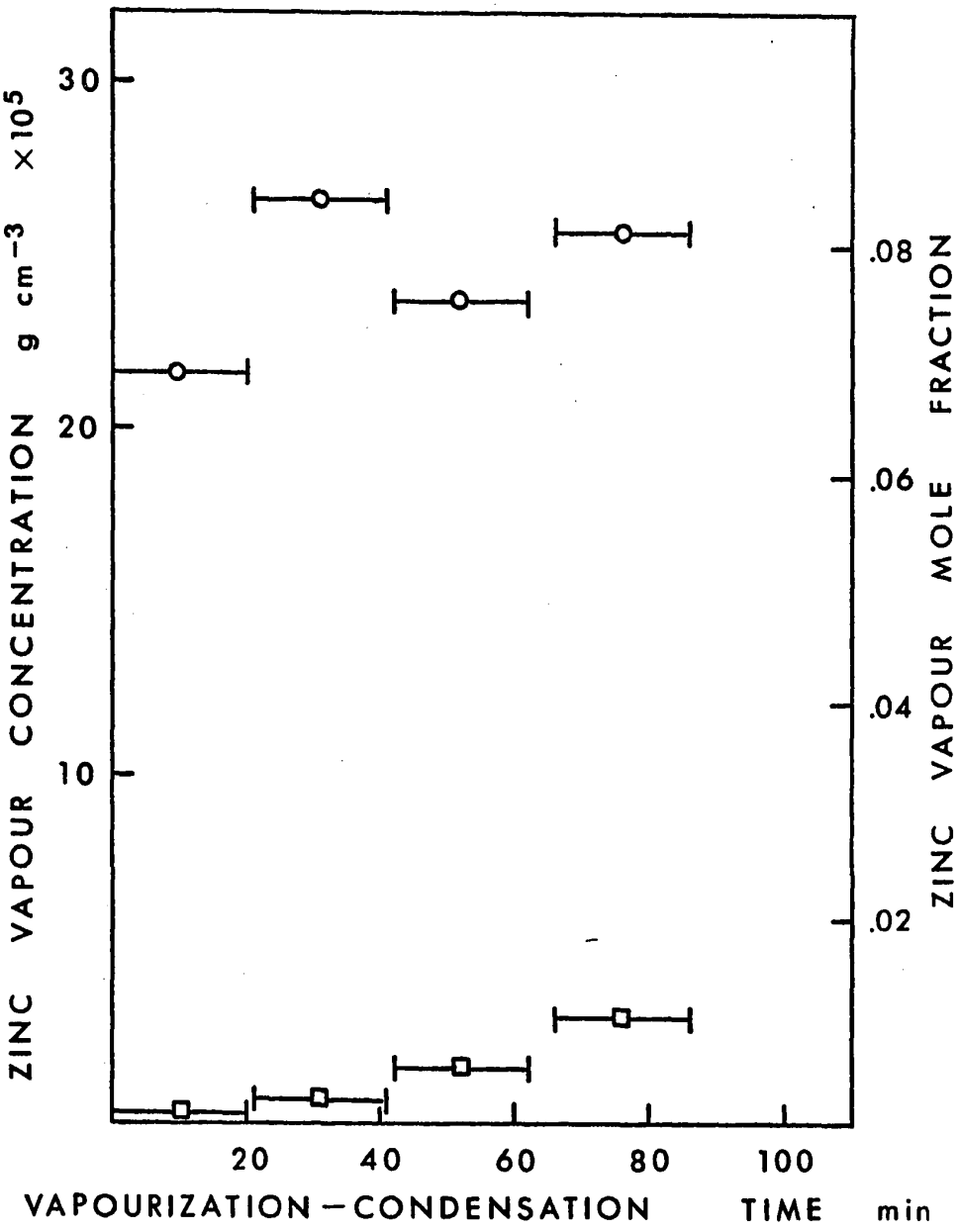

FIGURE 3.-14: Typical zinc vapour condensation results (bubbling), (lead bath temperature 700°C)

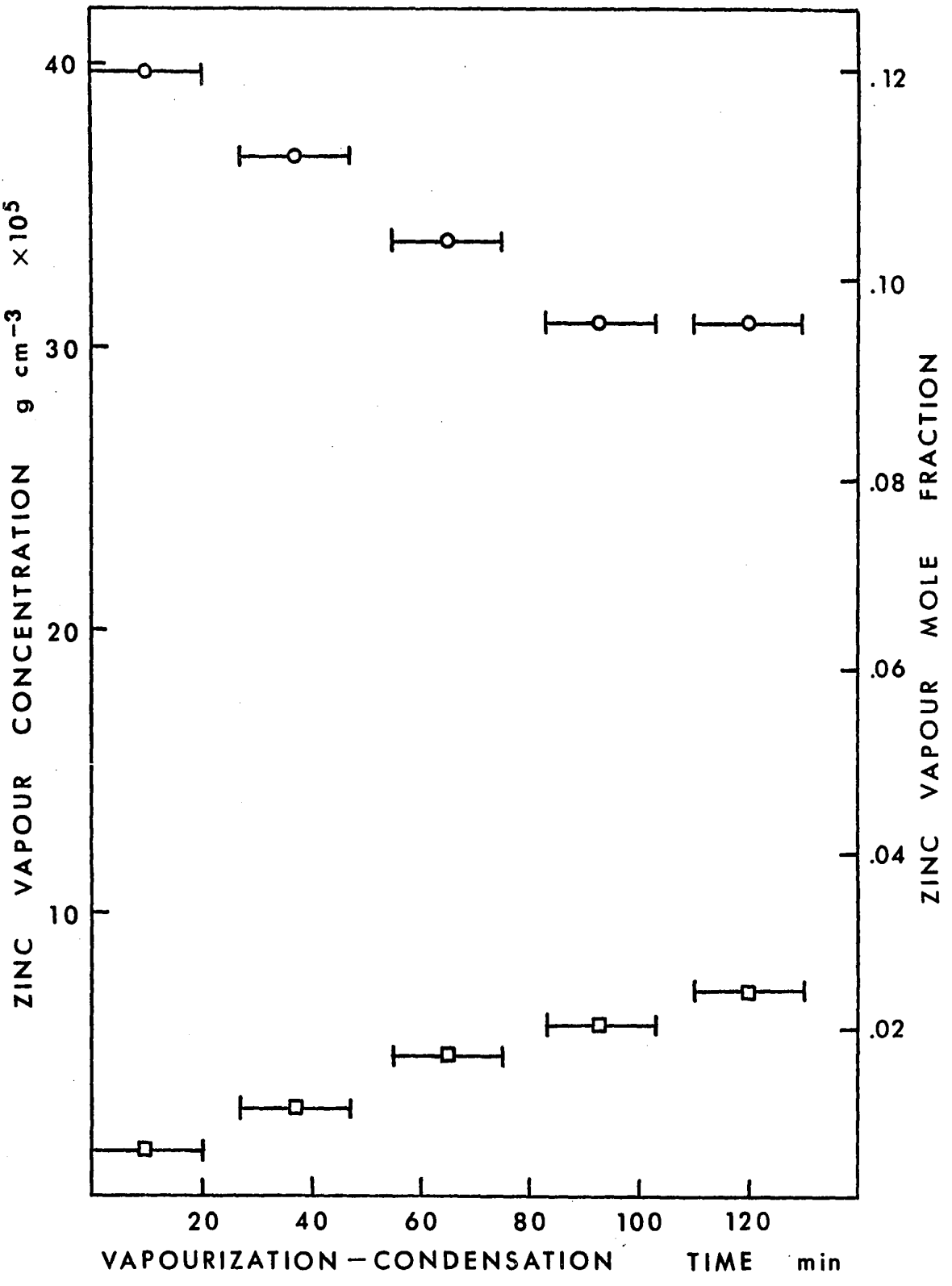

FIGURE 3.-15: Typical zinc vapour condensation results (bubbling), (lead bath temperature 750°C)

3.4.6 CONDENSATION FROM A GAS JET

Thirteen experiments were performed involving condensation of zinc vapour into liquid lead from a zinc-laden argon gas jet. In all cases the zinc laden gas stream input to the condenser was produced by jetting of argon onto the liquid zinc surface.

The condensation jetting experiments were designed to:

1) investigate the efficiency of condensation of zinc vapour on liquid lead from a zinc-laden argon gas jet;
2) investigate the effect of lead bath temperature on the condensation efficiency;
3) determine the mechanisms of zinc vapour condensation into liquid lead from a zinc-laden argon gas jet.

Figure 3.-16 shows a typical plot of zinc concentration in the input and the output condenser gases versus experiment running time.

The lower zinc-in-gas concentration in the output gases indicates that a considerable amount of condensation takes place but it can be noticed that the output zinc concentration in the gas stream increases rapidly with time.

The effect of lead bath temperature on the condensation efficiency can be illustrated by comparing Figure 3.-16 with Figure 3.-17. The zinc-in-gas concentration in the output gas stream is shown to decrease with decreasing lead bath temperature, i.e., the condensation efficiency increases with decreasing lead bath temperature.

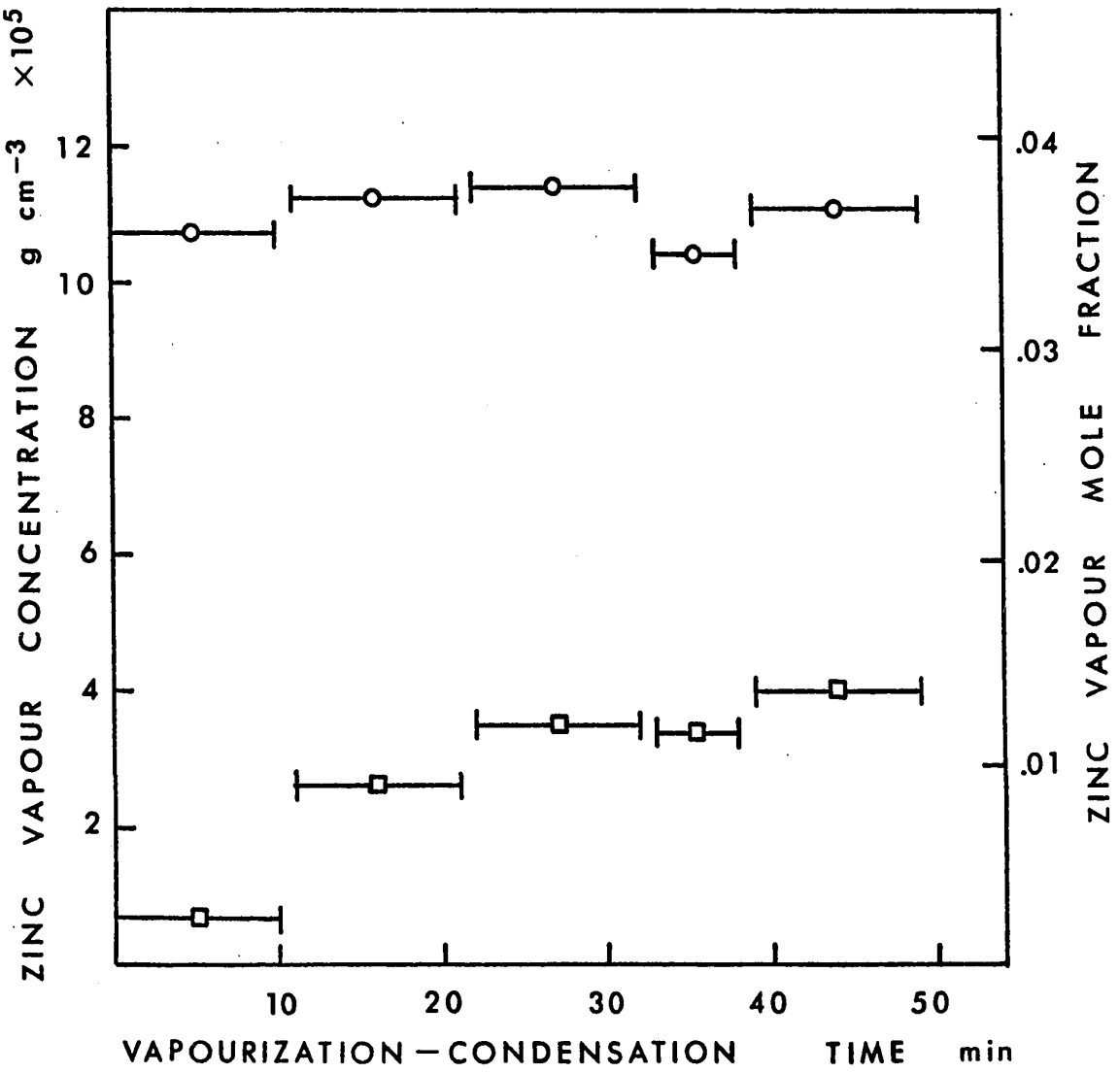

FIGURE 3.-16: Typical zinc vapour condensation results (jetting), (lead bath temperature 650°C).

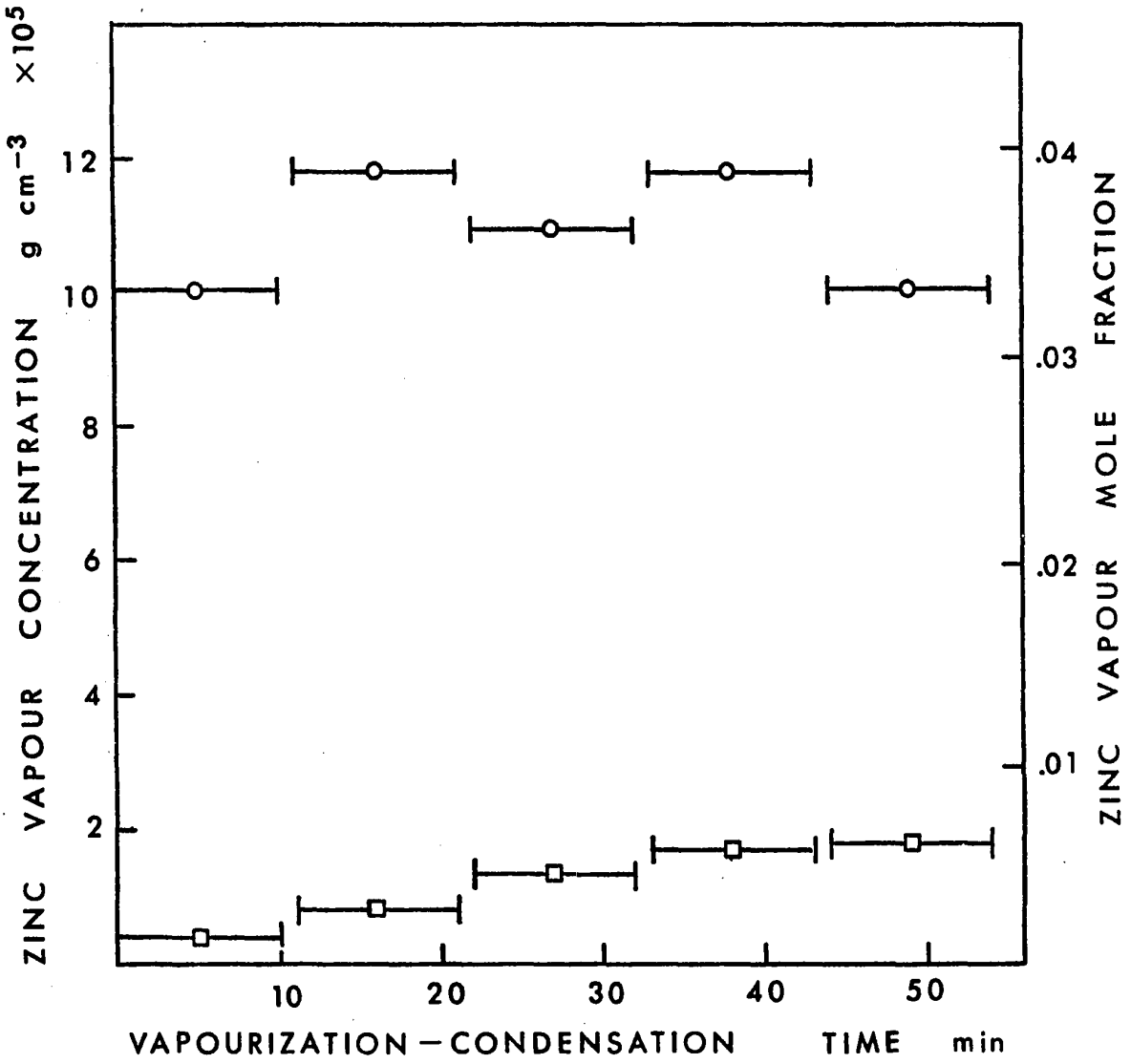

FIGURE 3.-17: Typical zinc vapour condensation results (jetting), (lead bath temperature 600°C).

It can also be noticed that the zinc-in-gas concentration in the exit gases from the condenser increases with increasing time of condensation.

Comparison of the bubbling and the jetting condensation results shows that a higher condensation efficiency was achieved with the bubbling configuration of condensation than with the jetting configuration.

CHAPTER IV

DISCUSSION

The results of the experimental investigation are discussed under the following headings:

1) Vapourization from liquid zinc into rising argon bubbles.
2) Vapourization from liquid zinc into a jet of argon.
3) Problems in interpreting the vapourization results.
4) Condensation of zinc vapour into lead from rising zinc-argon bubbles.
5) Condensation of zinc vapour into lead from a jet of zinc-argon gas.

The results are first discussed in terms of the proximity to equilibrium conditions, i.e., observed zinc partial pressures are compared with those which would be expected at equilibrium. Secondly, the rates of vapourization are discussed in terms of established mass transfer relationships.

Vapourization and condensation mechanisms are suggested.

4.1 VAPOURIZATION OF ZINC FROM LIQUID ZINC INTO RISING ARGON BUBBLES

The zinc vapour concentration results have been summarized in Figure 3.-7. It was shown that the gas zinc concentration increases markedly with temperature. This behaviour can be explained in terms of equilibrium zinc partial pressure over pure liquid zinc.

Figure 4.-1 shows a plot of equilibrium zinc partial pressure in mm Hg versus temperature. A comparison of Figure 4.-1 and Figure 3.-7 shows that there is a close correlation between the measured zinc vapour concentrations and the equilibrium zinc partial pressure. This observation led to plotting the experimental results in the form of measured average zinc partial pressures versus temperature.

Figure 4.-2 summarizes the measured zinc partial pressures in the vapourizer output gas and compares these measured values with the equilibrium zinc partial pressure over pure liquid zinc (solid line).

The figure shows that the measured average zinc vapour pressures tend to be higher than the equilibrium zinc vapour pressures, at any given temperature. On the other hand, the measured values seem to depend on temperature the same way as the equilibrium values. It could then be concluded that the zinc-argon stream produced was "supersaturated" with zinc vapour. This being physically improbable, it is believed that the supersaturation was likely due to the splashing of zinc into a higher temperature zone as has been mentioned in section 3.4.2. This result will be discussed in detail in section 4.3.

4.1.1 RATE CONTROLLING MECHANISMS IN VAPOURIZATION EXPERIMENTS (BUBBLING)

Since pure liquid zinc was used in the vapourization experiments, there can be no resistance to mass transfer in the liquid phase. Assuming interfacial steps and heat transfer for vapourization to be rapid, in view of the high thermal conductivity of liquid metal, the most probable

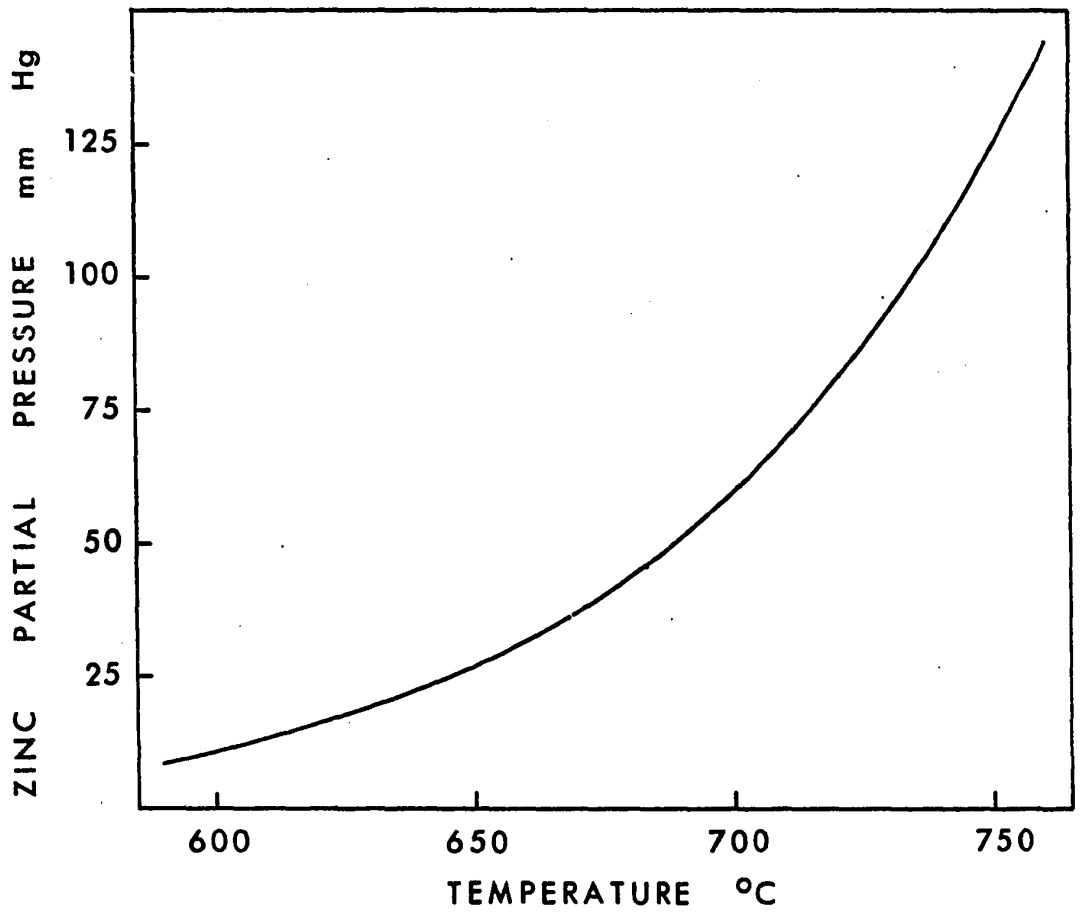

FIGURE 4.-1: Temperature dependence of the equilibrium zinc vapour pressure over pure liquid zinc.

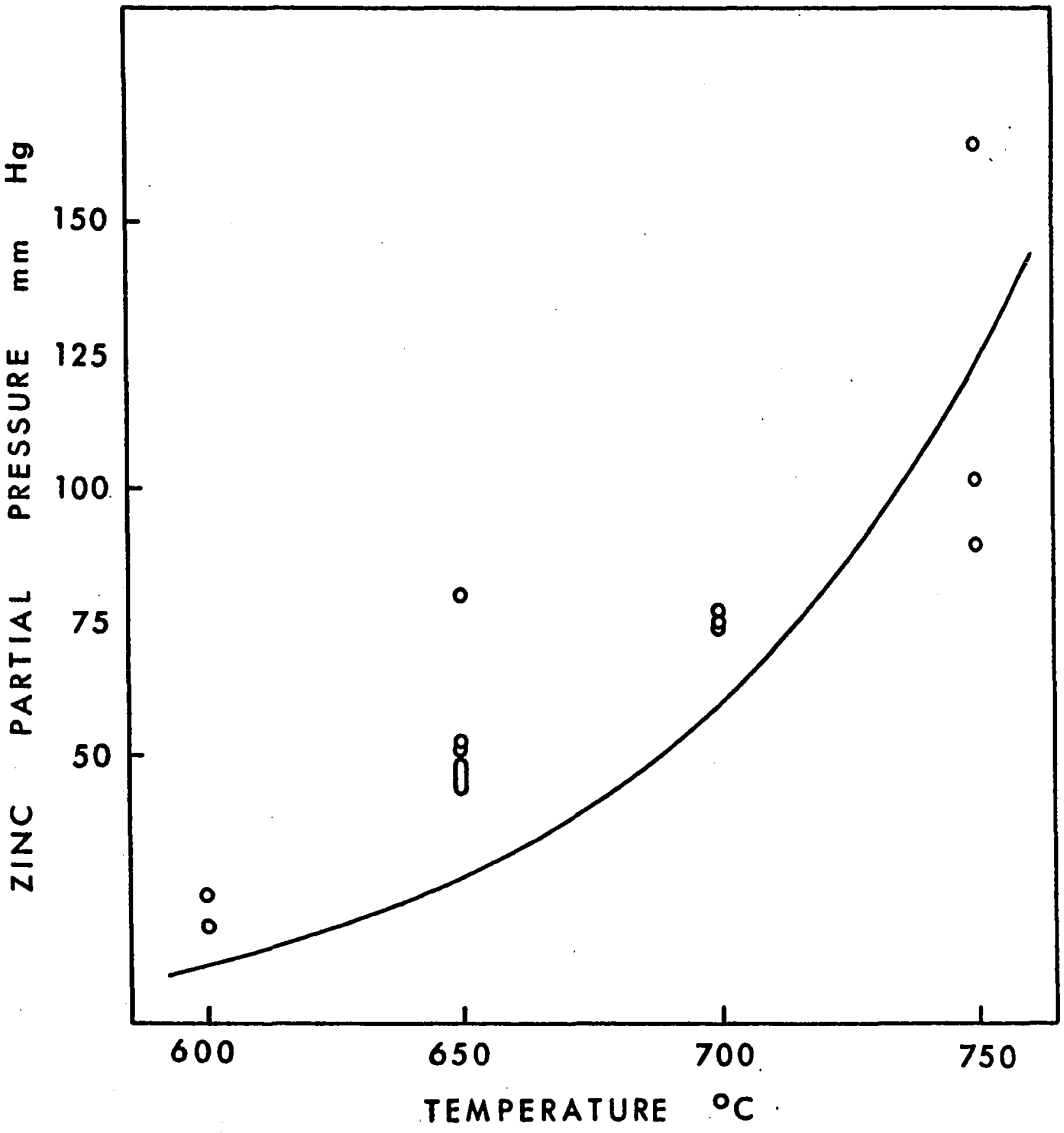

FIGURE 4.-2: Comparison between the experimental bubbling vapourization results and the equilibrium zinc vapour pressure over pure liquid zinc.

rate controlling step in the bubbling experiments should involve mass transfer of zinc vapour through argon.

Furthermore it can be assumed that the gas in the bubbles was in turbulent motion and well mixed. The rate controlling step can thus be assumed to be zinc mass transfer due to a concentration gradient in the gas phase between the gas adjacent to the zinc, and the gas in the bulk of the bubble.

Based on these assumptions it is possible to estimate the bulk zinc vapour content in rising bubbles after various heights of rise, i.e., after various contact times.

The rate of vapourization of zinc can be given by an equation of the form

$$\frac{dn_{Zn}}{dt} = k_g \cdot A_b \cdot (C^*_{Zn} - C^B_{Zn}) \qquad 4.-1$$

where n_{Zn} = number of g-moles of zinc in a bubble

k_g = equivalent mass transfer coefficient of zinc in the gas phase (argon), $cm \cdot sec^{-1}$

t = time, sec

A_b = equivalent bubble surface, cm^2

C^*_{Zn}, C^B_{Zn} = zinc concentrations at the interface and the bulk of the gas phase respectively

Writing the zinc concentration, C_{Zn}, according to the ideal gas law expression:

$$C_{Zn} = \frac{P_{Zn}}{RT}$$

equation 4.-1 can be rewritten:

$$\frac{dn_{Zn}}{dt} = \frac{k_g \cdot A_b}{RT} \cdot (P^*_{Zn} - P^B_{Zn}) \qquad 4.-2$$

The gas phase mass transfer coefficient, k_g, can be related to the bubble volume and the gas phase diffusion coefficient, the exact analytical expression depending on the bubble size and shape. Reference to the extensive results on bubble rising velocities in liquids by Haberman and Morton[22] shows that in low viscosity liquids (which is the case for liquid metals) bubbles are spherical up to a volume of 10^{-4} cm^3; bubbles have an ellipsoidal shape in the volume range 10^{-4} to $5 \times 10^{-1} cm^3$; and bubbles have a spherical cap shape for volumes in excess of 0.5 cm^3.

Bubble volumes were not directly measured in the present liquid metal experiments but reference to the work of Davidson and Amick[23] on bubbling rates and bubble sizes for vertical tubes, backed by observations of tubes facing downwards in tap water shows that, for the experimental volume flowrates, the bubble volumes would be between 1 and 5 cm^3. Thus the bubbles are in the spherical cap range and the gas phase mass transfer coefficient can be described by the analytical expression for the spherical cap bubble regime[24]:

$$k_g = .924 \cdot D^{1/2}_{ZnAr} \cdot g^{1/4} \cdot V^{-1/12} \qquad 4.-3$$

where D_{ZnAr} = diffusion coefficient of zinc in argon, $cm^2 \cdot sec^{-1}$

g = acceleration of gravity ($= 981$ $cm \cdot sec^{-2}$)

V = bubble volume, cm^3

Thus the appropriate gas mass transfer coefficient can be computed provided that the diffusion coefficient D_{ZnAr} is known.

Although no direct measurements of D_{ZnAr} have been made, it is possible to predict with good accuracy (± 10%) the diffusivity of zinc in argon using the empirical Chapman Enskog equation[25]:

$$D_{AB} = .001853 \cdot \frac{\sqrt{T^3 (1/2M_A + 1/M_B)}}{P \cdot \sigma_{AB} \cdot \Omega_{D,AB}} \qquad 4.-4$$

where T = temperature, ^oK

M_A, M_B = molecular weight of gases A and B respectively

P = total pressure, Atm.

σ_{AB} = Lennard-Jones parameter, "collision diameter," $\mathring{A}$

$\Omega_{D,AB}$ = dimensionless function of temperature and intermolecular potential fields "collision integral"

Taking $T = 923^oK$, $\Omega_{D,ZnAr} = .9845$,[25] $P = 1$ Atm,

$\sigma_{ZnAr} = 2.984\ \mathring{A}$,[25] the diffusivity of zinc in argon at 650°C

becomes $D_{ZnAr} = 1.2\ cm^2 \cdot sec^{-1}$

These mass transfer coefficient and diffusion data could be applied to the integration of equation 4.-2 to obtain P_{Zn}^B with respect to time of bubble rise (t) but this integration is rather difficult because the relation between n_{Zn} and P_{Zn}^B is complicated and it is easier to integrate with respect to the total pressure P on the bubble. The derivation of a suitable differential equation is as follows. Starting with the ideal gas law:

$$P \cdot V = n \cdot R \cdot T \qquad 4.-5$$

and differentiating with respect to pressure P, then:

$$V + P\frac{\partial V}{\partial P} = \frac{\partial n}{\partial P} RT \qquad 4.-6$$

In the case of zinc vapourization into an argon bubble

$$n = n_{Zn} + n_{Ar} \qquad 4.-7$$

and since there is no argon mass accumulation in the bubble

$$\frac{\partial n}{\partial P} = \frac{\partial n_{Zn}}{\partial P} = \frac{dn_{Zn}}{dt} \cdot \frac{dt}{dP} \qquad 4.-8$$

Combining Equations 4.-8 and 4.-2 yields

$$\frac{\partial n}{\partial P} = \frac{k_g \cdot A_b}{R \cdot T} \left(P^*_{Zn} - P^B_{Zn}\right) \frac{1}{dP/dt} \qquad 4.-9$$

For a rising bubble

$$\frac{dP}{dt} = -U \cdot \rho \cdot g \qquad 4.-10$$

where U = bubble rising velocity, $cm \cdot sec^{-1}$

ρ = liquid density, $g \cdot cm^{-3}$

and Equation 4.-9 becomes:

$$\frac{\partial n}{\partial P} = \frac{k_g \cdot A_b}{U \cdot \rho \cdot g} \cdot \frac{(P^B_{Zn} - P^*_{Zn})}{RT} \qquad 4.-11$$

Final substitution in equation 4.6 yields:

$$V + P\frac{\partial V}{\partial P} = \frac{k_g \cdot A_b}{U \cdot \rho \cdot g} \left(P^B_{Zn} - P^*_{Zn}\right) \qquad 4.-12$$

The bubble equivalent surface A_b is given by:

$$A_b = 4.82 \cdot V^{2/3} \qquad 4.-13$$

while bubble rising velocities for spherical cap bubbles are given by[22]:

$$U = .80 g^{1/2} V^{1/6} \qquad 4.-14$$

Insertion of the values of k_g, A_b, U in Equation 4.-12 finally yields:

$$V + P \frac{\partial V}{\partial P} = \frac{.924 \cdot D_{ZnAr}^{1/2} \cdot 4.82}{.80 \cdot g^{5/4} \cdot \rho} \cdot V^{5/12} \left(P_{Zn}^{B} - P_{Zn}^{*} \right) \qquad 4.-15$$

Since the bubble was initially free of zinc, the bulk zinc pressure in the bubble is given by $P_{Zn}^{B} = \frac{PV - P^{in}V^{in}}{V}$ 4.-16

and Equation 4.-15 becomes:

$$V + P \frac{\partial V}{\partial P} = .00016532 \; V^{5/12} \left(\frac{PV - P^{in}V^{in}}{V} - P_{Zn}^{*} \right) \qquad 4.-17$$

where P^{in} = initial bubble pressure

V^{in} = initial bubble volume, cm^3

Equation 4.-17 has been numerically integrated for a lance depth of 10 cm and initial bubble volumes of 1, 2, 5, 10 cm^3.

For the numerical integration initial values were given for pressure and bubble volume, and $\frac{\partial V}{\partial P}$ was calculated from equation 4.-17. Then ΔV was calculated from:

$$\Delta V = \Delta P \cdot \frac{\partial V}{\partial P} \qquad 4.-18$$

using pressure increments of -100 dynes $\cdot$ cm^{-2}. The new values of pressure and volume were calculated from:

$$P = P + \Delta P$$

$$V = V + \Delta V$$

and the calculation was started again.

The results of these calculations are illustrated in Figure 4.-3 where the height of bubble rise is plotted versus zinc mole fraction in the gas phase. The maximum equilibrium value of zinc mole fraction is also known.

It can be readily seen that argon bubbles of initial volumes between 1 and 5 cm^3 become virtually saturated with zinc vapour (650°C) after rising 5 to 10 cm in the zinc bath.

During the experiments the lance depth was between 5 and 10 cm and the measured zinc vapour pressures were greater than the equilibrium partial pressures. It can therefore be concluded that the suggested rate controlling mechanism is in basic agreement with the experimental results, i.e., bubble saturation is very quickly reached during bubble rise in liquid zinc.

4.2 VAPOURIZATION FROM LIQUID ZINC INTO A JET OF ARGON

As in the case of zinc vapourization into argon bubbles, the jetting vapourization results suggest a close correlation between the measured zinc vapour concentrations and the equilibrium zinc vapour pressures (compare Figures 3.-11 and 4.-1).

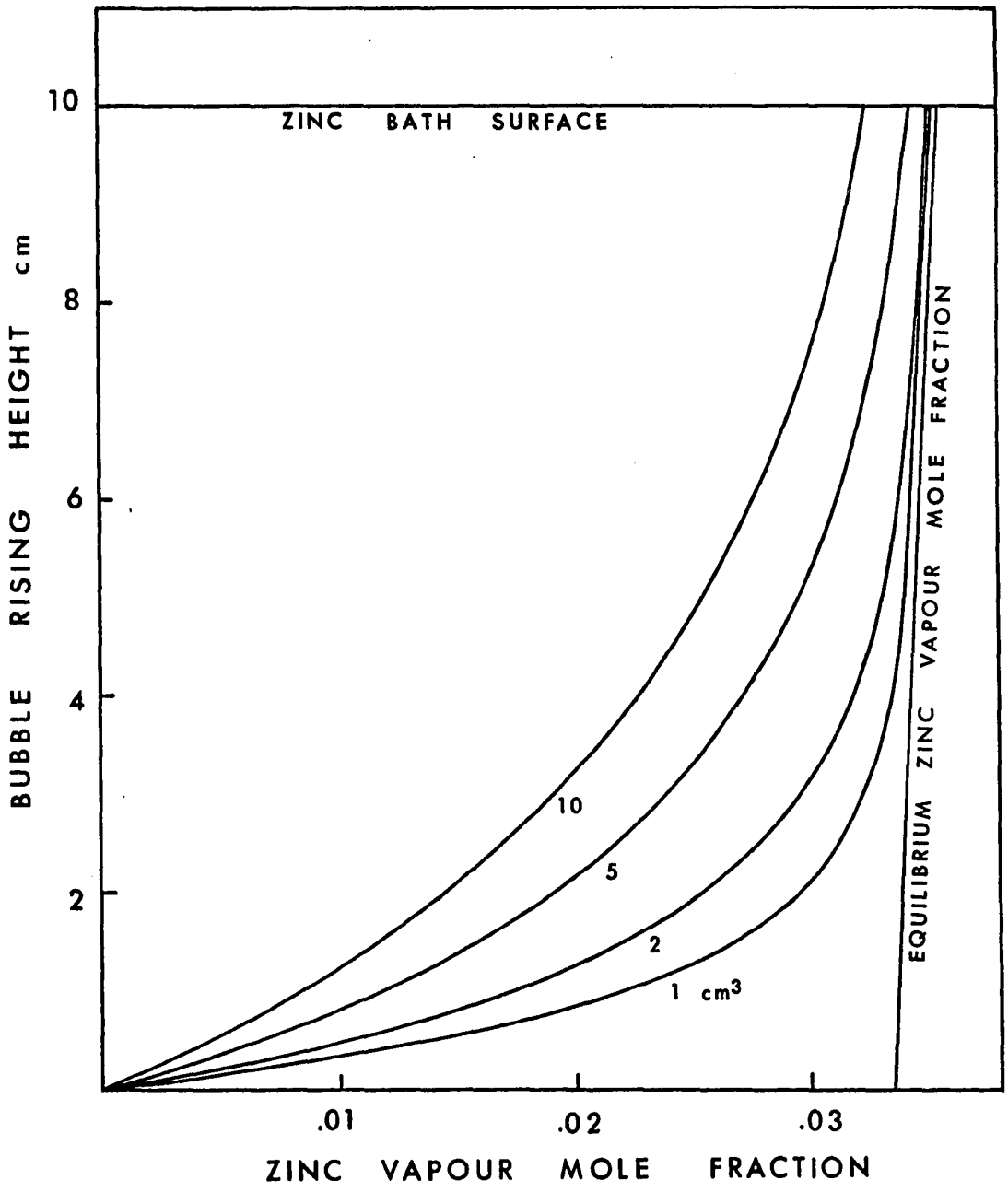

FIGURE 4.-3: Calculated zinc pick-up by argon rising bubbles.

Figure 4.-4 is a plot of the measured average zinc vapour pressures in mm Hg versus zinc bath temperature. The solid line represents the equilibrium zinc vapour pressure over pure liquid zinc. The lance height above the liquid zinc surface was 2.5 cm in all these experiments and the volumetric flowrate of argon was between 750 and 1400 $cm^3 \cdot min^{-1}$ measured at N.T.P. (lance diameter was 0.24 cm).

The experimental points agree within the limits of experimental accuracy with the equilibrium zinc vapour pressure curve. This implies that equilibrium has been reached between the gas-liquid zinc interface and the bulk of the gas phase.

The achievement of equilibrium between the bulk of the gas phase and the liquid-gas interface is of importance to the jetting condensation experiments and is further discussed in section 4.5.

4.3 PROBLEMS IN INTERPRETING THE VAPOURIZATION RESULTS

As mentioned in sections 3.4.2 and 4.1 the experimental results of zinc vapourization into argon bubbles showed:

1) a high scatter of the measured zinc vapour pressures in the vapourizer output gas;
2) measured zinc vapour pressures higher than the equilibrium zinc vapour pressures over pure liquid zinc.

These results could not be explained in terms of experimental inaccuracies. Two alternative explanations could be given for this phenomenon.

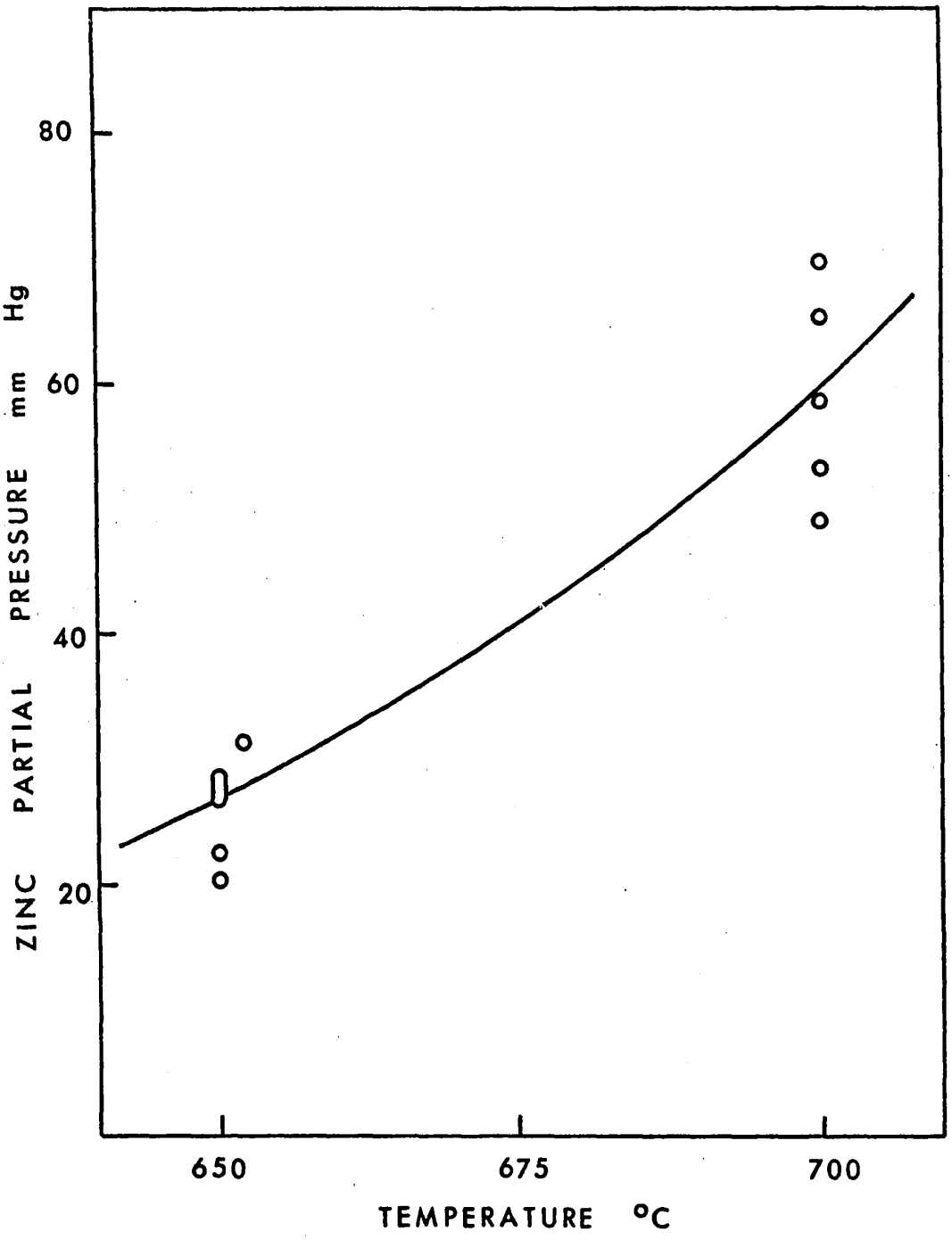

FIGURE 4.-4: Comparison between the experimental jetting vapourization results and the equilibrium zinc vapour pressure over pure liquid zinc.

1) The agitation of the zinc bath by the rising argon bubbles might have resulted in the generation of very small zinc droplets that were carried via the gas stream into the sampling tubes. These particles might subsequently have been deposited in the sampling tubes (either on the walls or on the filters) resulting in excessively high apparent zinc vapour pressures.

A calculation based on Stokes' law showed that for the average upward gas velocities in the vapourizer (max $3cm \cdot sec^{-1}$) the maximum radius of zinc droplets that could be carried in the gas stream was 14.3 microns. The creation of such droplets is considered very improbable in view of the high surface energies of such small droplets of metal.

2) The second explanation could have been that bubbling resulted in upward splashing of liquid zinc droplets which adhered to the walls of the vapourizer above the zinc bath. Since the temperature of the vapourizer above the liquid zinc surface was maintained at a temperature higher than that of the zinc bath to prevent any condensation on the vapourizer walls, these drops would have a higher equilibrium zinc vapour pressure than the bath itself. Thus vapourization of the zinc droplets adhering to the wall, would result in "supersaturated" (with respect to the zinc bath temperature) vapourizer gas output. Figure 4.-5 shows a typical temperature profile for the vapourizer unit.

Two observations confirm this second explanation:

a) Zinc droplets were actually observed on the vapourizer walls upon disassembling.

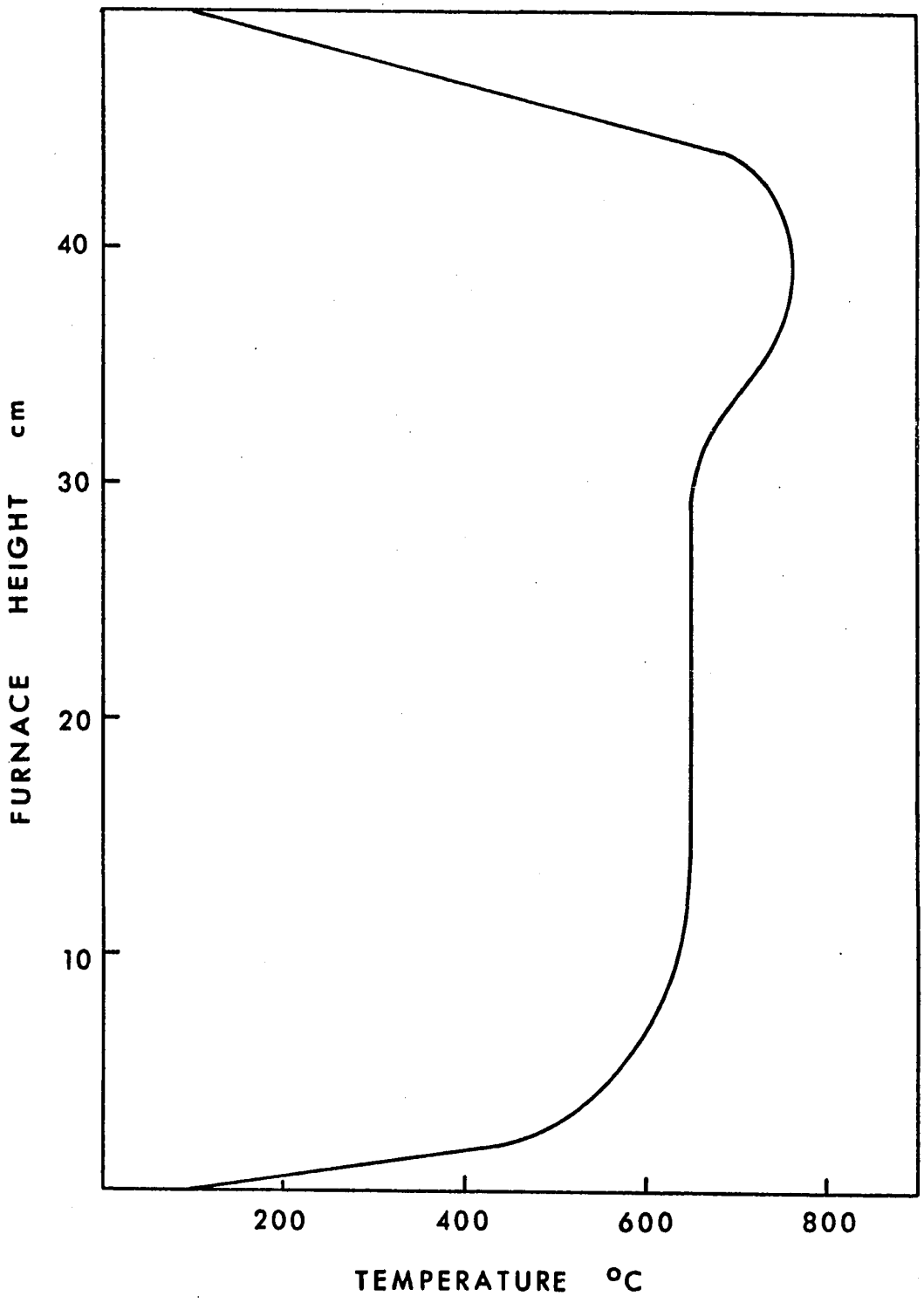

FIGURE 4.-5: Typical temperature profile of the vapourizer.

b) Abnormal behaviour was observed during the jetting vapourization experiments which immediately followed the bubbling vapourization experimental programme and also during the experiments which immediately followed the melting of new zinc in the zinc crucible.

Figure 4.-6 is, for example, a plot of experimental zinc vapour pressure versus time for four jetting vapourization experiments which immediately followed the bubbling vapourization programme. The solid line represents the equilibrium zinc vapour pressure over liquid zinc at the experimental temperature (650°C). The vapourizer was not opened for cleaning between the bubbling and the jetting experiments.

The abnormal behaviour is shown by very high initial zinc vapour pressure values and a downwards trend of the zinc vapour pressure values which continues through the four experiments until it reaches its normal level, i.e., the equilibrium partial pressure of zinc.

It is almost certain that this behaviour is due to the evaporation of zinc droplets remaining on the vapourizer walls from the previous bubbling experiments. As these droplets evaporated during the experiments, the apparent zinc vapour pressure decreased until the droplets had completely evaporated, whereupon the measured zinc vapour pressure reached the equilibrium partial pressure level.

Similar behaviour was observed during experiments which immediately followed replacement and melting of new zinc in the vapourizer crucible, as shown in 4.-7, a plot of measured zinc vapour

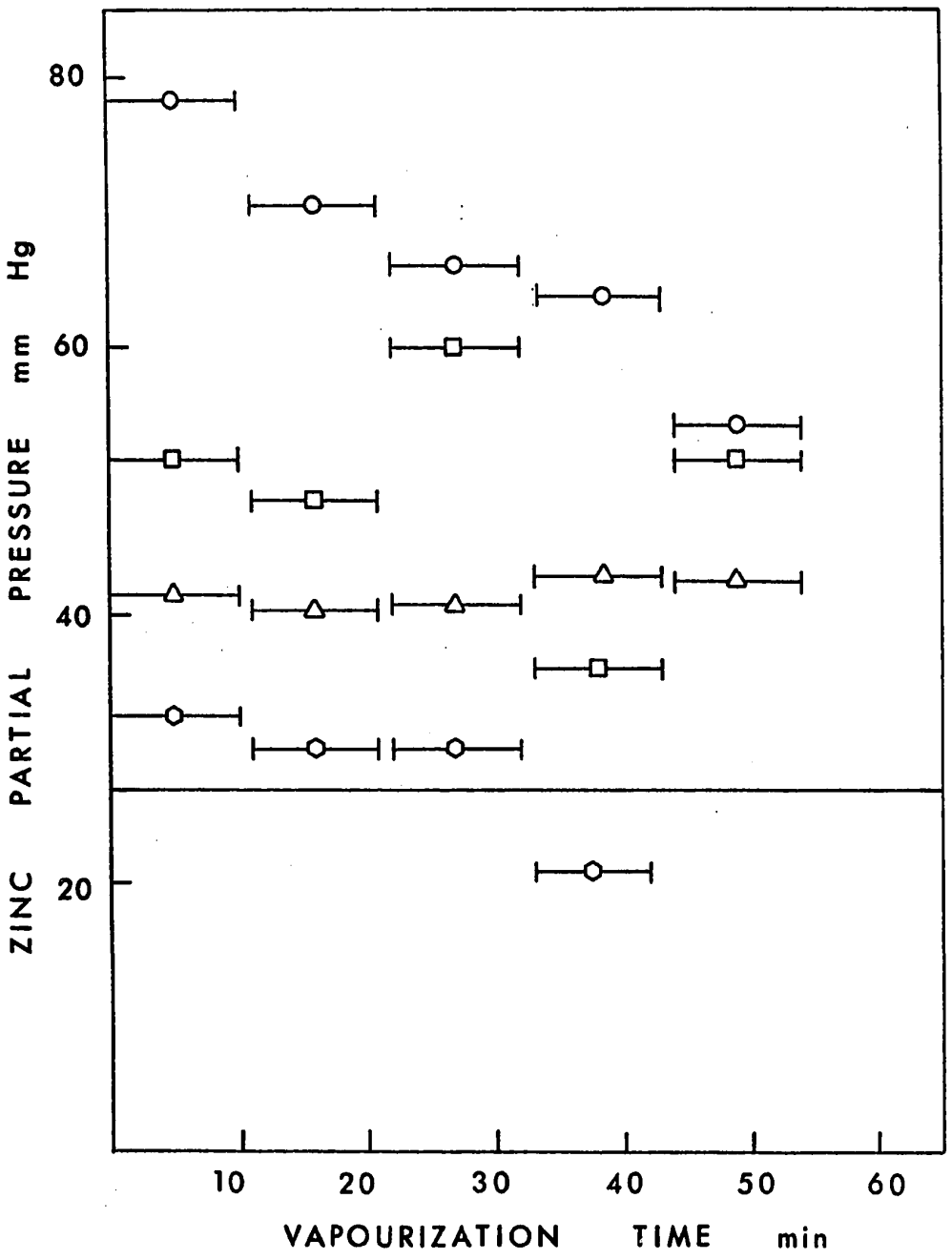

FIGURE 4.-6: Jetting vapourization results (jetting vapourization experiments immediately following the bubbling vapourization programme).

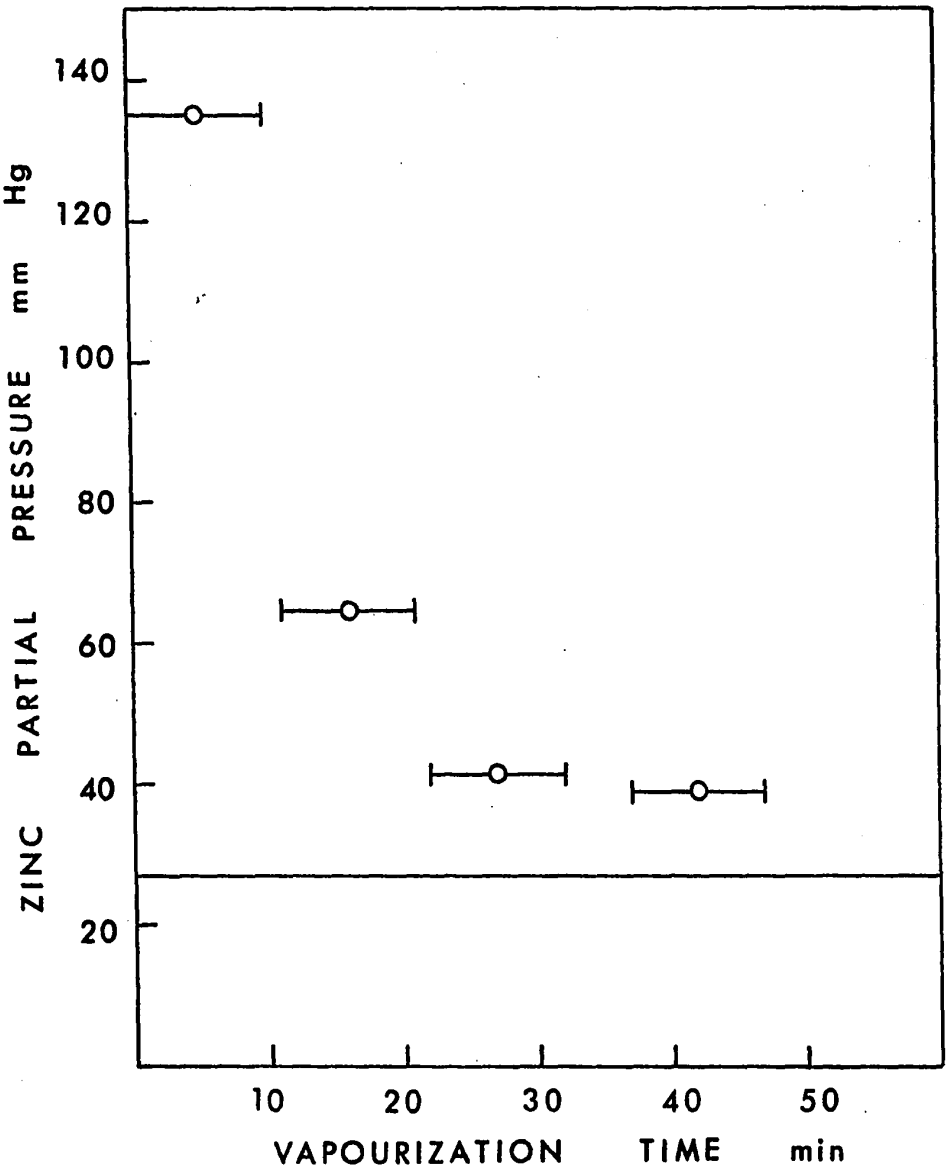

FIGURE 4.-7: Typical jetting vapourization results immediately following melting of new zinc.

pressure versus time. It is believed that this behaviour is also due to zinc being splashed onto the hot upper walls of the vapourizer, during the meltdown of the solid zinc.

It can be thus concluded that the excessively high measured zinc vapour pressure values, obtained in the vapourization experiments, especially the bubbling vapourization experiments, are due to these splashing effects.

It should be noted that in the early experiments the temperature of the upper vapourizer zone was not closely controlled. Care was taken to ensure that the temperature was at least 50°C higher than the melt temperature but in some experiments the temperature of this zone exceeded the melt temperature by 150°C. This is a likely explanation for the high scatter of zinc vapour pressure values obtained during the bubbling vapourization experiments. It can be noted also (Figure 4.-2) that an excess temperature of 100°C can account for the highest observed excess P_{Zn} values.

4.4 CONDENSATION EXPERIMENTS

The condensation results are treated in terms of equilibrium pressures in the same manner as the vapourization results. In this case, however, the condenser output zinc vapour pressure is not compared with the equilibrium zinc vapour pressure over pure liquid zinc but with the equilibrium zinc vapour pressures over liquid zinc-lead alloys.

The compositions of the lead-zinc alloys depended directly on the amounts of zinc vapour condensed in lead and thus on condensation time. The concentrations of zinc in the liquid alloys were not measured experimentally but, rather, they have been calculated from the weights of zinc condensed in the weighed amounts of lead.

The weights of zinc condensed were in turn calculated from the concentrations of zinc-in-gas into and out of the condenser as indicated by the sampling tubes. The quantities of gas into and out of the condenser were also used in the calculation. The zinc mass balance is:

$$G \cdot C_{Zn}^{in} = G \cdot C_{Zn}^{out} + W_{Zn}^{cond.}$$

where G = total volume of argon gas passed, cm^3

C_{Zn}^{in}, C_{Zn}^{out} = concentrations of zinc in the input and output gases, $g \cdot cm^{-3}$ of argon

$W_{Zn}^{cond.}$ = weight of zinc condensed

As can be noted, this balance assumes a 100% material balance, which would seem to be justified in the closed system employed.

4.5 CONDENSATION OF ZINC VAPOUR INTO LEAD FROM ZINC-ARGON GAS BUBBLES

Figure 4.-8 is a typical experimental plot of the ratio:

$$P_{Zn} / P_{Zn}^{o}$$

where P_{Zn} = measured zinc vapour pressure in the output gas from the condenser.

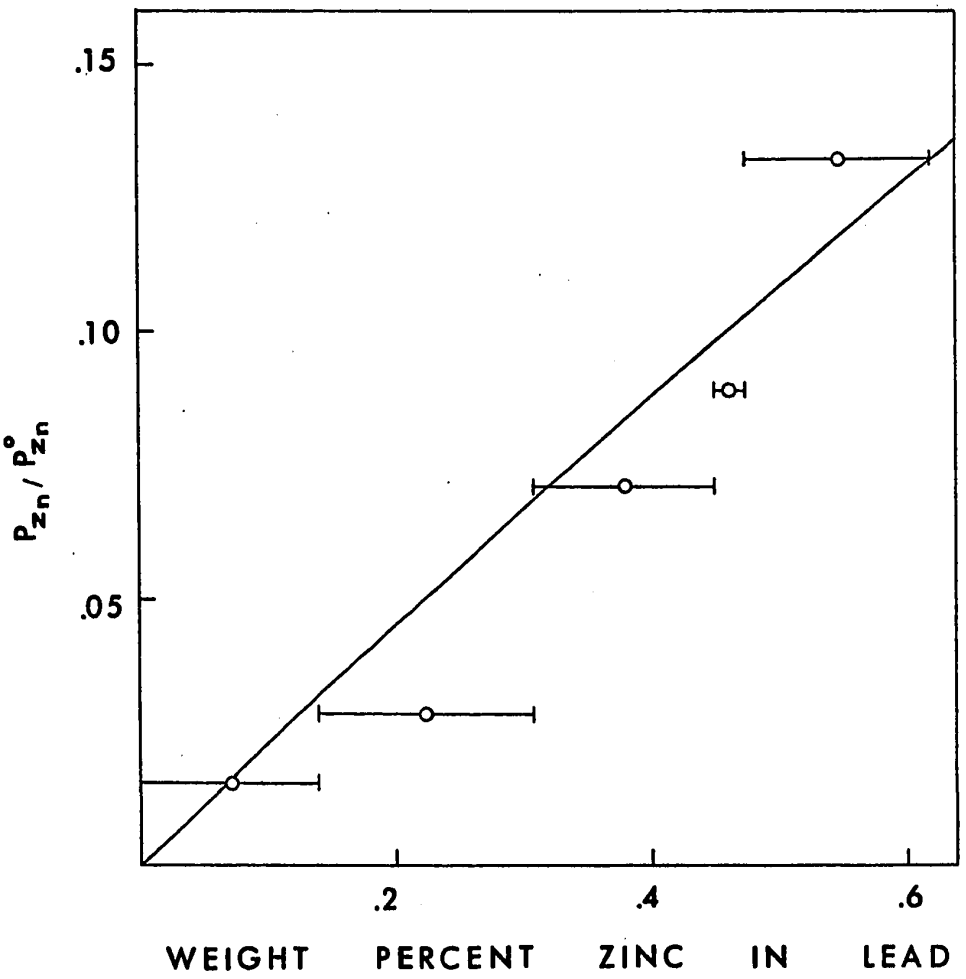

FIGURE 4.-8: Typical bubbling condensation results (lead bath temperature 700°C).

P^{o}_{Zn} = equilibrium zinc vapour pressure over pure liquid zinc at the experimental temperature.

versus percent zinc in lead.

The solid line represents the activity of zinc in the zinc-lead alloy as a function of weight percent zinc as reported by Hultgren.[19] Since the equilibrium ratio P_{Zn} / P^{o}_{Zn} is equivalent to activity, the measured ratio would equal a_{Zn} if equilibrium were achieved.

The measured zinc vapour pressure values are average values over the time of blowing through each sampling tube, while the weight of zinc in lead is the cumulative total at the midpoint of the blowing time for each sample tube. The arrows show the range of the bath composition for each experimental point.

It can be seen that within the limits of experimental accuracy the points follow the equilibrium curve. This means that the achievement of equilibrium between the gas phase in the bubbles and the liquid phase was virtually complete during the rise of the bubble through the liquid lead.

Figure 4.-9 is again a plot of the P_{Zn}/ P^{o}_{Zn} ratio versus weight percent of zinc in lead. The solid line represents zinc activity[19] in the alloy versus weight percent of zinc in the alloy. The high measured values in one of the experiments are probably due to a splashing effect similar to the splashing effect observed in the vapourization experiments, and which would lead to high P_{Zn} values in the condenser exit gases. This problem was avoided in the later experiments by decreasing the temperature of the upper condenser zone to the temperature of the lead bath.

This change was made as it was determined in the first experiments that the output zinc vapour pressures were too low for condensation

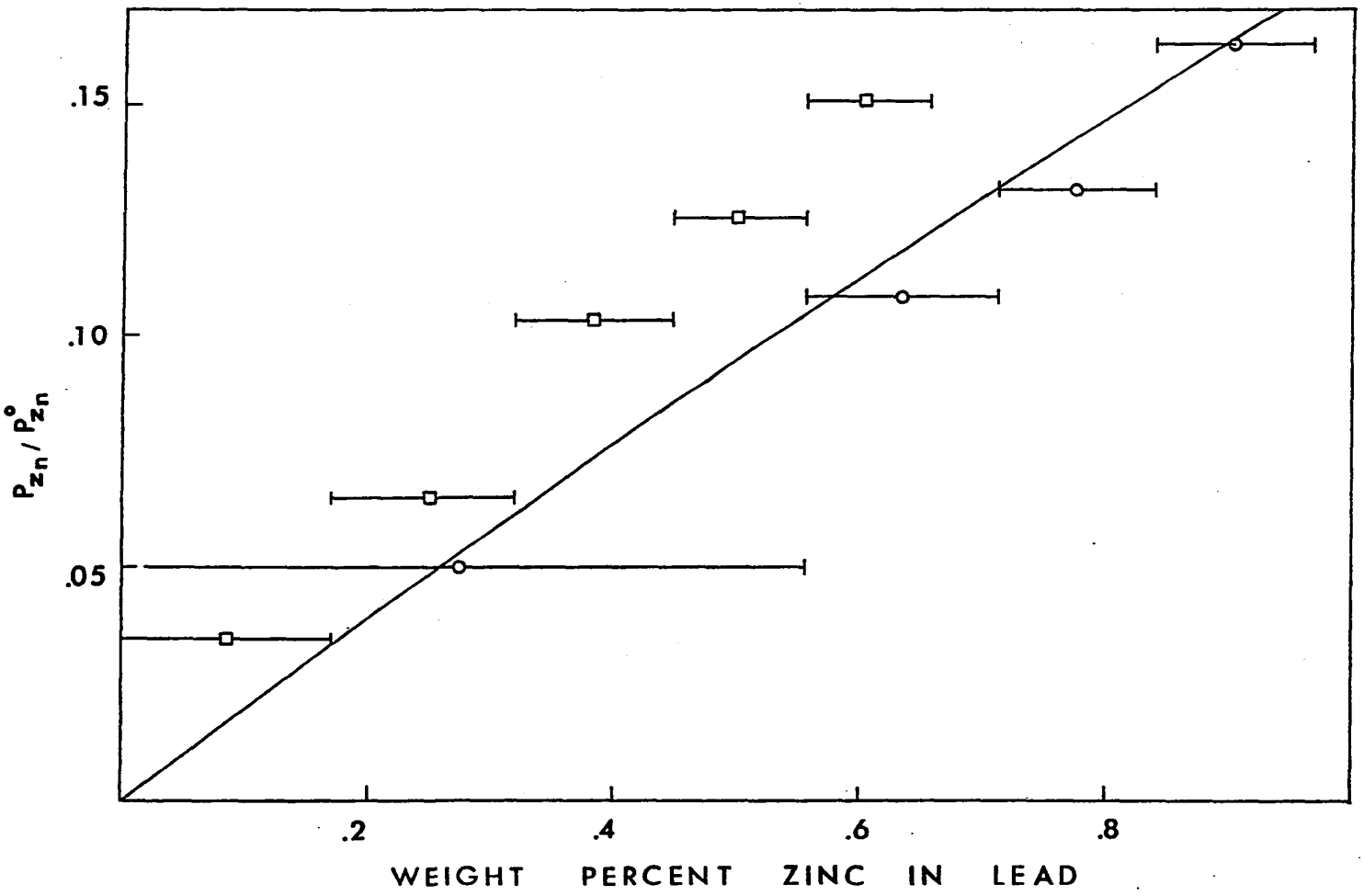

FIGURE 4.-9: Bubbling condensation results (lead bath temperature 750°C)

on the condenser walls to occur.

4.5.1 RATE CONTROLLING MECHANISMS IN BUBBLING CONDENSATION EXPERIMENTS

It can be assumed that the interfacial resistance to mass transfer of zinc vapour from the bubble to the liquid phase is negligible. It can also be assumed that the heat transfer for condensation is rapid. It then follows that the main resistance to zinc mass transfer should be diffusion and located in the gas and/or the liquid phases. The gas phase diffusional resistance was initially expected to be the rate controlling step.

In addition it is assumed that both the gas and the liquid phases are well mixed and thus the zinc vapour condensation process involves transfer of zinc vapour from the bulk of the gas phase to the bulk of the liquid phase.

Based on these assumptions it is possible to express the zinc mass transfer rate:

$$\frac{dn_{Zn}}{dt} = -k_g A_b \left(C^{B}_{Zn,g} - C^{*}_{Zn,g} \right) = -k_\ell A_b \left(C^{*}_{Zn,\ell} - C^{B}_{Zn,\ell} \right) \quad 4.-19$$

where n_{Zn} = g-moles of zinc in the bubble

k_g = zinc mass transfer coefficient in the gas phase $cm \cdot sec^{-1}$

k_ℓ = zinc mass transfer coefficient in the liquid phase (liquid lead), $cm \cdot sec^{-1}$

A_b = equivalent bubble surface, cm^2

$C^{B}_{Zn,\ell}$, $C^{*}_{Zn,\ell}$ = zinc concentrations in the bulk and the interface respectively, liquid phase, g-moles·cm^{-3}

$C^{B}_{Zn,g}$, $C^{*}_{Zn,g}$ = zinc vapour concentrations in the bulk and the interface respectively, gas phase, g-moles·cm^{-3}

As in the case of the vapourization experiments, the bubble volume was between 1 and 5 cm^3 falling in the range of the spherical cap bubbles. Thus, the mass transfer coefficients for the gas and the liquid phase are given by:[24]

$$k_g = .924 \cdot D_{ZnAr}^{1/2} \cdot g^{1/4} \cdot V^{-1/12} \qquad 4.-3$$

$$k_\ell = .924 \cdot D_{ZnPb}^{1/2} \cdot g^{1/4} \cdot V^{-1/12} \qquad 4.-20$$

The diffusivity of zinc in argon, D_{ZnAr} was calculated in section 4.1.1.

The diffusivity of zinc in lead can be estimated from the theoretical approach of Walls and Upthegrove:[26]

$$D_{ZnPb} = \frac{\kappa \cdot T}{2 \cdot \pi \cdot r_{Zn} \cdot (2b+1) \cdot \mu_{Pb}} \qquad 4.-21$$

where κ = Boltzmann's constant

T = temperature, ^{o}K

r_{Zn} = zinc atomic radius, cm

b = ratio of zinc atomic radius over interatomic distance

μ_{Pb} = absolute viscosity of liquid lead, poise

Taking $T = 923^{o}K$, $r_{Zn} = 1.47 \times 10^{-8}cm$, $b = .437$, $\mu_{Pb} = 1.47 \times 10^{-2}$ poises, the diffusivity of zinc in lead at $650^{o}C$ becomes:

$$D_{ZnPb} = 5 \times 10^{-5} cm^2 sec^{-1}$$

Equation 4.-19 can be rewritten as:

$$-A_b \frac{dn_{Zn}}{dt} = \frac{1}{\frac{RT}{k_g} + \frac{1}{k_\ell \cdot m}} \left(P^B_{Zn} - C^B_{Zn,\ell/m} \right) \qquad 4.-22$$

where m = the equilibrium partition coefficient between liquid and gas phases.

$$m = \frac{C^*_{Zn,\ell}}{P^*_{Zn}} = .17 \text{ g-atoms } cm^{-3} \text{ atm}^{-1} \text{ at } T = 923^{o}K$$

The terms $\frac{RT}{k_g}$ and $\frac{1}{k_\ell \cdot m}$ represent the diffusional resistances in the gas and the liquid phase respectively. Comparison between the two diffusional resistance terms shows that the ratio of the gas phase resistance over the liquid phase resistance is 85, i.e., that the liquid phase resistance accounts for only 1% of the overall diffusional resistance. Thus, the rate controlling step in zinc transfer from the bulk of the bubble to the bulk of the liquid zinc-lead alloy is gas phase mass transfer.

The zinc mass transfer rate is, therefore, given by:

$$\frac{dn_{Zn}}{dt} = -k_g A_b \cdot \frac{P^B_{Zn} - C^B_{Zn,\ell/m}}{RT} \qquad 4.-23$$

It then follows (see section 4.1.1):

$$\frac{\partial n}{\partial P} = \frac{k_g \cdot A_b}{U \rho g} \cdot \frac{P^B_{Zn} - C^B_{Zn,\ell/m}}{RT} \qquad 4.-24$$

and finally

$$V + P \frac{\partial V}{\partial P} = .00016532 \cdot V^{5/12} \left(\frac{P^{in}_{Zn} \cdot V^{in} + PV - P^{in}V^{in}}{V} - \frac{C^B_{Zn,\ell}}{m} \right) \qquad 4.-25$$

where P^{in}_{Zn} = the zinc pressure in the bubble as it is introduced into the lead.

Equation 4.-25 has been integrated numerically for a lance depth of 10 cm and initial bubble volumes of 1, 2, 5, 10 cm^3. The bulk zinc concentration in the liquid phase was taken equal to 0 and the initial zinc vapour pressure equal to .035 atm, a typical pressure introduced from the vapourizer (jet configuration).

The numerical integration method used was identical to that used for the integration of equation 4.-17.

Figure 4.-10 summarizes the results of this integration and shows a plot of height of rise versus zinc mole fraction in the bubble. It is readily seen that for bubble volumes between 1 and 5 cm^3, the zinc pressure in a rising bubble virtually reaches equilibrium values after a rise between 5 and 10 cm. It is clear that bubble volume is an important factor affecting the condensation efficiency, in view of the high efficiencies required from an industrial zinc condenser.

It can also be stated that for the experimental conditions, equilibrium between the gas phase and the liquid lead-zinc alloy should

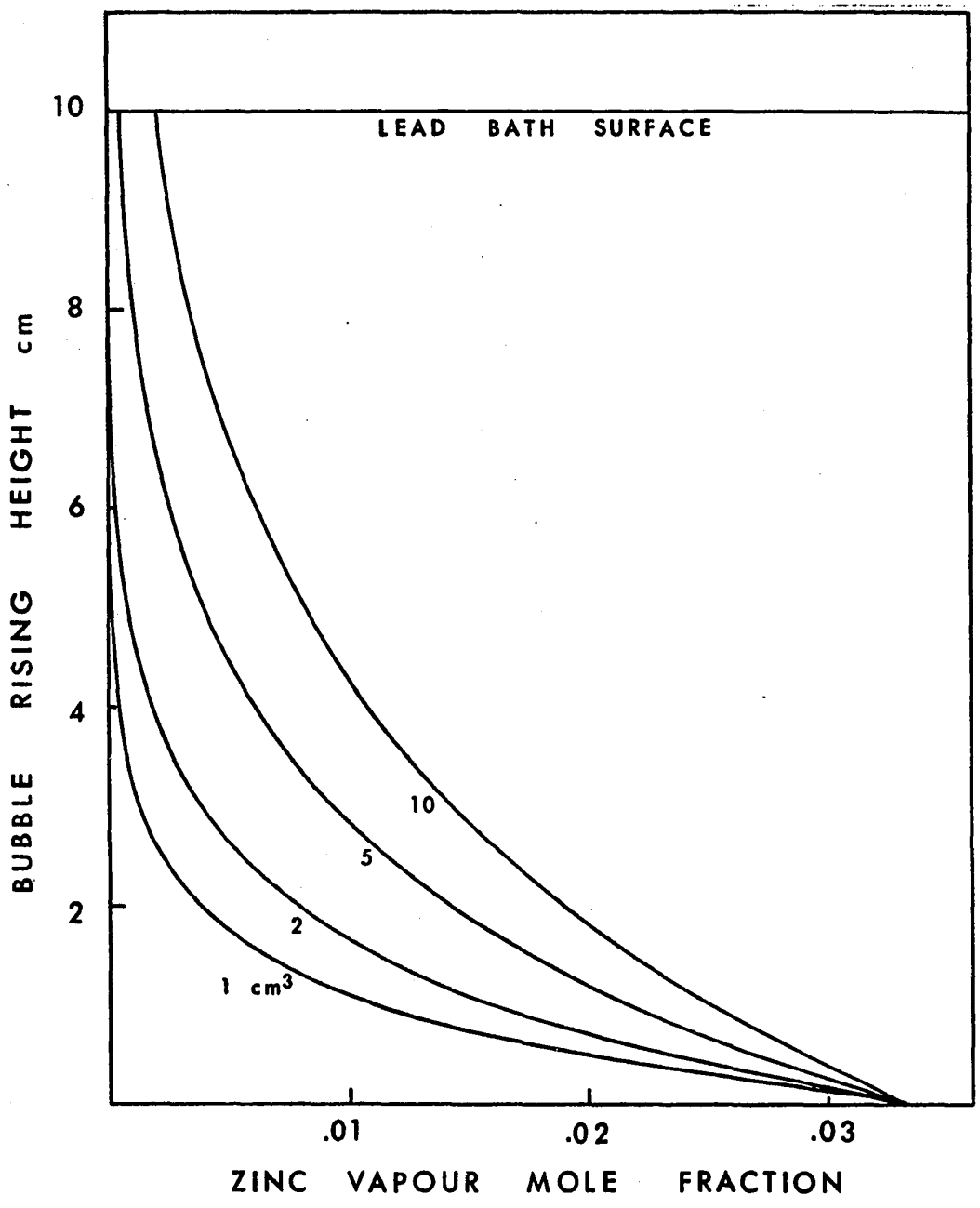

FIGURE 4.-10: Calculated zinc vapour loss from rising zinc-argon gas bubbles.

be expected according to the model developed above. The experimental results showed that such an equilibrium was actually reached and thus the validity of the theoretical model (i.e., mass transfer in the gas phase) is supported.

4.6 CONDENSATION OF ZINC VAPOUR INTO LEAD FROM A JET OF ZINC ARGON GAS

The experimental results of condensation from gas jets are shown in Figures 4.-11 to 4.-17, plotted as the ratio of measured zinc pressure over the equilibrium zinc vapour pressure over pure liquid zinc, versus weight percent zinc in lead. The solid lines represent the activity[19] of zinc in the zinc-lead alloy of composition equivalent to the experimental amount of zinc absorbed, assuming a well mixed liquid phase.

It can be seen that the experimental results show a strong departure from the activity curves, i.e., the exit gas zinc pressures are considerably higher than those which would be obtained if equilibrium between the bulk of the gas phase and the bulk of the liquid phase were achieved.

This result is equivalent to saying that a zinc concentration gradient exists between the two phases and that there is a significant resistance to mass transfer in the system.

Returning to the results of the vapourization of zinc into a jet of argon gas experiments, it can be remembered that near equilibrium pressures were obtained; and thus the resistance to mass transfer in

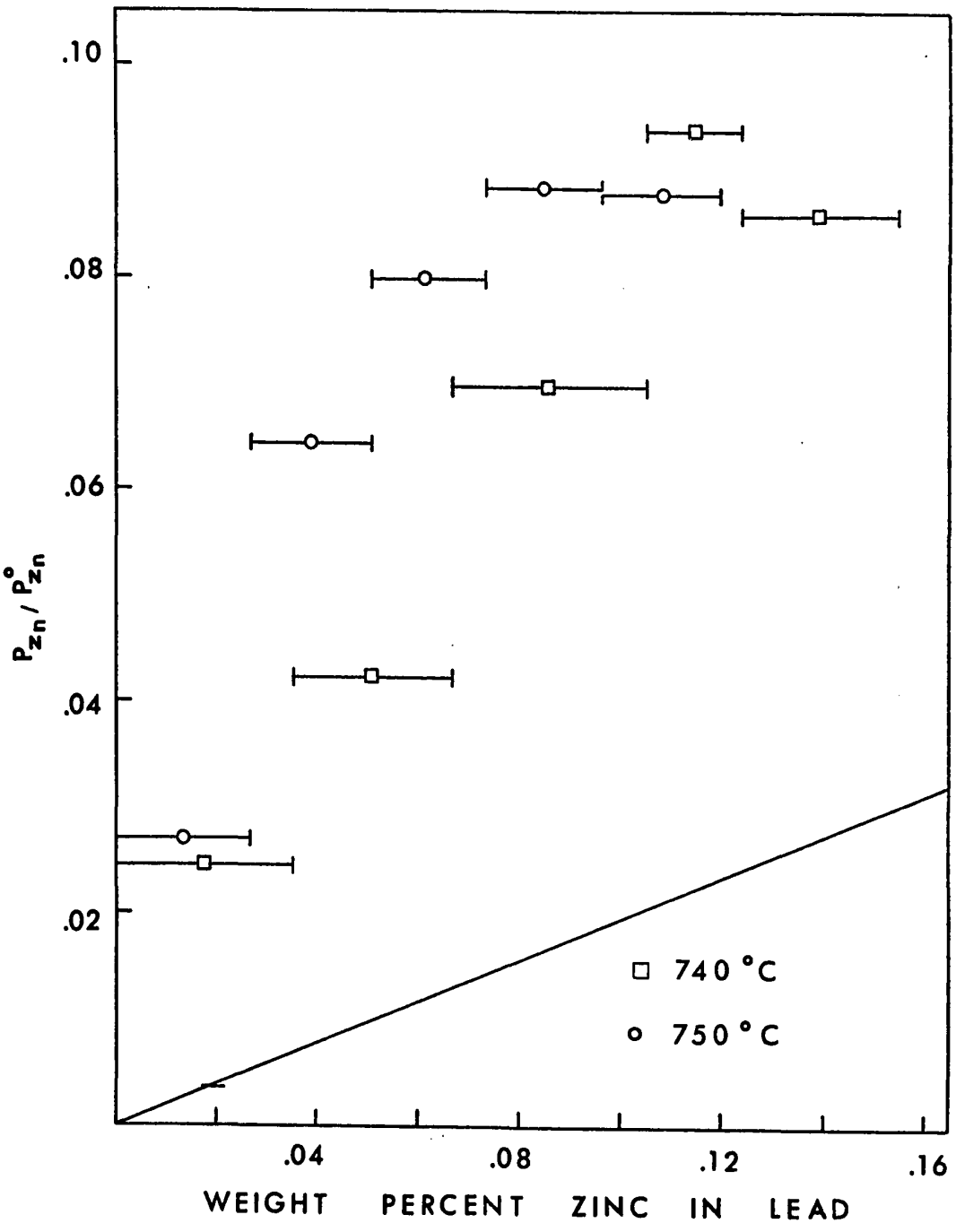

FIGURE 4.-11: Jetting condensation results (lead bath temperature 740°C, 750°C).

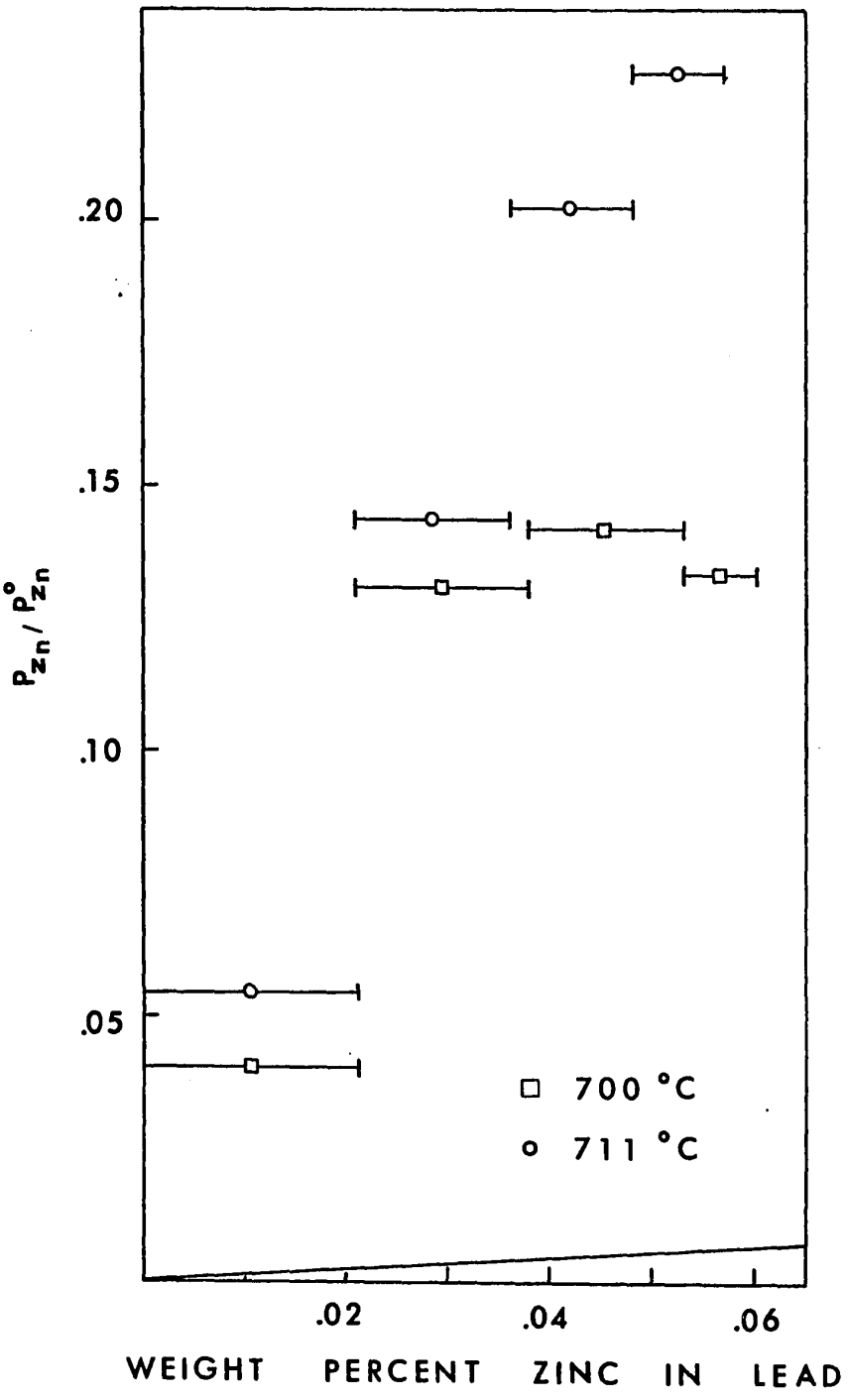

FIGURE 4.-12: Jetting condensation results (lead bath temperature 700°C, 711°C)

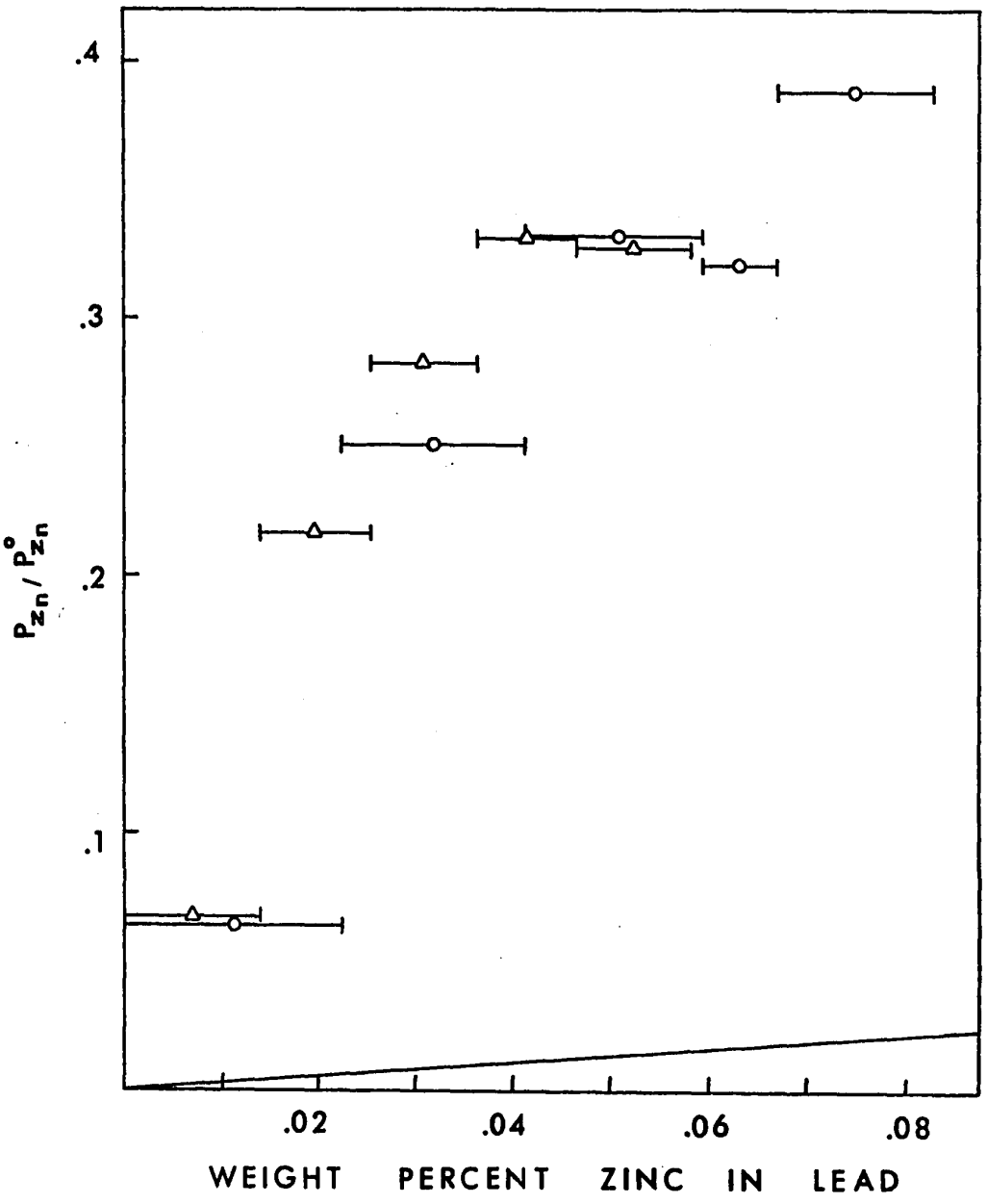

FIGURE 4.-13: Jetting condensation results (lead bath temperature 650°C).

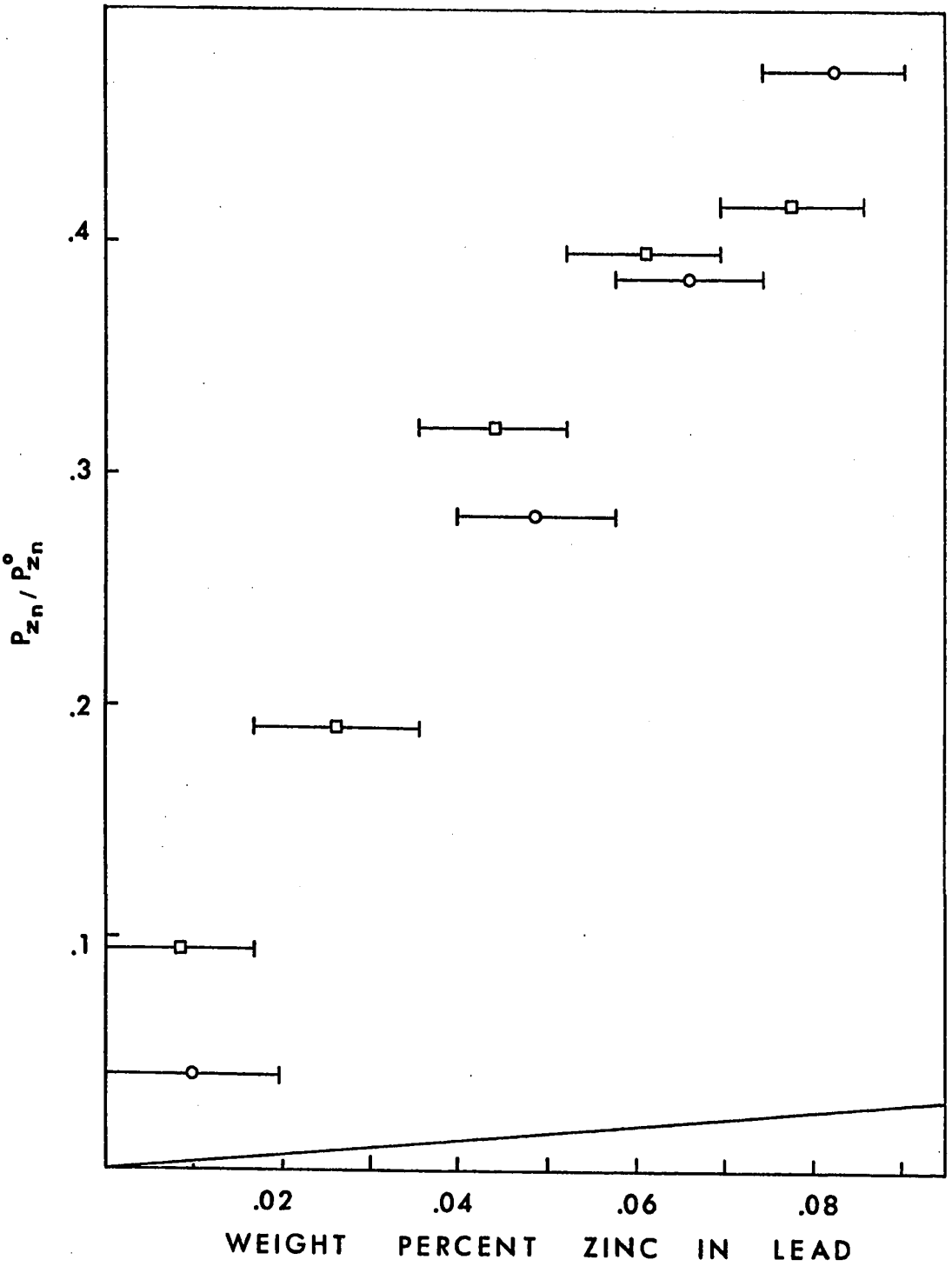

FIGURE 4.-14: Jetting condensation results (lead bath temperature 600°C.

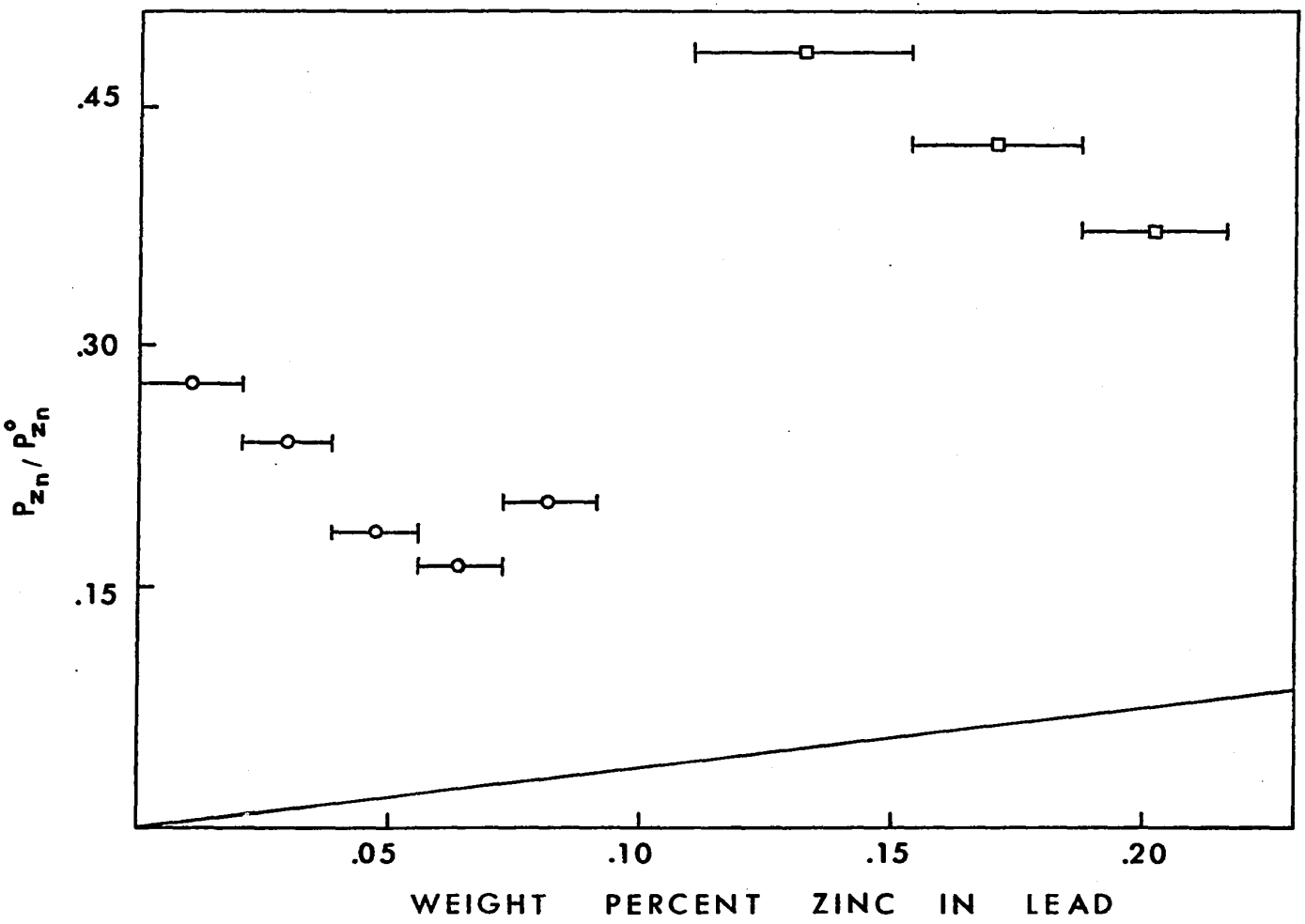

FIGURE 4.-15: Jetting condensation results (lead bath temperature 550°C).

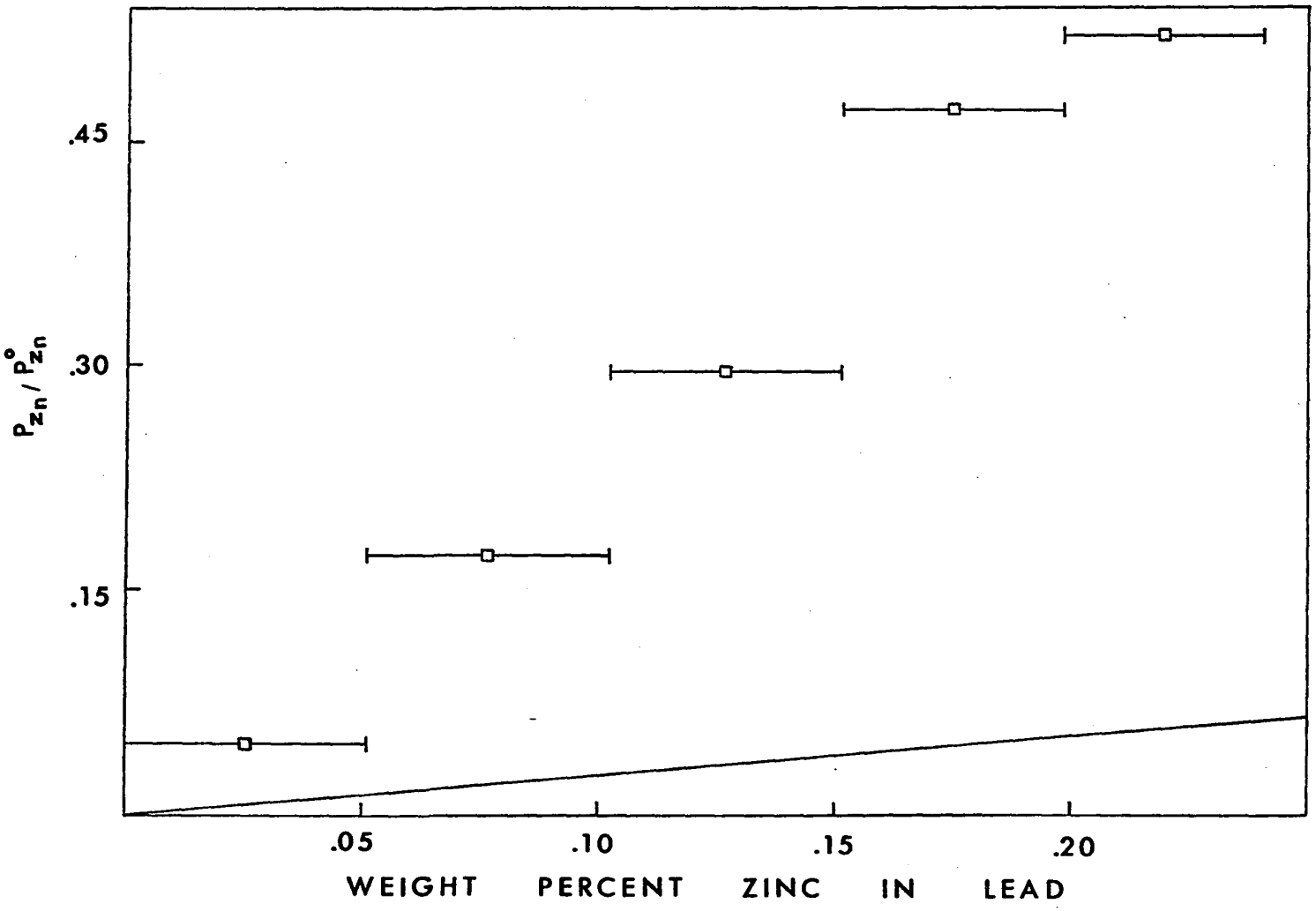

FIGURE 4.-16: Jetting condensation results (lead bath temperature 650°C).

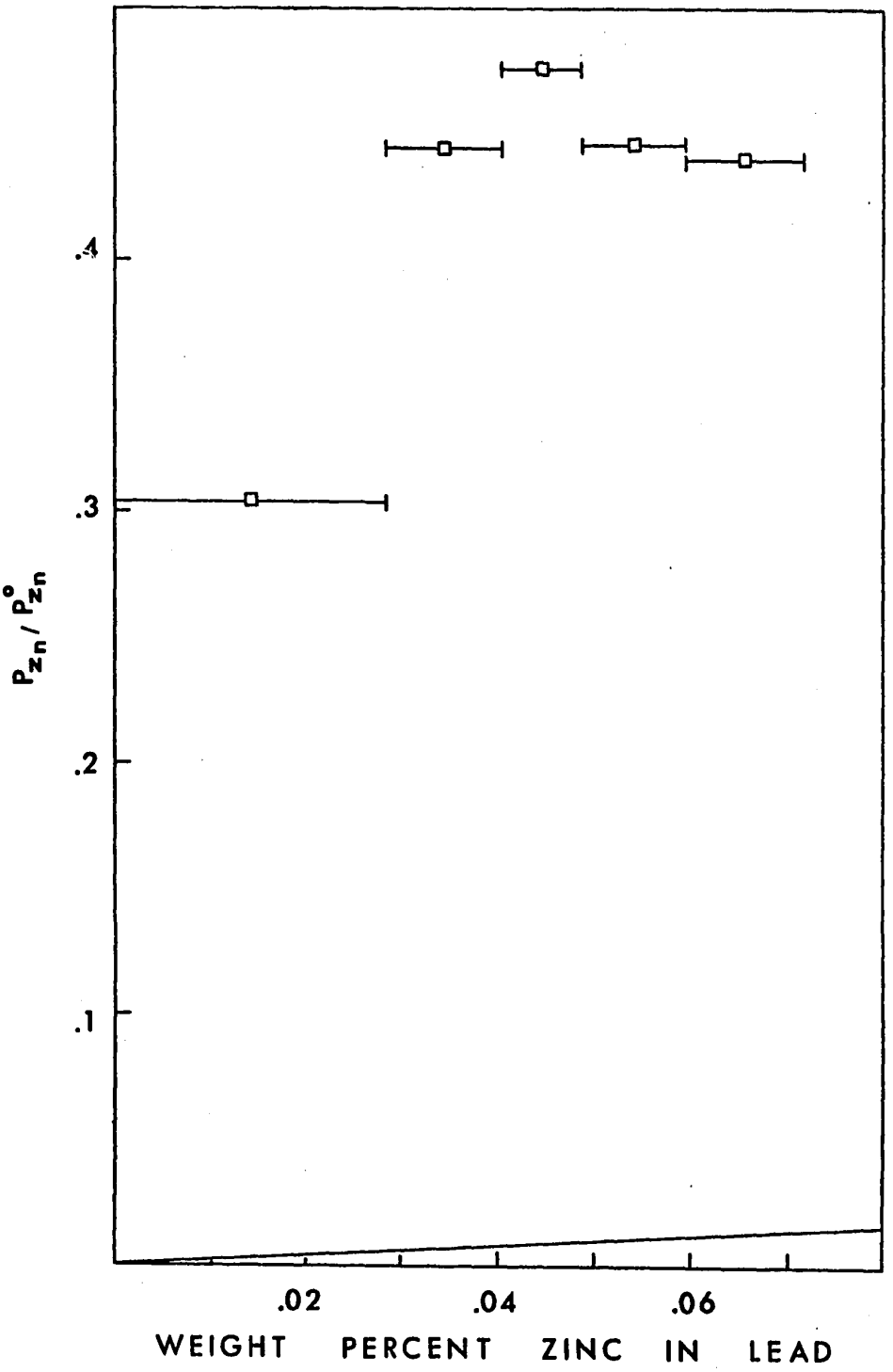

FIGURE 4.-17: Jetting condensation results (lead bath temperature 750°C).

the gas phase must have been small.

Thus, in the condensation experiments it is reasonable to likewise assume that equilibrium conditions exist between the bulk of the gas phase and the gas-metal interface since the volumetric flowrates were reasonably close in the vapourization and condensation experiments (i.e., volumetric flowrate, vapourization = 12.8 cm^3 sec^{-1} N.T.P., volumetric flowrate, condensation = 10.0 cm^3 sec^{-1} N.T.P.). In other words, it is reasonably assumed that $P^B_{Zn} = P^*_{Zn}$,

where P^B_{Zn}, P^*_{Zn} = zinc vapour pressures in the bulk gas and at the gas metal interface respectively.

Thus,

$$C^*_{Zn,\ell} = m\, P^B_{Zn} \qquad \forall\ t > 0 \qquad 4.-26$$

$$\frac{\partial n_{Zn}}{\partial t} = \frac{P^{in}_{Zn} - P^B_{Zn}}{RT}\ \dot{V} \qquad x = 0,\ \forall\ t > 0 \qquad 4.-27$$

where $C^*_{Zn,\ell}$ = zinc concentration in the lead bath at the gas-metal interface

t = time

m = equilibrium partition coefficient $\dfrac{C^*_{Zn,\ell}}{P^*_{Zn}}$

n_{Zn} = number of gram-atoms of zinc in the lead bath

P^{in}_{Zn} = input zinc vapour pressure in the jet

$\dot{V}$ = volumetric flowrate of the jet

x = distance of a point in the lead bath from the gas-metal interface.

The controlling step of the mass transfer of zinc vapour from the gas phase to the liquid phase was thus assumed to be mass transfer through the liquid lead. Two models were tentatively used to describe the mass transfer process.

Model 1: Stagnant Lead Bath

The lead bath was assumed to be stagnant and the mass transfer mechanism involving diffusion of zinc in a finite column of liquid lead. Fick's second law equation:

$$\frac{\partial C_{Zn,\ell}}{\partial t} - D_{ZnPb} \cdot \frac{\partial^2 C_{Zn,\ell}}{\partial x^2} = 0$$

with boundary conditions

$$C_{Zn,\ell} = 0, \quad \forall \ x, \quad t = 0$$

where $C_{Zn,\ell}$ = concentration of zinc in liquid lead

was numerically solved, simultaneously with equations 4.-26, 4.-27. The numerical solution of these equations yielded computed values of the zinc vapour pressure in the exit gas (P^B_{Zn}), the zinc concentration profile in liquid lead, and the average zinc concentration in the liquid lead. The results are plotted in Figure 4.-18 as P^B_{Zn} / P^o_{Zn} versus weight percent zinc in lead and they are compared with the experimental results. It can be seen that the computed values are considerably higher than the measured values indicating that some stirring must have been occurring in the lead bath.

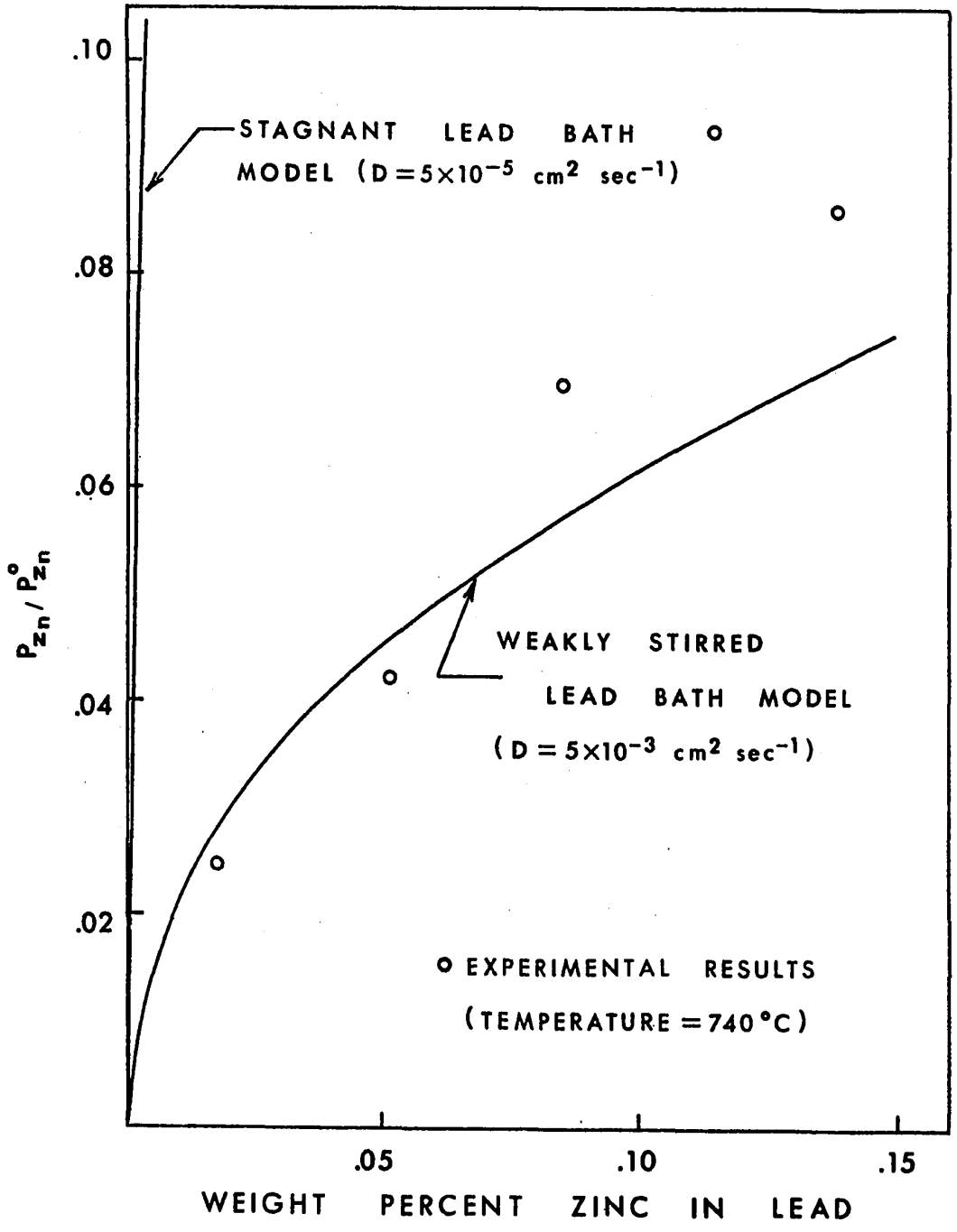

FIGURE 4.-18: Comparison between jetting condensation experimental results and computed values from assumed mass transfer models.

Model 2: Weakly Stirred Lead Bath

The liquid lead bath was assumed to be weakly stirred as a result of the mechanical action of the gas jet on it and a zinc concentration profile of the error function form was assumed to be established in the liquid metal bath. This assumption was suggested by the experimental work of Davenport, Wakelin and Bradshaw[27] who showed that an impinging gas jet could only slightly stir a liquid metal bath even at very high jet momentum values.

Values as high as 10^{-2} cm^2 sec^{-1} were given to an apparent diffusion coefficient (eddy diffusivity), and a numerical method was used to solve Fick's second law equation. An example computed curve for P^B_{Zn}/ P^o_{Zn} is again plotted in Figure 4.-18 versus weight percent zinc in lead, in this case for an eddy diffusivity of 5×10^{-3} cm^2 sec^{-1}. As expected the computed values more closely approximate those obtained in the experiments. It can be noted, however, that the shapes of the computed and experimental curves are somewhat different.

It appears therefore that none of the above models completely describes the condensation of zinc from the impinging zinc-argon gas jets.

It is interesting to note, however, that the measured exit zinc vapour pressures were always lower than the equilibrium vapour pressures of zinc over pure liquid zinc at the condenser temperature, even when the liquid lead temperatures were lower than the dew point temperature of the zinc-argon gas mixtures introduced into the condenser.

This was observed in four experiments, as shown in Table 4.A, which gives the average condenser input zinc vapour pressure, the input gas dew point, the lead bath temperature, the equilibrium zinc vapour pressure over pure liquid zinc at the condenser temperature and the maximum measured exit zinc vapour pressure for these four experiments.

TABLE 4.A

CONDENSER CONDITIONS, JETTING CONFIGURATION

Input zinc vapour press. mm Hg	Input gas dew point °C	Lead bath temperature °C	Equil. zinc vap. press. mm Hg	Max. exit vap. press. mm Hg
28.00	653	600	11.13	4.64
28.00	653	600	11.13	5.09
27.00	650	550	4.09	1.14
65.00	705	650	27.01	14.00

Table 4.A shows that in all these experiments the lead bath temperature was lower than the zinc dewpoint temperature in the input gas. The table also shows, however, that the exit gas zinc pressure was always lower than the equilibrium zinc vapour pressure over pure liquid zinc. This result indicates that a pure zinc phase was not present in the condenser (say by nucleation on the condenser walls) and thus that physical liquefaction of pure zinc followed by absorption in the liquid lead does not occur.

The condensation process is better described, therefore, as absorption of zinc vapour into lead.

4.7 INDUSTRIAL IMPLICATIONS

In this section, some improvements in zinc condensation methods are suggested. An analysis of the possible choice of a zinc bubble condenser, as an alternative to the lead splash condenser for zinc blast furnace gases is given below.

It has been shown from the experimental study that a high condensation efficiency was achieved in the bubbling condensation experiments. It has also been shown that bubble rising heights of 5 cm to 10 cm are sufficient for equilibrium to be reached between the gas phase and the liquid phase. In other words the experimental condensation efficiency achieved was equal to the theoretical maximum condensation efficiency.

In addition, a bubble condenser is preferable to a splash condenser from an engineering point of view for these reasons:

1) It has very few moving parts and thus has consequently lower maintenance costs.
2) It can be more readily made gas tight to prevent zinc vapour oxidation due to air leakage into the condenser.
3) It has a lower construction cost.

Industrial data show, moreover, that metal recoveries in bubble and splash condensers (the bubble condenser is coupled with the St. Joseph Lead Co. electrothermic furnace, while the zinc splash condenser is coupled with the vertical retort) are approximately the same, between 93 and 97%. Since the condensation conditions (temperature,

zinc-in-gas concentration, enthalpy) are comparable for the two condenser types, it can be stated that the two condensation configurations, i.e., bubbling and splashing are likely to be equally efficient.

It is believed that a bubble condenser would be the best solution for the problem of condensation of zinc vapour from zinc blast furnace gases.

4.7.1 THE USE OF LEAD OR OF ZINC IN THE BUBBLE CONDENSER

Perhaps the biggest question in condenser design is whether it is necessary to use liquid lead as the shock cooling condensing medium in a bubble condenser for zinc blast furnace gas or whether zinc itself would be a suitable condensing medium. The use of zinc would have the advantages of:

1. The step of separating lead and zinc phases would be eliminated.
2. Rather than using cooling launders open to the atmosphere as is now employed with the lead splash condenser, heat extraction would be accomplished by means of submerged, watercooled pipes in the condenser.
3. A zinc product, uncontaminated with lead would be produced from zinc oxide sinter.
4. The pumping of large quantities of liquid lead would be eliminated.

The first advantage lead might be considered to have is its low melting point 327^{o}C as compared with that of zinc, 419^{o}C. This

lower melting point indicates that a greater shock-cooling effect can be obtained with the cooler lead medium.

On the other hand, the industrial condensers are never operated at less than 450°C, in order to avoid solidification of any condensing zinc, so that with closer operating control, say in an internally cooled bubble condenser, a zinc condenser could be operated virtually as cool as the present lead condensers are now run. In addition an internally cooled bath would not let the cooling medium increase in temperature as does the present lead splash condenser in which the temperature of the lead rises to 600°C during its countercurrent passage through the condenser.

The second advantage of a lead condenser is that the zinc is dissolved in lead and hence it is at less than unit activity. Hence the thermodynamic tendency for oxidation by the reaction

$$Zn_{(\ell)} + CO_2 = CO + ZnO_{(s)}$$

is reduced.

If the present lead condenser conditions are considered, however, in which the output zinc in lead concentration is 2.25 weight percent (molar fraction of zinc .068), the activity of zinc in the lead is 0.4. Thus the equilibrium zinc vapour pressure over pure liquid zinc is 0.08 atm, while the equilibrium pressure over the zinc lead alloy is 0.032 atm. Calculation of the free energy of the reaction:

$$Zn_{(v)} + CO_2 = CO + ZnO_{(s)}$$

for the above two values of zinc vapour pressure according to equation:

$$\Delta G_T = \Delta G_T^o - R\,T\,\ln \frac{P_{Zn} \cdot P_{CO_2}}{P_{CO}}$$

the partial pressures of carbon monoxide and carbon dioxide being:

P_{CO_2} = .12 atm, P_{CO} = .25 atm, yields:

ΔG_T = -10,600 cals mole^{-1} for P_{Zn} = 0.08 atm, and

ΔG_T = - 8,800 cals mole^{-1} for P_{Zn} = 0.032 atm.

Thus, the thermodynamic tendency for zinc back oxidation is only slightly reduced by using liquid lead rather than liquid zinc as the condensing medium.

It can be seen, then, that the advantages for a lead medium are not clear cut. It may be that at the temperature for which the use of zinc is envisaged (450^{o}C), the back oxidation reaction, though thermodynamically favoured in blast furnace gas, will be kinetically sluggish.

In summary then, the advantages of a zinc condenser in the bubble configuration warrant further attention.

4.7.2 DESIGN CALCULATION OF FULL SCALE BUBBLE CONDENSER

In this section the size and design of a bubble condenser to be coupled with a zinc blast furnace is evaluated. The calculations are valid for either zinc or lead to be used as the cooling liquid metal and the design of the existing industrial bubble condensers has been taken as a basis. The scale-up factors used are based on:

1) the size of existing industrial condensers in relation to their capacities;
2) the assumption that the most important factor affecting the condenser design is the volume of gases to be handled.

The latter assumption is justified by the dependence of the rate of approach to equilibrium on bubble size and of rising velocity (and hence residence time) on bubble size (see Figure 4.-10). Thus, the most important design criterion is expected to be the ratio of the condenser cross sectional area to the volumetric gas flowrate.

Table 4.B shows the operating conditions of a proposed condenser to cover the condensation requirements of an industrial scale zinc blast furnace.

TABLE 4.B

OPERATING CONDITIONS OF ZINC BLAST FURNACE[13]

Zinc production		100 tons/day
Gas input temperature		1050°C
Gas output temperature		450°C
Liquid metal temperature		450°C
Gas composition:	Zn	8%
	CO	25%
	CO_2	12%
	N_2	55%
Total gas volume		1400 m^3 min^{-1}
Heat to be extracted		10^5 Kcals min^{-1}

The dimensions of industrial retort bubble condensers for various rated condensation capacities are shown in Table 4.C.

TABLE 4.C

DIMENSIONS OF INDUSTRIAL BUBBLE CONDENSERS

Condenser production capacity tons/day	Gas volume $m^3\ min^{-1}$	Heat evolved $Kcals\ min^{-1}$	Cross sectional height in.	Cross sectional crown width in.	Condenser length feet
5	2.65	2×10^3	38	28	10
30	16.0	12×10^3	51	36	22
50	26.5	20×10^3	56	40	31

It can be noted that the volumetric flowrate from the blast furnace is some 50 times larger than that throughout the largest existing bubble condensers so that considerably larger units would have to be used. It is believed that the best solution would be the use of a system of twin condensers coupled with a zinc blast furnace. The option for a system of two condensers is suggested because:

1) it provides for small size condensers which are easy to control;
2) it provides for a high versatility.

The design of the proposed twin condensers was done by extrapolation based on the designs of existing industrial bubble condensers. Figure 4.-19 shows a plot of cross section dimensions of industrial bubble condensers versus volumetric flowrate of input gases. The design dimensions of the proposed condensers cross section were found using this plot for a gas flowrate of 700 $m^3\ min^{-1}$ (each condenser).

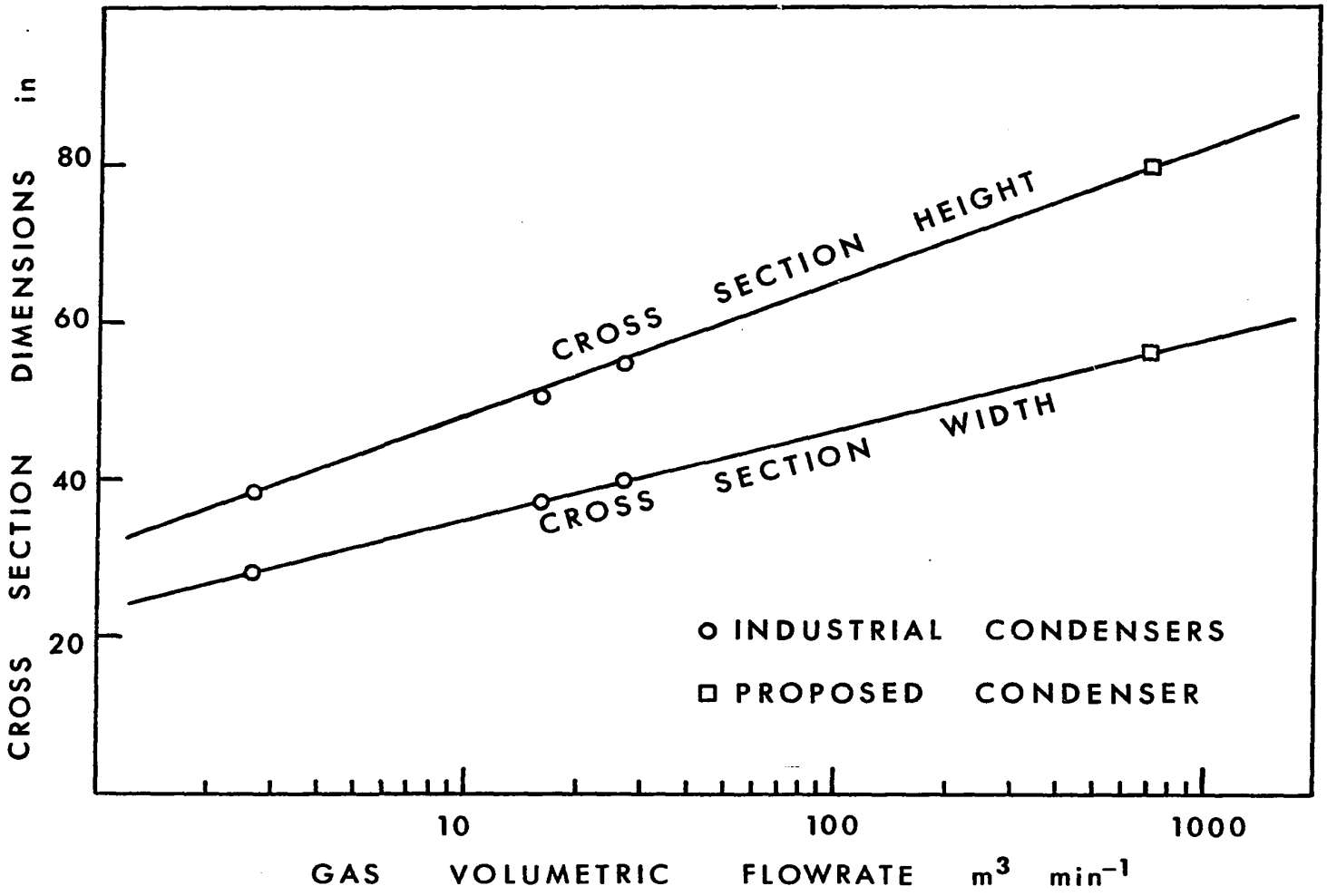

FIGURE 4.-19: Dependence of the bubble condenser cross section dimensions on the gas throughput.

The dimensions of these condensers are shown in Table 4.D.

TABLE 4.D

DIMENSIONS OF ZINC BLAST FURNACE TWIN BUBBLE CONDENSERS

Cross section height	80 in
Cross section crown width	56 in
Condenser length	30 ft
Condenser chamber slope	6^{o}

It should be noted that the length of the condenser has not been increased for two reasons:

1) the length and the slope of the condenser chamber are interrelated and it is believed that a slope of 6^{o} is close to the lower limit of condenser chamber slope for a smooth operation;
2) the length of the old industrial condensers was increased in order to provide enough surface area for heat exchange since these old condensers were cooled externally by water sprays.[3] Since the methods of internal cooling by means of submerged water pipes are now in use, the proposed condensers could be short and internally cooled by water circulation.

The heat to be removed from each of these condensers is 5×10^{4} Kcals min^{-1}. If water is used as the cooling medium, assuming a water input temperature of $20^{o}C$ and a water output temperature of $70^{o}C$, the volume of water to be circulated through the water cooling pipes to absorb the heat evolved from the gases cooling and the zinc condensation would be 1 m^{3} min^{-1} in each condenser.

4.8 SUGGESTIONS FOR FUTURE EXPERIMENTAL WORK

The present work has established the validity of bubbling as a method for condensation of zinc vapour on liquid lead.

Some suggestions for future work to further exploit the results presented in this thesis and to widen the scope of this method include:

1) Further exploration of the liquid lead temperature effect on the condensation efficiency mainly towards the lower temperature range, i.e., down to 450°C.
2) Further exploration of the gas flowrate effect on the condensation efficiency.
3) Repetition of the vapourization and condensation experiments with mixtures of nitrogen, carbon monoxide, carbon dioxide as the carrying gas. The rates of liquid zinc and zinc vapour reoxidation could be studied in this series of experiments.
4) An experimental program with liquid zinc as the condensing medium using an inert carrying gas to study the rates of condensation of zinc vapour on liquid zinc.
5) An experimental program with liquid zinc as the condensing medium and mixtures of N_2, CO, CO_2 as the zinc vapour carrying gas, to explore the possibility of substituting liquid zinc for liquid lead in industrial practice.

4.9 CONCLUSIONS

1) Methods were successfully developed for the production of zinc vapour/argon gas mixtures of required composition and flowrate.
2) The condensation of zinc vapour from argon-zinc gas mixtures into liquid lead was studied using two different contacting methods: jetting and bubbling.
3) High rates and efficiencies of condensation were obtained using the bubbling configuration. The experimental results were compatible with mass transport control in the gas phase.
4) Condensation rates and efficiencies are lower from impinging gas jets than from rising bubbles.
5) The condensation of zinc vapour on liquid lead was shown to be chemical absorption of zinc into the lead rather than physical liquefaction.
6) It is suggested that the condensation of zinc vapour from zinc blast furnace gas can be performed by use of liquid zinc instead of liquid lead as the coolant metal.
7) A bubble vacuum condenser is proposed as a better alternative to the lead splash condenser at present coupled with zinc blast furnaces.

APPENDIX A

EXPERIMENTAL RESULTS

A.1

SIMPLE VAPOURIZATION EXPERIMENTS (BUBBLING)

Experiment No.	Flowrate $cm^3 min^{-1}$	Lance Depth cm	Bath Temperature °C	Blowing Time min	Zinc Weight g	Zinc Concentration $g\ cm^{-3} \times 10^5$	Zinc Molar Fraction (Gas Phase)	Zinc Partial Pressure mm Hg	Zinc Pressure Max. Fluctuation %	Vapourization Rate g-moles sec^{-1}
5	870	7.5	600 ±5	4	.32	9.0	.030	22.7	16.1	2.18
				5	.38	8.5	.028	31.6		
				8	.69	9.7	.032	24.4		
				10	.83	9.3	.031	23.5		
				12	1.06	9.9	.033	25.0		
				14	1.39	11.2	.037	28.0		
				1	.855	9.6	.032	24.2		
6	870	5	600 ±5	4	.20	5.6	.019	14.3	21.1	1.62
				6	.32	6.0	.020	15.3		
				8	.52	7.3	.024	18.5		
				10	.66	7.4	.025	18.8		
				12	.85	7.9	.026	20.2		
				14	1.05	8.4	.028	21.3		
				1	.063	7.1	.024	18.1		
7	870	10	650 ±5	4	.63	17.7	.057	43.4	7.1	3.74
				7	1.01	16.2	.053	40.0		
				8	1.13	15.9	.051	39.2		
				10	1.50	16.8	.055	41.5		
				12	1.73	16.2	.053	40.0		
				14	2.00	16.0	.052	39.6		
				1	.147	16.5	.053	40.6		

A.1 (Cont'd)

SIMPLE VAPOURIZATION EXPERIMENTS (BUBBLING)

Experiment No.	Flowrate $cm^3 min^{-1}$	Lance Depth cm	Bath Temperature °C	Blowing Time min	Zinc Weight g	Zinc Concentration $g\ cm^{-3} \times 10^5$	Zinc Molar Fraction (Gas Phase)	Zinc Partial Pressure mm Hg	Zinc Pressure Max. Fluctuation %	Vapourization Rate $g\text{-moles}\ sec^{-1}$
				4	.595	16.7	.054	41.2		
				6	.93	17.4	.056	42.8		
				8	1.24	17.4	.056	42.8		
8	870	7.5	650 ±5	10	1.61	18.1	.058	44.4	6.0	4.03
				12	1.99	18.6	.060	45.6		
				14	2.30	18.4	.059	45.2		
				1	.158	17.7	.057	43.6		
				4	.71	19.9	.064	48.6		
				6	1.01	18.9	.061	46.4		
9	870	5	650 ±5	10	1.64	18.4	.059	45.1	8.1	4.18
				12	1.86	17.4	.056	42.8		
				14	2.16	17.3	.056	42.6		
				1	.164	18.4	.059	45.1		
				4	1.04	29.2	.091	69.1		
				6	1.68	31.5	.097	73.9		
				8	2.30	32.3	.099	75.7		
10	870	10	700 ±5	10	2.87	32.2	.099	75.6	6.5	7.09
				12	3.40	31.8	.098	74.7		
				14	3.79	30.4	.094	71.7		
				1	.278	31.2	.097	73.5		

A.1 (Cont'd)

SIMPLE VAPOURIZATION EXPERIMENTS (BUBBLING)

Experiment No.	Flowrate $cm^3 min^{-1}$	Lance Depth cm	Bath Temperature °C	Blowing Time min	Zinc Weight g	Zinc Concentration $g\ cm^{-3} \times 10^5$	Zinc Molar Fraction (Gas Phase)	Zinc Partial Pressure mm Hg	Zinc Pressure Max. Fluctuation %	Vapourization Rate g-moles sec^{-1}
11	870	7.5	700±5	4	1.04	29.2	.091	69.1	18.9	7.47
				6	1.69	31.6	.098	74.3		
				8	2.28	32.0	.099	75.1		
				10	3.00	33.7	.103	78.7		
				12	3.40	31.8	.098	74.7		
				14	4.88	39.2	.118	89.9		
				1	.293	32.9	.101	77.0		
12	870	5	700±5	4	.94	26.4	.083	63.1	24.6	7.27
				6	1.40	26.2	.082	62.6		
				8.5	2.28	30.1	.094	71.1		
				10	3.00	33.7	.103	78.7		
				12	3.82	35.7	.109	83.0		
				14	4.98	40.0	.120	91.5		
				1	.285	32.0	.099	75.1		
14	870	10	750±2	4	1.36	38.2	.116	88.0	53.7	10.2
				7	2.24	35.9	.110	83.4		
				10	3.20	35.9	.110	83.4		
				5.5	3.40	69.4	.192	146.1		
				8.25	3.40	46.3	.137	104.1		
				1	.402	45.2	.134	101.9		

A.1 (Cont'd)

SIMPLE VAPOURIZATION EXPERIMENTS (BUBBLING)

Experiment No.	Flowrate $cm^3 min^{-1}$	Lance Depth cm	Bath Temperature °C	Blowing Time min	Zinc Weight g	Zinc Concentration $g\ cm^{-3} \times 10^5$	Zinc Molar Fraction (Gas Phase)	Zinc Partial Pressure mm Hg	Zinc Pressure Max. Fluctuation %	Vapourization Rate g-moles sec^{-1}
				4	1.42	39.9	.120	91.4		
				5.5	1.78	36.4	.111	84.2		
15	870	7.5	750±2	7	2.34	37.6	.114	86.7	6.5	8.85
				8.5	3.08	40.7	.122	93.0		
				10	3.58	40.2	.121	92.1		
				1	.346	39.0	.117	89.6		
				4	3.35	94.1	.244	185.3		
				5.5	3.53	73.1	.198	150.6		
16	870	5	750±2	7	4.97	79.8	.215	163.4	16.7	18.3
				8.75	6.27	80.5	.216	164.3		
				10	6.82	76.6	.208	158.1		
				1	.718	80.7	.216	164.6		

A.2

INTEGRATED BUBBLING VAPOURIZATION AND BUBBLING CONDENSATION EXPERIMENTS

Experiment No.	Vapourizer Sampling Flowrate $cm^3\ min^{-1}$	Lance Depth cm	Bath Temperature °C	VAPOURIZER: Blowing Time mins	Zinc Weight g	Zinc Concentration $g \cdot cm^{-3} \times 10^6$	Zinc Molar Fraction (gas phase)	Zinc Partial Pressure mm Hg	Zinc Pressure Max. Fluctuation %	Vapourization Rate g-moles sec^{-1}	Condenser Flowrate $cm^3\ min^{-1}$	Lance depth cm	Bath Temperature °C	CONDENSER: Blowing Time min	Zinc Weight g	Zinc Concentration $g\ cm^{-3} \times 10^6$	Zinc Molar Fraction (gas phase)	Condensation Rate g-moles sec^{-1}	Condensation Efficiency %
				7	.97	16.4	.053	40.4						30					
				7	1.26	21.3	.068	51.7						30	1.12	58.0	.015	11.2	78
				7	1.26	21.3	.068	51.7						30	1.27	66.0	.017	12.8	75
A2	850	7.5	650±2	7	1.33	22.5	.071	54.3	22.1	4.53	850	10	750±2	30					
				7	1.40	23.7	.075	57.1						30	1.92	99.0	.025	19.1	63
				7	1.24	21.0	.067	51.1											
				5	1.68	39.7	.120	92.0						20	.287	16.0	.006	4.2	95
				5	1.56	36.7	.112	86.0						20	.552	30.8	.011	8.1	90
				5	1.43	33.8	.104	79.8						20	.887	49.6	.017	12.8	84
A3	850	7.5	650±5	5	1.31	30.8	.096	73.5	15.4	7.44	890	10	750±5	20	1.08	60.5	.020	15.6	81
				5	1.31	30.8	.096	73.5						20	1.30	72.7	.024	18.7	77
				5	1.46	34.4	.105	81.1											
				11	.308	16.5	.053	40.7						11	.089	13.3	.0045	3.4	94
				10	.383	22.5	.072	54.7						10	.096	15.9	.0054	4.2	93
A5	170	7.5	650±2	10	.558	32.8	.101	77.1	35.6	5.06	600	10	750±2	10	.099	16.3	.0056	4.3	93
				10	.493	29.0	.090	69.0						10	.071	11.8	.0040	3.1	95
				10	.461	27.1	.085	64.8						10	.079	13.0	.0044	3.4	94
				10	.435	25.6	.081	61.2											
				10	.399	33.5	.075	56.8						10	.096	15.8	.0054	4.1	92
				10	.444	26.1	.082	62.5						10	.109	18.0	.0061	4.6	91
A6	170	5	650±5	10	.347	20.4	.065	46.7	32.8	4.27	600	10	750±5	10	.097	16.0	.0055	4.2	92
				10	.399	23.5	.074	56.7						10	.100	16.5	.0056	4.3	92
				10	.247	14.5	.047	36.1						10	.116	19.3	.0066	5.0	90
				10	.367	21.6	.069	52.4											
				10	.341	20.1	.064	47.9						10	.0385	6.4	.0022	1.6	97
				10	.428	25.2	.079	59.3						10	.0460	7.6	.0026	1.9	96
A7	170	5	655±2	10	.396	23.3	.074	55.1	13.4	4.39	600	10	695±2	10	.0495	8.2	.0028	2.1	96
				10	.356	20.9	.067	50.0						10	.0525	8.7	.0030	2.2	96
				10	.368	21.7	.069	51.5						10	.0395	6.5	.0022	1.6	97
				10	.378	22.2	.071	53.8											

INTEGRATED JETTING VAPOURIZATION AND JETTING CONDENSATION EXPERIMENTS

Experiment No.	Vapourizer Sampling Flowrate $cm^3\ min^{-1}$	Lance Depth cm	Bath Temperature °C	VAPOURIZER Blowing Time mins	Zinc Weight g	Zinc Concentration $g \cdot cm^{-3} \times 10^5$	Zinc Molar Fraction (gas phase)	Zinc Partial Pressure mm Hg	Zinc Pressure Max. Fluctuation %	Vapourization Rate g-moles sec^{-1}	Condenser Flowrate $cm^3\ min^{-1}$	Lance depth cm	Bath Temperature °C	CONDENSER Blowing Time min	Zinc Weight g	Zinc Concentration $g\ cm^{-3} \times 10^6$	Zinc Molar Fraction (gas phase)	Condensation Rate g-moles sec^{-1}	Condensation Efficiency %
				10	.553	32.5	.100	76.2						10	.0568	9.4	.0032	2.4	96
				10	.493	29.0	.090	68.7						10	.0583	9.6	.0033	2.5	96
A9	170	-3	650±2	10	.463	27.2	.085	64.9	20.2	5.40	600	0	745±5	10	.0643	10.6	.0036	2.7	96
				10	.443	26.1	.082	62.3						10	.0603	10.0	.0034	2.6	96
				11	.408	21.8	.069	52.9						11	.0800	11.6	.0040	3.0	95
				10	.465	27.3	.086	65.0											
				10	.366	21.5	.069	51.9						10	.0629	10.4	.0035	2.6	95
				10	.342	20.1	.064	48.6						10	.1075	17.7	.0060	4.5	91
A10	170	-3	650±5	10	.429	25.2	.079	60.1	28.9	4.07	600	-3	740±5	10	.177	29.2	.0099	7.5	85
				10	.249	14.6	.048	36.1						10	.237	39.2	.0133	10.0	80
				10	.366	21.5	.069	51.9						10	.217	35.9	.0122	9.2	82
				10	.351	20.6	.066	49.7											
				10	.287	16.9	.055	41.6						10	.0788	13.0	.0044	3.3	92
				10	.277	16.3	.053	40.2						10	.188	31.1	.0105	8.0	81
A11	170	-3	650±5	10	.279	16.4	.053	40.6	3.5	3.33	600	-3	750±5	10	.232	38.4	.0130	9.9	76
				10	.297	17.4	.056	43.0						10	.258	42.7	.0144	11.0	74
				10	.294	17.3	.056	42.7						10	.256	42.4	.0143	10.9	74
				10	.287	16.9	.055	41.6											
				10	.223	13.1	.043	32.5						10	.0566	9.4	.0032	2.4	91
				10	.205	12.1	.040	30.0						10	.186	30.7	.0104	7.9	72
A12	170	-3	650±5	10	.205	12.1	.040	30.0	27.2	2.25	600	-3	700±5	10	.202	33.3	.0113	8.5	70
				8	.113	8.3	.028	20.9						8	.151	24.9	.0106	8.0	72
				10	.194	11.4	.037	28.3											
				10	.231	13.6	.044	33.5						10	.090	14.9	.0051	3.8	88
				10	.216	12.7	.042	31.5						10	.241	39.8	.0135	10.2	68
A13	170	-3	652±2	10	.216	12.7	.042	31.5	8.7	2.5	600	-3	711± 2	10	.342	56.5	.0190	14.3	54
				10	.196	11.5	.038	28.7						10	.386	63.8	.0214	16.1	49
				10	.215	12.7	.041	31.3											

A.3 (Cont'd)

INTEGRATED JETTING VAPOURIZATION AND JETTING CONDENSATION EXPERIMENTS

				VAPOURIZER								CONDENSER						
Experiment No.	Vapourizer Sampling Flowrate $cm^3\ min^{-1}$	Lance Depth cm	Bath Temperature °C	Blowing Time mins	Zinc Weight g	Zinc Concentration $g\ cm^{-3} \times 10^5$	Zinc Molar Fraction (gas phase)	Zinc Partial Pressure mm Hg	Zinc Pressure Max. Fluctuation %	Vapourization Rate g-moles sec^{-1}	Condenser Flowrate $cm^3\ min^{-1}$	Lance Depth cm	Bath Temperature °C	Blowing Time min	Zinc Weight g	Zinc Concentration $g\ cm^{-3} \times 10^8$	Zinc Molar Fraction (gas phase)	Condensation Rate g-moles sec^{-1}	Condensation Efficiency %
				10	.182	10.7	.035	26.6						10	.046	6.7	.0023	1.7	94
				10	.191	11.3	.037	28.0						10	.161	26.6	.0090	6.8	75
A15	170	-3	650±2	10	.194	11.4	.038	28.3	4.7	2.2	600	-3	650±2	10	.213	35.2	.0119	9.0	67
				5	.089	10.5	.035	26.1						5	.103	34.1	.0115	8.7	68
				10	.189	11.1	.037	27.7						10	.249	41.2	.0139	10.5	62
				10	.187	11.0	.036	27.4											
				10	.143	8.4	.028	21.4						10	.0422	7.0	.0024	1.8	92
				10	.143	8.4	.028	21.4						10	.137	22.6	.0077	5.9	74
A16	170	-3	650±2	10	.153	9.0	.030	22.8	8.9	1.8	600	-3	650±2	10	.179	29.5	.0100	7.6	67
				10	.155	9.1	.030	23.1						10	.209	34.5	.0117	8.9	61
				10	.165	9.7	.033	24.9						10	.207	34.2	.0116	8.8	62
				10	.152	8.9	.030	23.0											
				10	.171	10.1	.033	25.3						10	.0242	4.0	.0014	1.1	96
				10	.201	11.8	.039	29.5						10	.0502	8.3	.0028	2.1	92
A17	170	-3	650±5	10	.186	10.9	.036	27.4	9.8	2.2	600	-3	600±5	10	.0832	13.7	.0047	3.6	87
				10	.201	11.8	.039	29.5						10	.102	16.9	.0058	4.4	84
				10	.188	11.1	.037	27.8						10	.108	17.9	.0061	4.6	84
				10	.189	11.1	.037	27.9											
				10										10	.0099	1.6	.306	1.5	98
				11	.209	11.2	.037	28.1						11					
				10	.197	11.6	.038	29.1						10	.0732	12.1	.0042	3.1	89
A18	170	-3	650±5	10	.192	11.3	.037	28.4	1.3	2.2	600	-3	600±5	10	.100	16.5	.0056	4.3	85
				10	.191	11.2	.037	28.3						10	.124	20.4	.0069	5.3	81
				10	.192	11.3	.037	28.5											

A.3 (Cont'd)

INTEGRATED JETTING VAPOURIZATION AND JETTING CONDENSATION EXPERIMENTS

Experiment No.	Vapourizer Sampling Flowrate $cm^3\ min^{-1}$	Lance Depth cm	Bath Temperature °C	VAPOURIZER Blowing Time mins	Zinc Weight g	Zinc Concentration $g \cdot cm^{-3} \times 10^5$	Zinc Molar Fraction (gas phase)	Zinc Partial Pressure mm Hg	Zinc Pressure Max. Fluctuation %	Vapourization Rate g-moles sec^{-1}	Condenser Flowrate $cm^3\ min^{-1}$	Lance Depth cm	Bath Temperature °C	CONDENSER Blowing Time min	Zinc Weight g	Zinc Concentration $g\ cm^{-3} \times 10^6$	Zinc Molar Fraction (gas phase)	Condensation Rate g-moles sec^{-1}	Condensation Efficiency %
A19	170	-3	650±5	10	1.076	63.3	.178	135.5						10	.376	62.2	.0209	15.8	88
				10	.466	27.4	.086	65.3	136	5.3	600	-3	550±2	10	.0467	7.7	.0026	2.0	97
				12	.330	16.2	.053	39.9						12	.0485	6.7	.0023	1.7	96
				10	.237	13.9	.046	34.6						10	.0355	5.9	.0020	1.5	96
				10	.455														
A20	170	-3	650±5	11	.212	11.3	.037	28.3						11	.0287	4.3	.0015	1.1	96
				10	.180	10.8	.035	26.5						10	.0237	3.9	.0013	1.0	96
				10	.176	10.4	.034	25.9	6.3	2.1	600	-3	550±5	10	.0181	3.0	.0010	.8	97
				10	.180	10.6	.035	26.5						10	.0159	2.6	.0009	.7	97
				10	.178	10.5	.035	26.2						10	.0201	3.3	.0011	.8	97
				10	.182	10.7	.035	26.7											
A21	170	-3	700±5	10	.440	25.8	.081	62.4						10	.0300	4.9	.0017	1.3	98
				10	.462	27.2	.085	65.3						10	.109	18.0	.0061	4.7	93
				10	.480	28.2	.088	67.6	4.9	5.4	600	-3	650±5	10	.243	40.2	.0136	10.4	84
				10	.480	28.2	.088	67.6						10	.297	49.2	.0166	12.7	81
				10	.452	26.6	.083	64.0						10	.331	54.8	.0184	14.1	78
				10	.463	27.2	.085	65.3											
A22	170	-3	700±5	10	.523	30.8	.095	72.4						10	.926	153.1	.0498	37.8	46
				10	.502	29.5	.092	69.7						10	1.386	229.1	.0728	55.2	21
				10	.496	29.1	.091	68.9	4.1	5.8	600	-3	750±5	10	1.491	246.4	.0778	59.0	16
				10	.494	29.0	.090	68.7						10	1.391	229.9	.0730	55.4	21
				10	.499	29.4	.091	69.4						10	1.371	226.6	.0720	54.6	22
				10	.503	29.6	.092	69.9											

A.4

INTEGRATED JETTING VAPOURIZATION AND BUBBLING CONDENSATION EXPERIMENTS

				VAPOURIZER										CONDENSER					
Experiment No.	Vapourizer Sampling Flowrate $cm^3\ min^{-1}$	Lance Depth cm	Bath Temperature °C	Blowing Time mins	Zinc Weight g	Zinc Concentration $g\cdot cm^{-3} \times 10^5$	Zinc Molar Fraction (gas phase)	Zinc Partial Pressure mm Hg	Zinc Pressure Max. Fluctuation %	Vapourization Rate g-moles sec^{-1}	Condenser Flowrate $cm^3\ min^{-1}$	Lance depth cm	Bath Temperature °C	Blowing Time min	Zinc Weight g	Zinc Concentration $g\ cm^{-3} \times 10^6$	Zinc Molar Fraction (gas phase)	Condensation Rate g-moles sec^{-1}	Condensation Efficiency %
				25	.853	51.7	.151	114.1						25	.717	21.4	.0073	5.5	95
				15	.298	30.1	.093	70.9						15	1.032	51.3	.0173	13.1	82
A23	65	-3	715±5	15	.266	26.9	.084	63.9	51.0	12.2	1350	8	750±5	15	1.227	61.0	.0205	15.6	76
				15	.280	28.3	.088	66.9						15	1.537	76.5	.0255	19.3	71
				15	.339														
				20	.285	21.6	.069	52.6						20	.073	3.6	.0012	.9	98
				20	.351	26.6	.083	63.7						20	.131	6.5	.0022	1.7	97
A24	65	-3	700±5	20	.313	23.7	.075	57.3	11.5	6.7	1010	8	700±5	20	.323	16.0	.0054	4.2	93
				2	.052	39.4	.119	90.7						2	.033	16.3	.0056	4.3	93
				20	.339	25.7	.081	61.8						20	.607	30.1	.0102	7.8	87
				20	.322	24.4	.077	58.7											
				20	.239	18.1	.058	44.6						20	.131	5.5	.0022	1.7	97
				20	.313	23.7	.075	57.4						20	.186	9.2	.0031	2.4	95
A25	65	-3	700±5	20	.297	22.5	.072	54.7	17.1	6.0	1010	6	650±5	20	.229	11.3	.0039	3.0	94
				20	.305	23.1	.073	56.1						20	.335	16.6	.0056	4.3	92
				20	.288	21.8	.070	53.2											

ACKNOWLEDGEMENTS

Sincere appreciation is extended to Professor W.G. Davenport for supervision and assistance given during the course of this work.

Thanks are due to Professor W.M. Williams, Chairman, Department of Metallurgical Engineering, McGill University, and to Professor R.I.L. Guthrie for their interest and encouragement.

The author wishes to extend his thanks to Mr. M. Knoepfel for his invaluable technical assistance.

The author is indebted to the International Nickel Company of Canada Limited for providing generous financial assistance.

LIST OF SYMBOLS

Symbol		Units
ΔH^{o}_{T}	Standard enthalpy of reaction at temperature T°K	cal g-mole^{-1}
ΔG^{o}_{T}	Standard free energy of reaction at temperature T°K	cal g-mole^{-1}
K	Reaction equilibrium constant	suitable units
P	Pressure	atm.
P_x	Partial pressure of x gas in a mixture of gases	atm.
P^{o}_{x}	Equilibrium partial pressure of vapour x over the corresponding pure liquid	atm.
P^{in}	Initial value of total pressure	atm.
n_x	Number of moles of compound x	dimensionless
a_{Zn}	Activity of zinc in a zinc-lead alloy	dimensionless
t	Time	sec.
k_g	Gas phase mass transfer coefficient	cm sec^{-1}
k_ℓ	Liquid phase mass transfer coefficient	cm sec^{-1}
A_b	Equivalent bubble surface area (assuming spherical shape)	cm^2
V_b	Bubble volume	cm^3
$C^{*}_{Zn,g}$	Zinc interfacial concentration, gas phase	g-mole cm^{-3}
$C^{B}_{Zn,g}$	Zinc bulk concentration, gas phase	g-mole cm^{-3}
$C^{*}_{Zn,\ell}$	Zinc interfacial concentration, liquid phase	g-mole cm^{-3}
$C^{B}_{Zn,\ell}$	Zinc bulk concentration, liquid phase	g-mole cm^{-3}

Symbol		Units
R	Gas law constant	cal g-mole^{-1} ^{o}K^{-1}
T	Temperature	^{o}K
D_{AB}	Diffusion coefficient of solute A in solvent B	cm^2 sec^{-1}
g	Gravitational acceleration	cm sec^{-2}
M	Molecular weight	dimensionless
σ_{AB}	Collision diameter (Lennard-Jones parameter)	$\mathring{A}$
$\Omega_{D,AB}$	Collision integral	dimensionless
U	Bubble rising velocity	cm sec^{-1}
ρ	Liquid density	g cm^{-3}
m	Equilibrium partition coefficient between liquid and gas phases	g-atom cm^{-3} atm^{-1}
$\dot{V}$	Jet volumetric flowrate	cm^3 sec^{-1}
κ	Boltzmann constant	g cm^2 sec^{-2} ^{o}K^{-1}
μ_{Pb}	Absolute viscosity of liquid lead	poise

LIST OF FIGURES

Figure		Page
1.-1	Horizontal Retort Furnace	4
1.-2	Schematic diagram of vertical retort	6
1.-3	St. Joseph Lead Company electrothermic zinc furnace	7
1.-4	Bubble vacuum condenser	10
1.-5	Zinc splash condenser	11
1.-6	Diagrammatic arrangement of zinc blast furnace	13
2.-1	Condensation of zinc vapour from vertical retort gas	25
2.-2	Condensation of zinc vapour from zinc blast furnace gas	27
2.-3	The separation of zinc from lead (lead-zinc phase diagram)	34
3.-1	Schematic diagram of experimental apparatus . .	38
3.-2	Arrangement of vapourizer access pipes	40
3.-3	View of the experimental furnace.	43
3.-4	View of the experimental furnace.	43
3.-5	Schematic and wiring diagram of one side of the furnace	46
3.-6	Typical vapourization results (bubbling).	54
3.-7	Zinc vapourization results (bubbling)	56
3.-8	Zinc vapourization rates (bubbling)	58
3.-9	Typical vapourization results (jetting).	60
3.-10	Effect of new zinc meltdown on zinc-in-gas concentration	62

Figure		Page
3.-11	Zinc vapourization results (jetting)	63
3.-12	Zinc vapourization rates (jetting)	65
3.-13	Typical zinc condensation results (bubbling) (lead bath temperature 650°C)	67
3.-14	Typical zinc vapour condensation results (bubbling), (lead bath temperature 700°C) . . .	68
3.-15	Typical zinc vapour condensation results (bubbling), (lead bath temperature 750°C) . . .	69
3.-16	Typical zinc vapour condensation results (jetting), (lead bath temperature 650°C)	71
3.-17	Typical zinc vapour condensation results (jetting), (lead bath temperature 600°C)	72
4.-1	Temperature dependence of the equilibrium zinc vapour pressure over pure liquid zinc	76
4.-2	Comparison between the experimental bubbling vapourization results and the equilibrium zinc vapour pressure over pure liquid zinc	77
4.-3	Calculated zinc pick-up by argon rising bubbles.	84
4.-4	Comparison between the experimental jetting vapourization results and the equilibrium zinc vapour pressure over pure liquid zinc	86
4.-5	Typical temperature profile of the vapourizer. .	88
4.-6	Jetting vapourization results (jetting vapourization experiments immediately following the bubbling vapourization programme)	90
4.-7	Typical jetting vapourization results immediately following melting of new zinc	91
4.-8	Typical bubbling condensation results (lead bath temperature 700°C)	94
4.-9	Bubbling condensation results (lead bath temperature 750°C)	96

Figure		Page
4.-10	Calculated zinc vapour loss from rising zinc-argon gas bubbles	101
4.-11	Jetting condensation results (lead bath temperature 740°C, 750°C)	103
4.-12	Jetting condensation results (lead bath temperature 700°C, 711°C)	104
4.-13	Jetting condensation results (lead bath temperature 650°C)	105
4.-14	Jetting condensation results (lead bath temperature 600°C)	106
4.-15	Jetting condensation results (lead bath temperature 550°C)	107
4.-16	Jetting condensation results (lead bath temperature 650°C)	108
4.-17	Jetting condensation results (lead bath temperature 750°C	109
4.-18	Comparison between jetting condensation experimental results and computed values from assumed mass transfer models.	112
4.-19	Dependence of the bubble condenser cross section dimensions on the gas throughput.	121

LIST OF TABLES

Table		Page
1.A	Vertical Retort Furnaces	8
2.A	Free Energy of Reaction 2.-1 and Free Energy of Formation of ZnO	18
2.B	Free Energy and Equilibrium Constant of Reaction 2.-1	18
2.C	Temperature and Composition of Zinc Furnaces' Exhaust Gases	22
2.D	Working Conditions of the Vacuum-Bubble Condenser	31
2.E	Working Conditions of the Lead Zinc Splash Condenser	32
3.A	Distribution of Heating Elements in the Furnace .	45
4.A	Condenser Conditions, Jetting Configuration . . .	114
4.B	Operating Conditions of Zinc Blast Furnace . . .	119
4.C	Dimensions of Industrial Bubble Condensers . . .	120
4.D	Dimensions of Zinc Blast Furnace Twin Bubble Condensers	122

REFERENCES

1. Mathewson, C.H., "Zinc: The Science and Technology of the Metal, Its Alloys and Compounds," Reinhold Publishing Corp., New York, 1959.
2. Maier, C.G., "Zinc Smelting from a Chemical and Thermodynamic Viewpoint," Bull. U.S. Bur. Mines, Vol. 324, 1930, pp. 54-69.
3. Najarian, H.K., "Wheaton-Najarian Vacuum Condenser," Trans. Am. Inst. Mining Met. Engrs. 159, 165, 1944, pp. 164-175.
4. Mahler, G.T., Handwerk, E.C., "Condensing Zinc Vapor," U.S. Patent 2,494,552, Jan. 17, 1950.
5. Handwerk, E.C., Mahler, G.T., "Zinc Condenser," U.S. Patent 2,494,551, Jan. 17, 1950.
6. Robson, S., "Condensation of Zinc from Its Vapor in Gaseous Mixtures," U.S. Patent 2,583,668, Jan. 29, 1952.
7. Robson, S., Derham, L.J., "Improvements in the Production of Zinc," British Patent 686,585, Jan. 28, 1953.
8. Lumsden, J., "The Physical Chemistry of the Imperial Smelting Furnace," paper presented at the I.S.P. Conference at Bristol, England, June 12, 1963.
9. Morgan, S.W.K., "The Production of Zinc in a Blast Furnace," Trans. Inst. Mining Met., 66, Part II, pp. 553-65, 1956-57.

10. Wicks, C.E., Block, F.F., "Thermodynamic Properties of 65 Elements—Their Oxides, Halides, Carbides, and Nitrides," U.S. Bureau of Mines Bulletin No. 605, 1962.

11. Björling, G., "Ein Beitrag zur Thermodynamik der Kondensation von Zink," Z. Erzbergbau und Metallhüttenw., 7, pp. 69-73, 1954.

12. "AIME World Symposium on Mining and Metallurgy of Lead and Zinc," New York, 1970.

13. Gray, P.M.J. and Woods, S.E., "Production Capacity of the Imperial Smelting Furnace," 9th Commonwealth Mining and Metallurgical Congress, London, 1969, paper no. 9.

14. Truesdale, E.C., Warring, R.K., "Reduction Equilibria of Zinc Oxide and Carbon Monoxide," J. Am. Chem. Soc., 1941, Vol. 63, pp. 1610-21.

15. Kitchener, J.A., Ignatowicz, S., "The Reduction Equilibria of Zinc Oxide and Zinc Silicate with Hydrogen," Trans. Faraday Soc. 1951, Vol. 47, pp. 1278-86.

16. Wilder, T.C., "The Free Energy of Formation of $ZnO_{(s)}$ for the Temperature Range 420°C to 908°C," Trans. Metall. Soc. AIME 245, June 1969, pp. 1370-72.

17. Coughlin, T.P., "Heats and Free Energies of Formation of Inorganic Oxides," U.S. Bur. of Mines Bull., No. 542, 1959.

18. Denbigh, K., "The Principles of Chemical Equilibrium," Cambridge University Press, 1966.

19. Hultgren, R., Orr, R.L., Anderson, P.D., Kelley, K.K., "Selected Values of Thermodynamic Properties of Metals and Alloys," John Wiley and Sons, Inc., New York, 1963.

20. Todd, D.D., Oates, W.A., "A Calorimetric Study of the Thermodynamic Properties of Lead-Zinc Alloys in the Molten State," J. Inst. Metals, Vol. 93, pp. 302-8.

21. Warner, N.A., "The Absorption of Zinc Vapour in Molten Lead. Countercurrent Absorption in a Packed Column," Chem. Eng. Science, 1956, Vol. II, pp. 161-182.

22. Haberman, W.L., Morton, R.K., "An Experimental Study of Bubbles Moving in Liquids," Amer. Soc. of Civil Eng. Trans., Vol. 121, 1956, pp. 227-250.

23. Davidson, L., Amick, E.H., "Formation of Bubbles at Horizontal Orifices," A.I. Ch. Eng. J., Vol. 2, pp. 337-42.

24. Baird, M.H.I., Davidson, J.F., "Gas Absorption by Large Rising Bubbles," Chem. Eng. Sci., 1962, Vol. 17, p. 87.

25. Bird, R.B., Stewart, W.E., Lightfoot, E.N., "Transport Phenomena," John Wiley and Sons, New York, 1966, pp. 510-11.

26. Walls, H.A., Upthegrove, W.R., "Theory of Liquid Diffusion Phenomena," Acta Metg. 1964, Vol. 12, pp. 461-71.

27. Davenport, W.G., Wakelin, D.H., Bradshaw, A.V., "Interaction of Both Bubbles and Gas Jets with Liquids," Heat and Mass Transfer in Process Metallurgy, The Inst. of Min. and Met., London, 1966, pp. 207-240.